UNIVERSITY OF TRENTO

Department of Mathematics

Doctoral School in Mathematics

Ph.D. Thesis

A Geometric Singular Perturbation approach to epidemic compartmental models

Advisor:

Prof. Andrea Pugliese

Candidate:

Mattia Sensi

Academic Year 2019 - 2020

Contents

Acknowledgements **III**

1 Introduction **1**

2 A geometric analysis of the SIR, SIRS and SIRWS epidemiological models **5**
2.1 Introduction . . . 5
2.2 Preliminaries . . . 7
2.2.1 Fast-slow systems . . . 7
2.2.2 Entry-exit function . . . 8
2.3 Analysis of the SIR, SIRS and SIRWS models . . . 9
2.3.1 SIR model . . . 9
2.3.2 Applying the entry-exit function . . . 14
2.3.3 SIRS model . . . 17
2.3.4 SIRWS model . . . 19
2.3.4.1 Periodic orbits . . . 22
2.3.4.2 Bifurcation analysis . . . 26
2.4 Summary and Outlook . . . 29

3 A geometric analysis of the SIRS epidemiological model on a homogeneous network **33**
3.1 Introduction . . . 33
3.2 Formulation of the SIRS model on a network . . . 34
3.2.1 The model . . . 35
3.2.2 Moment closures . . . 37
3.3 Analysis of the model . . . 38
3.3.1 Fast-slow model . . . 38
3.3.2 Fast limit . . . 41
3.3.3 Equilibria of the perturbed system . . . 45
3.3.4 Slow manifold . . . 46
3.3.5 Rescaling . . . 47
3.3.6 Entry-exit function . . . 50
3.3.7 Application of the entry-exit formula to the parabola . . . 51
3.4 Bifurcation analysis and numerical simulations . . . 53
3.5 Summary and Outlook . . . 58

4 Bibliography **59**

Acknowledgements

Firstly, I would like to express my sincere gratitude to my advisor Prof. Andrea Pugliese, for his expert and wise guidance, for the constant and precise supervision, and for his limitless patience over the course of my Ph.D. studies. I sincerely hope we will continue working together in the future. Moreover, I want to thank the reviewers, Prof. Mathieu Desroches and Prof. Stephen Schecter, for their precious feedback on the content of this thesis.

Secondly, I wholeheartedly thank Prof. Hildeberto Jardón-Kojakhmetov and Prof. Christian Kuehn for the opportunity to study and work with them in the months I have spent in München, and the following year and a half. Our collaboration fundamentally shaped my thesis, and directed my main research over the last two years. Moreover, I am grateful to Prof. Tommaso Lorenzi, for a prolonged but ultimately rewarding joint effort, the result of which unfortunately is not included in this thesis.

Thirdly, I would like to thank all my fellow Ph.D. students at the University of Trento, in particular Nicolò Cangiotti, Marco Capolli, Claudia De Lazzari and Sara Sottile, for their friendship and encouragement during the time we spent together in Trento.

Fourthly, I must acknowledge all my friends from Padova, Amsterdam and Trento, now scattered throughout Europe: Maddalena Barbari, Roberto Bocchi, Carlo Borriello, Filippo Canevarolo, Luca Colombi, Claudio Corbellini, Giovanni Di Salvo, Vittoria Fiore, Marco Fraccaroli, Pietro Frazzarin, Arianna Gardellin, Franco Guida, Reka Kadar, Leonardo Lerer, Daniele Mammi, Francesco Marzola, Casper Oelen, Giovanni Righetto, Riccardo Rizzo, Michele Stecconi, Francesco Torelli, Sofia Zambelli and everybody I most likely forgot to name.

Lastly, I would like to thank my family, for the continuous interest in my work and, more importantly, my well-being; and Eva, for her love and support over the last several months: I would not have survived the quarantine without her.

1. Introduction

This thesis is rooted in the extremely broad field of mathematical epidemiology. More precisely, in the two main chapters we provide an analysis of multiple mathematical models of infectious diseases, under the characteristic assumption that the mechanisms involved evolve on time scales which differ by many orders of magnitude. As we will explain shortly, such an assumption is of interest, and justified, in this and various other contexts.

Multiple time scales are extremely common in natural phenomena; instances of time scales separation are present in engineering, ecology, chemistry, celestial mechanics, and many more fields [30, 51]. The study of such phenomena has been tackled through various methods of singular perturbation, which eventually evolved in the branch of mathematics which is now called Geometric Singular Perturbation Theory, or GSPT, as we will denote it throughout this introduction.

The fundamental idea of GSPT is the use of a small quantity, possibly originating from the ratio of the time scales involved, as a perturbation parameter. The pioneering paper by Fenichel [20] is often considered to be the foundation stone of GSPT, although perturbed systems had been studied for decades already.

Indeed, in the vast field of perturbed systems, we must mention the works of Tikhonov, Levinson, Hoppensteadt and Friedrichs & Wasow. We briefly recall the contributions to the theory these five authors made.

Tikhonov's main result in this field, also known as Tikhonov's theorem, regards systems of the form

$$\begin{aligned} \frac{\mathrm{d}x}{\mathrm{d}t} &= f(x,z,t), \\ \mu\frac{\mathrm{d}z}{\mathrm{d}t} &= g(x,z,t), \end{aligned} \tag{1.1}$$

where $0 < \mu \ll 1$ is a small parameter, $x = x(t) \in \mathbb{R}^m$, $z = z(t) \in \mathbb{R}^n$, with $m, n \geq 1$, f and g are functions of class $\mathcal{C}^k$, with k as large as needed. If we let $\mu \to 0$, system (1.1)becomes

$$\begin{aligned} \frac{\mathrm{d}x}{\mathrm{d}t} &= f(x,z,t), \\ z &= \phi(x,t), \end{aligned} \tag{1.2}$$

with $z = \phi(x,t)$ a solution of $g(x,z,t) = 0$. We define the so-called "adjoined system"

$$\frac{\mathrm{d}z}{\mathrm{d}t} = g(x,z,t), \tag{1.3}$$

where both x and t are considered parameters. In this setting, in 1952, Tikhonov proved that, on a finite interval $t \in (0,T]$, solutions of system (1.1) tend to corresponding solutions of system (1.2) as $\mu \to 0$, under the assumption that $z = \phi(x,t)$ is a stable root of system (1.3).

In 1950, Levinson published a paper [57] regarding a different kind of perturbed system, namely

$$\frac{\mathrm{d}x}{\mathrm{d}t} = f\frac{\mathrm{d}u}{\mathrm{d}t} + \varphi, \quad \epsilon\frac{\mathrm{d}^2u}{\mathrm{d}t^2} + g\frac{\mathrm{d}u}{\mathrm{d}t} + h = 0, \tag{1.4}$$

where f, φ, g and h are all regular enough functions of $x \in \mathbb{R}^n$, and u, t and ϵ, which are, instead, all scalar.
Taking the limit as $\epsilon \to 0$ in system (1.4), we obtain

$$\frac{\mathrm{d}y}{\mathrm{d}t} = f\frac{\mathrm{d}v}{\mathrm{d}t} + \varphi, \quad g\frac{\mathrm{d}v}{\mathrm{d}t} + h = 0, \tag{1.5}$$

where the variables were renamed for ease of notation.
Fix a starting time $t_0 = \alpha$; under some closeness assumptions between $x(\alpha)$ and $y(\alpha)$, $u(\alpha)$ and $v(\alpha)$, $\frac{\mathrm{d}u}{\mathrm{d}t}(\alpha)$ and $\frac{\mathrm{d}v}{\mathrm{d}t}(\alpha)$, Levinson proved that the solutions of systems (1.4) and (1.5) remain close for any finite interval $t \in [\alpha, \beta]$, for any $\alpha < \beta < +\infty$, for ϵ small enough. We refer to [57] for the precise formulation of this theorem and its proof.

Hoppensteadt, in his 1966 paper [34], extended Tikhonov's results on closeness of the orbits for systems of the form

$$\begin{aligned} x' &= f(t, x, y, \epsilon), \\ \epsilon y' &= g(t, x, y, \epsilon) \end{aligned}$$

to unbounded intervals $t \in [\alpha, \infty)$.

Lastly, we recall a paper by Friedrichs and Wasow, which predates the three cited so far. In their 1946 paper [21], the authors analysed another specific class of systems of ODEs of the form

$$\begin{aligned} X_i' &= F_i(X_1, \ldots, X_n), \quad i = 1, 2, \ldots, n-1 \\ \epsilon X_n' &= F_n(X_1, \ldots, X_n), \end{aligned} \tag{1.6}$$

giving conditions on the $\epsilon \to 0$ limit system under which system (1.6) admits periodic orbits.

In a series of papers written and published in the 1970s, Fenichel then proposed his main contribution, in the form of two theorems. He studied systems in a form identical to the ones studied by Tikhonov, with a slightly different notation. Namely,

$$\begin{aligned} x' &= \epsilon f(x, y, \epsilon), \\ y' &= g(x, y, \epsilon), \end{aligned} \quad \text{equivalent, for } \epsilon > 0, \text{ to} \quad \begin{aligned} \dot{x} &= f(x, y, \epsilon), \\ \epsilon\dot{y} &= g(x, y, \epsilon), \end{aligned} \tag{1.7}$$

where from the leftmost system to the rightmost one we simply rescale the time from τ, the so-called *slow time variable*, to $t = \tau/\epsilon$, the *fast time variable*. The prime and the overdot indicate, respectively, the derivative with respect to τ and t. In general, $x \in \mathbb{R}^l$, $y \in \mathbb{R}^m$, $0 < \epsilon \ll 1$, and f and g sufficiently regular.
Systems (1.7) are said to be in *standard form*, because the variables x are globally slow (notice the small parameter multiplying their derivatives), whereas the variables y are globally fast.
The two systems correspond to two distinct limit systems as $\epsilon \to 0$, namely

$$\begin{aligned} x' &= 0, \\ y' &= g(x, y, 0), \end{aligned} \quad \text{and} \quad \begin{aligned} \dot{x} &= f(x, y, 0), \\ 0 &= g(x, y, 0), \end{aligned} \tag{1.8}$$

called the *layer equation* and the *reduced system*, respectively. In the layer equation, the variables x do not evolve in time, as they remain constant, and are considered parameters upon whose variation the fast dynamics of y may change as well. The manifold described by the equation $g(x, y, 0) = 0$ is the *critical manifold*, and it is of fundamental importance; we denote it with $\mathcal{C}_0$.

In this setting, Fenichel proved two theorems.
Suppose there exists an m-dimensional compact submanifold $\mathcal{M}_0$, possibly with boundary, contained in $\mathcal{C}_0$. Moreover, the manifold $\mathcal{M}_0$ is assumed to be *normally hyperbolic*, meaning that the eigenvalues of the Jacobian $\mathrm{D}_x f(x, y, 0)|_{\mathcal{M}_0}$ are bounded away from the imaginary axis.
With such assumptions, the first theorem states that the submanifold $\mathcal{M}_0$ "survives" the perturbation, assuming ϵ is "small enough". This means that there exists a manifold $\mathcal{M}_\epsilon$, *locally invariant* under the flow of (1.7), which is $\mathcal{O}(\epsilon)$ close, and diffeomorphic, to $\mathcal{M}_0$. Local invariance means that trajectories may enter or leave $\mathcal{M}_\epsilon$ only through its boundary.
The second theorem regards the corresponding stable and unstable manifolds of $\mathcal{M}_0$, which are proved to survive the perturbation in a similar fashion. We refer to [51, 30, 40] for more recent and in-depth treatises on Fenichel theory. However, we will give a more formal introduction to the subject in Section 2.2.

The presence of parameters differing by many orders of magnitudes from one another is surprisingly common in real-world scenarios, and they often give rise to rich dynamics. Indeed, Fenichel's theory was applied to famous models such as the FitzHugh-Nagumo equation [51], Van der Pol oscillator [24, 83], and to many other models of phenomena such as enzyme reactions [62, 28], pattern formation [30], etc. However, as often happens in mathematical biology, the systems analysed might not be in the standard form (1.7). Instead, they are presented in the non-standard form

$$\begin{aligned} x' &= f(x, y, \epsilon), \\ y' &= g(x, y, \epsilon), \end{aligned} \quad \text{or, in short,} \quad z' = H(z, \epsilon), \tag{1.9}$$

in which no variable is *globally* fast or slow with respect to the other, but only locally near critical sets of the phase space. This is the case of all the systems studied in this thesis, and the main focus of the recent treatise [86]. Moreover, the normal hyperbolicity assumption is often not satisfied on the whole critical manifolds, and points or sets of non-hyperbolicity must be treated carefully through more specialized analysis techniques.

In particular, the study of the simpler limit systems (1.8) is used to deduce information on the original perturbed system. We refer to Section 2.2 of this thesis for a slightly longer introduction to the subject, and to one specific, fundamental tool for our analysis: namely, the *entry-exit function*, also known in literature as way-in/way-out function [49], or Pontryagin delay [67].

Mathematical epidemiology is, now more than ever, an extremely important field, with evident and critical applications to real-world scenarios: a deep insight in the dynamics of infectious diseases is fundamental to formulate control responses and prevention strategies to epidemics.

Over the last century, many different approaches have been chosen to try to balance the trade-off between realism and complexity in epidemics modeling. The most famous and quoted paper dates back to 1927 [44], in which an SIR (Susceptible – Infected – Recovered) compartment model was described through the use of renewal equations. The mathematical literature regarding epidemics modelling has expanded considerably in the following decades, considering different models and various techniques, including but not limited to the use of ODEs, PDEs, SDEs, and analytical and numerical exploration of diseases spreading on various kinds of networks.

In particular, in this thesis we focus on compartmental models, expressed as systems of singularly perturbed ODEs, which include the possibility of loss of immunity (*i.e.*, the flow of individuals from the R compartment to the S compartment).

There are multiple real-life diseases characterized by parameters which differ by several orders of magnitudes [11, 43, 55, 70], *e.g.* the duration of infection vs. life expectancy, demographic turnover or immunity window; this hypothesis was assumed in [2, 76]. This difference gives rise to a separation of the phenomena involved into slow and fast ones, and this separation properly motivates the study of such diseases through GSPT [70, 73]. The rigorous application of GSPT

to epidemics models is still a relatively untrod path; however, we stress the contribution given in particular by [70], which was part of the inspiration of the works contained in this thesis, and [7, 29, 73, 85, 90]. The models we decided to study are of particular interest in the study of compartment epidemics models: apart from the well-known SIR model, we focused on the SIRS model (*i.e.*, a model in which it is possible to lose immunity, and flow from the R compartment to the S compartment) and on the SIRWS model. Both allow for loss of immunity, and the SIRWS model in particular introduces a compartment for individuals with "waning immunity": these are individuals who still have partial immunity to the disease, but are on their way to losing it; indeed, unless they encounter an Infected individual, which would boost their immunity and move them back to the R compartment, these individuals would eventually lose their immunity entirely, and become Susceptible again. Pertussis seems to be well modelled by this type of scheme; varicella infection has apparently a similar behaviour, where however individuals do not become susceptible to reinfection but to virus reactivation (zoster disease).

The research contained in this thesis aims at providing a novel point of view in the analysis of compartmental epidemic models, exploiting an hypothesis of time scale separation. Such an hypothesis, which as we said finds confirmation in different real world cases [10, 11, 55, 88], allows us to characterize the asymptotic behaviour of the underlying compartment models. In particular, we propose a geometric argument which reveals, with the aid of numerical simulations, whether a system will converge towards an (endemic) equilibrium, or it will be characterized by (un)stable limit cycles. This technique is particularly useful in high dimensional systems, for which analysis is harder, and which are often extremely stiff: our geometrical argument splits the perturbed model into its two limit systems, which instead are not stiff.

The main body of this thesis consists of two papers, the first accepted by the journal *Nonlinear Analysis: Real World Applications*, soon to appear in their April 2021 issue; the second submitted to *Journal of Mathematical Biology*, awaiting review. Both papers were co-authored with Hildeberto Jardón-Kojakhmetov, Christian Kuehn and Andrea Pugliese.

The first paper, which constitutes the first chapter of this thesis, studies, with tools from GSPT, three distinct compartment models, namely SIR with demography, SIRS without demography, and SIRWS (the "W" standing for "waning immunity") with demography. After the theoretical analysis, the results are complemented by bifurcation analysis; moreover, the main numerical geometrical argument is introduced and explained.

The second paper is a natural generalization of the SIRS model studied in the first one, and is contained in the second chapter of this thesis. The introduction of the network structure brings some more realism to the model, by dropping the homogeneous mixing hypothesis and allowing each individual to have contacts, which potentially spread the infection, with a finite number of "neighbors". In particular, this specific network structure is used to obtain, through the so-called pair approximation, a system of ODEs. This additional depth in the model unveils asymptotic behaviours which were not possible in the homogeneous mixing settings, namely convergence of the system towards stable limit cycles.

This thesis contains the main results we have reached over the course of my Ph.D. years. Throughout our analysis we found numerous unexplored paths and prompts, which we believe can lead to a significant amount of additional research; hence, we end both chapters with possible outlooks for future works.

2. A geometric analysis of the SIR, SIRS and SIRWS epidemiological models

2.1 Introduction

Epidemic modelling has grown from the pioneering 1927 article by Kermack and McKendrick [44] into a wide body of theory and applications to several diseases [1, 32, 42, 16, 63], used also for developing appropriate control strategies.

The model by Kermack and McKendrick [44], formulated as renewal equations, was of S-I-R type, meaning that individuals are classified as *Susceptibles* (S), *Infected* (I) or *Recovered* (R), and that the only possible transitions are $S \to I$ (new infection) and $I \to R$ (recovery with permanent immunity). As that model does not consider new births or deaths (other than because of the disease), it is appropriate for an epidemic that develops on a time-scale much faster than demographic turn-around. The epidemic SIR model was extended by Soper [77] and by Kermack and McKendrick [45] in a second paper, in which they allowed for immigration, reproduction and reinfection, arriving to the so-called SIR endemic model, that has been extensively analysed in the following decades [31], especially to investigate how to explain the apparent periodicities in the notifications of childhood diseases [76, 43]. The SIR endemic model can be seen as the basis, over which more complex and realistic models have been built.

The difference in time-scales between epidemic spread and demographic turnaround has been observed by several authors. Smith [76] introduced a small parameter ϵ as the ratio between the average lengths of the infection period and of life; he proved that, if the contact rate is a sinusoidal function of period 1 and ϵ is sufficiently small, a subharmonic bifurcation of a 2-periodic stable positive solution can occur. Andreasen [2] showed that, for ϵ small enough, the endemic equilibrium is always stable in a certain class of age-dependent SIR models. Diekmann, Heesterbeek and Britton [16] have exploited the fact that ϵ is a small parameter in an informal argument about the minimum community size in which a measles-like infection can persist. However, to our knowledge very few authors have systematically used geometric singular perturbation theory as a tool to investigate properties of epidemic models. We only know of the paper by Rocha *et al.* [70] that used singular perturbation methods for the analysis of a SIRUV model for a vector-borne epidemic, and we have recently been informed of [58].

Our main objective in this chapter is to show that under certain assumptions of the system parameters (namely the transition rates between states), tools from Geometric Singular Perturbation Theory (GSPT) are suitable to describe the intricate dynamics that such models exhibit due to the presence of multiple time scales.

The first part of the chapter is devoted to the classical SIR and SIRS epidemic models, that

we analyse in the limiting case of $\epsilon \to 0$. For such models, it is well known that, when $R_0 > 1$, there exists a unique endemic equilibrium, which is globally asymptotically stable.

The SIRS model analysed previously consists in a system of ODEs, in which individuals are assumed to switch from totally immune to totally susceptible. A more complex and insightful approach has been recently proposed by Breda *et al.* [8]. In the second part, we instead consider a model, named SIRWS, introduced for pertussis in [55], and partially analysed in [11]. In the model it is assumed that immunity wanes in two stages: after recovering from infection individuals are totally immune, but then immune memory starts to fade: if they are challenged by the pathogen when they are in the stage of partial immunity, they recover a complete immunity; otherwise, they completely lose immunity, and re-enter the susceptible stage. A distinction between fully and partially immune individuals was also studied, with a different modelling approach, in [78]. A large difference generally exists between the lengths of the infection period and of the period of temporary immunity; see, for instance the studies on the loss of vaccine-induced immunity [10, 88]). Thus we will assume a time-scale difference between recovery rate and the rate of immunity loss.

Our main results can be summarized as follows:

- For the fast-slow SIR and SIRS models we capture the transient behaviour from an initial introduction of the infection, and show that, when $R_0 > 1$, the dynamics leads, in the slow time-scale, to a neighbourhood of the endemic equilibrium, see Sections 2.3.1 and 2.3.3. Then convergence to the equilibrium can be established by local methods.

- For the fast-slow SIRWS model, in particular, we confirm the result obtained numerically in [11] that stable periodic epidemic outburst can exist. Moreover, we give a detailed description of the system parameters for which such behaviour occurs and the corresponding time scales involved, see Section 2.3.4.

Our mathematical analysis is largely based on GSPT, see more details in Section 2.2.

In such a context, it is worth mentioning that the models we study are not immediately, nor globally, in a standard singularly perturbed form, but in each model the fast-slow decomposition appears only in specific regions of the phase space, similarly to what is considered in e.g. [48, 53, 38]; see in particular the recent treatise [86], in which a thorough exploration of singular perturbation problems beyond the standard form is available. As it is usually the case in such biological models, the main difficulty for analysis is due to the loss of normal hyperbolicity of the critical manifold. To overcome this obstacle, we use here the so called entry-exit function, as presented by De Maesschalck and Schecter [13], which gives details regarding the behaviour of an orbit in regions where the critical manifold changes its stability properties. Moreover, for the modified SIRWS system we present a combination of analytical and numerical studies regarding the dependence of the dynamics with respect to some of the parameters, and compare our results with the ones obtained in [11]. In particular, we focus on the interplay between life expectancy (or birth/death rate) and boosting rate, and on how different values of these parameters can give rise to damped or sustained oscillations. Finally, the novelty of our analysis is not confined to the usage of GSPT in the context of the well-known SIR model, but we also show that our techniques can be potentially used in higher dimensional systems (as the SIRWS model). This is rather important since the well-studied SIR and SIRS models often depend on Lyapunov's method to show stability of trajectories [66], and it is known that Lyapunov functions are difficult to obtain. Our GSPT analysis does not require global Lyapunov functions.

The remainder of this chapter is arranged as follows: in Section 2.2 we provide some necessary mathematical preliminaries which will be later used for the analysis of the models. Afterwards, we

present in Section 2.3 the mathematical analysis of the SIR, SIRS, and the SIRWS epidemiological models. We finish in Section 2.4 with a summary and an outlook of open-problems regarding modelling and analysis of epidemiological models with fast-slow dynamics.

2.2 Preliminaries

In the main part of this chapter we study three compartment models whose dynamics evolve at distinct time scales. Therefore, we now provide a brief description of Geometric Singular Perturbation Theory (GSPT), and in particular of the entry-exit function [13], which is fundamental in our analysis.

2.2.1 Fast-slow systems

The term "fast-slow systems" is commonly used to model phenomena which evolve on two (or more) different time scales [4, 51]. Often such behaviour can be described by a singularly perturbed ordinary differential equation (ODE), that is

$$\begin{aligned} \epsilon \dot{x} &= f(x, y, \epsilon), \\ \dot{y} &= g(x, y, \epsilon), \end{aligned} \tag{2.1}$$

where $x = x(\tau) \in \mathbb{R}^m$, $y = y(\tau) \in \mathbb{R}^n$, with $m, n \geq 1$, are the fast and slow variables respectively, f and g are functions of class $\mathcal{C}^k$, with k as large as needed, and $0 < \epsilon \ll 1$ is a small parameter which gives the ratio of the two time scales. Here the overdot $(\dot{})$ indicates $\frac{\mathrm{d}}{\mathrm{d}\tau}$. The system (2.1) is formulated on the *slow time* scale τ. When studying fast-slow systems we often define a new *fast time* $t = \tau/\epsilon$ with which (2.1) can be rewritten as

$$\begin{aligned} x' &= f(x, y, \epsilon), \\ y' &= \epsilon g(x, y, \epsilon), \end{aligned} \tag{2.2}$$

where now the prime $(\,')$ indicates $\frac{\mathrm{d}}{\mathrm{d}t}$. Clearly, since we simply rescaled the time variable, systems (2.1) and (2.2) are equivalent for $\epsilon > 0$.

Fast-slow systems given by (2.1)-(2.2) are said to be *in standard form*. In a more general context, it is possible to have a fast-slow system given by

$$z' = F(z, \epsilon), \tag{2.3}$$

where the time scale separation is not explicit. In fact, many biological models [48, 53], among others, and in particular the models we study in this thesis are in such non-standard form.

The main idea of GSPT is to consider (2.1)-(2.2) in the limit $\epsilon \to 0$ and then use perturbation arguments to describe the dynamics of the full fast-slow system. The motivation behind this strategy is that one expects that the analysis of the limit systems ($\epsilon = 0$) is simpler compared to the analysis of (2.1)-(2.2) with $\epsilon > 0$.

Taking the limit $\epsilon \to 0$ in systems (2.1) and (2.2) yields, respectively

$$\begin{aligned} 0 &= f(x, y, 0), \\ \dot{y} &= g(x, y, 0), \end{aligned} \tag{2.4}$$

and

$$\begin{aligned} x' &= f(x, y, 0), \\ y' &= 0, \end{aligned} \tag{2.5}$$

where (2.4) is called *reduced subsystem* (or *slow subsystem*), and (2.5) is called *the layer equation* (or *fast subsystem*). We note that the reduced subsystem describes a dynamic evolution constrained to the set

$$\mathcal{C}_0 = \{x \in \mathbb{R}^m, y \in \mathbb{R}^n \mid f(x, y, 0) = 0\},$$

which is called the *critical manifold*. On the other hand, we note that $\mathcal{C}_0$ defines the set of equilibrium points of the layer equation. See for example [3, 56] for techniques to approximate and estimate such a manifold.

Fenichel's theorems, which are the basis of GSPT, require certain assumptions on $\mathcal{C}_0$. Namely, we suppose there exists an n-dimensional compact submanifold $\mathcal{M}_0$, possibly with boundary, contained in $\mathcal{C}_0$. Moreover, the manifold $\mathcal{M}_0$ is assumed to be *normally hyperbolic*, meaning that the eigenvalues of the Jacobian $\mathrm{D}_x f(x, y, 0)|_{\mathcal{M}_0}$ are bounded away from the imaginary axis. In such a setting, the following can be proved (see [20]):

Theorem 2.2.1. *For $\epsilon > 0$ sufficiently small, there exists a manifold $\mathcal{M}_\epsilon$, called* slow manifold*, which lies $\mathcal{O}(\epsilon)$ close to $\mathcal{M}_0$, is diffeomorphic to $\mathcal{M}_0$ and is locally invariant under the flow of (2.2).*

We note that the manifold $\mathcal{M}_\epsilon$ is usually not unique, but all the possible choices lie $\mathcal{O}(\epsilon^{-K/\epsilon})$-close to each other, for some $K > 0$. Therefore, in most cases the choice of slow manifold $\mathcal{M}_\epsilon$ does not change the analytical and numerical results.

With the usual definitions for stable and unstable manifolds (see, for example, equations (6.3) in [51])

$$W^{\mathrm{s}}(\mathcal{M}_0) = \{(x, y) : \phi_t(x, y) \to \mathcal{M}_0 \text{ as } t \to +\infty\},$$
$$W^{\mathrm{u}}(\mathcal{M}_0) = \{(x, y) : \phi_t(x, y) \to \mathcal{M}_0 \text{ as } t \to -\infty\},$$

where ϕ_t denotes the flow of system (2.5), Fenichel's second theorem ensures that $W^{\mathrm{s}}(\mathcal{M}_0)$ and $W^{\mathrm{u}}(\mathcal{M}_0)$ persist under perturbation as well:

Theorem 2.2.2. *For $\epsilon > 0$ sufficiently small, there exist manifolds $W^{\mathrm{s}}(\mathcal{M}_\epsilon)$ and $W^{\mathrm{u}}(\mathcal{M}_\epsilon)$ which lie $\mathcal{O}(\epsilon)$ close to and are diffeomorphic to $W^{\mathrm{s}}(\mathcal{M}_0)$ and $W^{\mathrm{u}}(\mathcal{M}_0)$ respectively, and are locally invariant under the flow of (2.2).*

However, local invariance does not imply the same strong property of $W^{\mathrm{s}}(\mathcal{M}_0)$ for $W^{\mathrm{s}}(\mathcal{M}_\epsilon)$, as trajectories might leave the latter as t increases, through its boundary.

In practical terms, Fenichel's theorems show that for $\epsilon > 0$ sufficiently small, the dynamics of (2.1)-(2.2) are a regular perturbation of the limit dynamics (2.4)-(2.5) within a small neighbourhood of the critical manifold.

When the manifold $\mathcal{M}_0$ is not normally hyperbolic, some more advanced tools, such as the *blow-up method* (see [37]), may need to be invoked. All of the systems we analyse below have one non-hyperbolic point in the biologically relevant region. Thus, in order to describe the relevant dynamics we need to use extra techniques besides Fenichel's theorems. Due to the properties of the models to be studied, it turns out that the *entry-exit function* [12, 13] is suitable.

2.2.2 Entry-exit function

The entry-exit function gives, in the form of a Poincaré map between two sections in phase space, an estimate of the behaviour of the orbits near the point in which the critical manifold changes stability (from attracting to repelling), in a class of singularly perturbed systems. Intuitively, the result can be interpreted as a "build up" of repulsion near the repelling part of the slow

manifold, which needs to compensate the attraction which was built up near the attracting part before the orbit can leave an $\mathcal{O}(\epsilon)$ neighbourhood of the critical manifold.

More specifically, this construction applies to systems of the form

$$\begin{aligned} x' &= f(x, y, \epsilon)x, \\ y' &= \epsilon g(x, y, \epsilon), \end{aligned} \tag{2.6}$$

with $(x, y) \in \mathbb{R}^2$, $g(0, y, 0) > 0$ and $\text{sign}(f(0, y, 0)) = \text{sign}(y)$. Note that for $\epsilon = 0$, the y-axis consists of normally attracting/repelling equilibria if y is negative/positive, respectively.

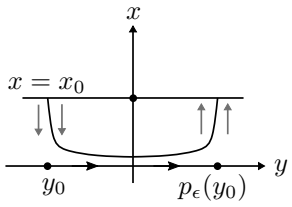

Figure 2.1: Visualization of the entry-exit map on the line $x = x_0$

Consider a horizontal line $\{x = x_0\}$. An orbit of (2.6) that intersects such a line at $y = y_0 < 0$ (entry) re-intersects it again (exit) at $y = p_\epsilon(y_0)$, as sketched in Figure 2.1. De Maesschalck [12] shows that, as $\epsilon \to 0$, the image of the return map $p_\epsilon(y_0)$ to the horizontal line $x = x_0$ approaches $p_0(y_0)$ given implicitly by

$$\int_{y_0}^{p_0(y_0)} \frac{f(0, y, 0)}{g(0, y, 0)} \mathrm{d}y = 0. \tag{2.7}$$

In the following sections, the entry-exit function p_0 plays a crucial role in the analysis of three different epidemiological models. In particular, the analysis of the SIRWS model relies on a multi-dimensional version of the entry-exit map, provided in a recent paper by Hsu and Ruan [35].

2.3 Analysis of the SIR, SIRS and SIRWS models

In this section we analyse three different epidemiological models, giving a short interpretation of the equations and then proceeding to use the techniques of GSPT, especially the entry-exit function, to deduce information about the behaviour of each one.

2.3.1 SIR model

We consider a SIR compartment model (presented in a similar form in [32]) as depicted in Figure 2.2 and with corresponding equations given as in (2.8)

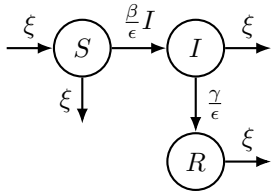

$$\begin{aligned}\dot{S} &= \xi - \xi S - \frac{\beta}{\epsilon} SI,\\ \dot{I} &= \frac{\beta}{\epsilon} SI - \frac{\gamma}{\epsilon} I - \xi I,\\ \dot{R} &= -\xi R + \frac{\gamma}{\epsilon} I,\end{aligned} \tag{2.8}$$

Figure 2.2: Flow diagram for (2.8).

where $S(\tau)$, $I(\tau)$, $R(\tau)$ denote the susceptible, infected and recovered proportion of the population respectively. Since the (S, I, R) variables represent fractions of a population, they are assumed to be non-negative for all $\tau \geq 0$. Observe that the non-negative octant of $\mathbb{R}^3$, to be denoted by $\mathbb{R}^3_{\geq 0}$, and in particular the set $\left\{(S, I, R) \in \mathbb{R}^3_{\geq 0} \mid 0 \leq S + I + R \leq 1\right\}$, are invariant under the flow of (2.8).

The parameter ξ in (2.8) refers to the birth rate and is assumed to be equal to the death rate. Furthermore, as depicted in Figure 2.2, we also assume that all individuals are born susceptible. Similarly, the parameters $\tilde{\beta} = \beta/\epsilon$ and $\tilde{\gamma} = \gamma/\epsilon$ are, respectively, the contact rate and the recovery rate of infectious individuals. In our analysis the parameters ξ, β and γ are of order $\mathcal{O}(1)$. Note that we introduce a small positive parameter $0 < \epsilon \ll 1$, which gives rise to the difference in magnitude between the large infection rate β/ϵ, the large recovery rate γ/ϵ and the birth/death rate. Such a difference represents a highly contagious disease with a short infection period.

Remark 1. *We notice that the total population $N := S + I + R$ in system (2.8) is governed by the ODE $\dot{N} = \xi(1 - N)$; hence, the total population converges exponentially fast to 1.*

As stated above, $S(\tau)$, $I(\tau)$ and $R(\tau)$ represent proportions of the population. Consistently the plane $\{S + I + R = 1\}$ is invariant for system (2.8) . Hence, we can assume $R = 1 - S - I$, which allows us to reduce (2.8) to

$$\begin{aligned}\dot{S} &= \xi - \xi S - \frac{\beta}{\epsilon} SI,\\ \dot{I} &= \frac{\beta}{\epsilon} SI - \frac{\gamma}{\epsilon} I - \xi I.\end{aligned} \tag{2.9}$$

By rescaling time, system (2.9) can also be written as

$$\begin{aligned}S' &= \epsilon\xi(1 - S) - \beta SI,\\ I' &= I(\beta S - \gamma - \epsilon\xi).\end{aligned} \tag{2.10}$$

We briefly recall definitions (3.1) and (3.2) from [86].

Definition 1. *Consider a perturbed system of n ODEs of the form*

$$z' = H(z, \epsilon) = h(z) + \epsilon G(z, \epsilon). \tag{2.11}$$

We call system (2.11) regular *if the set*

$$S_0 := \{z \in \mathbb{R}^n | H(z, 0) = h(z) = 0\}$$

is empty, or consists of isolated singularities. We call it singular *otherwise, and S_0 is then the critical manifold of system (2.11).*

Note that system (2.10) is a fast-slow singular system, which is not in the standard form (2.2), as it often occurs in biological models [48, 53, 86]. Later we perform a convenient rescaling that brings (2.10) into a standard form.

The corresponding critical manifold is the set $\mathcal{C}_0 = \{(S, I) \in \mathbb{R}^2 \,|\, I = 0\}$, and the slow flow along it is given by $S' = \xi(1 - S)$, which implies flow towards the point $S = 1$. In the $\epsilon \to 0$ limit, we recover from (2.10) the basic dynamics for the (S, I) couple in a standard SIR system (see [32]), namely

$$\begin{aligned} S' &= -\beta SI, \\ I' &= I(\beta S - \gamma). \end{aligned} \tag{2.12}$$

In particular, it follows from linearization of (2.12) along $\mathcal{C}_0$ that the critical manifold is attracting for $S < \frac{\gamma}{\beta}$, repelling for $S > \frac{\gamma}{\beta}$, and loses normal hyperbolicity at $S = \frac{\gamma}{\beta}$.

It is well known [33] that the basic reproduction number R_0^ϵ for system (2.10) is equal to $\frac{\beta}{\gamma+\epsilon\xi}$. From here on, we assume that its limiting value $R_0 = \beta/\gamma$ satisfies $R_0 > 1$. This implies that the disease is able to spread through the population, at least for ϵ small enough. In particular, as stated in the well known next Lemma [33, 44], the previous assumption implies that, for every initial condition $S(0) = S_0 > 1/R_0$, there exists a unique $S_\infty < 1/R_0$ such that a trajectory of (2.12) with initial conditions (S_0, I_0) converges towards $(S_\infty, 0)$ as $t \to +\infty$.

Lemma 1. *$\Gamma(S, I) = \gamma \ln(S) - \beta(S + I)$ is a constant of motion for system (2.12); all the orbits of the system in the first quadrant are heteroclinic to two points on the S-axis.*

Proof. By direct derivation with respect to time, we see that

$$\Gamma' = -\gamma\beta I - \beta SI + \beta SI + \gamma\beta I = 0.$$

Moreover, all the equilibria of system (2.12) belong to $I = 0$, i.e. the S-axis; they are attracting for $S < \frac{\gamma}{\beta}$, repelling for $S > \frac{\gamma}{\beta}$. We notice that

$$\frac{\mathrm{d}I}{\mathrm{d}S} = -1 + \frac{\gamma}{\beta S},$$

which implies that I is increasing if $S > \frac{\gamma}{\beta}$, and decreasing otherwise.
Finally, (2.12) is topologically equivalent, for $I > 0$, to the linear system

$$\begin{aligned} S' &= -\beta S, \\ I' &= \beta S - \gamma, \end{aligned}$$

which can be easily integrated to show heteroclinic orbits. □

From Lemma 1 we define $S_\infty \in (0, \frac{1}{R_0})$ to be the unique non-trivial solution of the equation $\Gamma(S, 0) = \Gamma(S_0, 0)$ where $S_0 > \frac{1}{R_0}$.

For future use, let us define the map

$$\Pi_1 : \{S \in (1/R_0, 1]\} \to \{S \in (0, 1/R_0)\} \tag{2.13}$$

that maps S_0 into S_∞, and which is induced by the flow of (2.12), or is equivalently given by Γ.

So far, we know that the solutions of (2.10) away from the critical manifold are close to $\Gamma(S, I)$ as shown in the right side of Figure 2.3. Therefore, the next step is to focus on a small region close to $\mathcal{C}_0$. That is, for the analysis that follows, we assume I to be $\mathcal{O}(\epsilon)$-small. In particular, and following Lemma 1, if we choose $I_0 \in \mathcal{O}(\epsilon^2)$, we have an explicit relation (up to a $\mathcal{O}(\epsilon)$ error) between S_∞ and S_0, namely, $\Gamma(S_\infty, 0) \approx \Gamma(S_0, I_0) = \Gamma(S_0, 0) + \mathcal{O}(\epsilon)$.

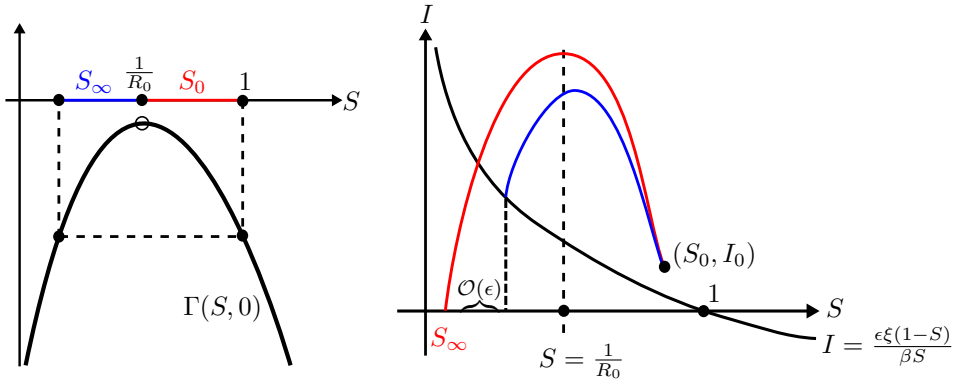

Figure 2.3: Left: function $\Gamma(S,0)$, intersection with horizontal lines give the starting and ending points of a heteroclinic orbit of the layer equation (2.12). Right: qualitative comparison between perturbed and unperturbed SIR systems in fast time scale. In red we show an orbit of (2.12) given by $\Gamma(S,I)=\Gamma(S_0,I_0)$ and in blue a small perturbation of it, the corresponding orbit of (2.10). Notice that $I_0\in\mathcal{O}(\epsilon^2)$.

Considering the signs of the derivatives in the perturbed system (2.10), we see that orbits spiral counterclockwise. Moreover, system (2.10) has a two equilibria, namely $(S,I)=(1,0)$ and one which is $\mathcal{O}(\epsilon)$-close to the point $(1/R_0,0)$, as shown in Figure 2.4, given by $(S,I)=(S_E,I_E):=(\frac{1}{R_0}+\epsilon\frac{\xi}{\beta},\alpha_\epsilon(S_E))$, where

$$\alpha_\epsilon(S)=\frac{\epsilon\xi(1-S)}{\beta S} \tag{2.14}$$

is obtained from the nullcline for S in (2.8). Regular perturbation arguments imply that an orbit of the perturbed system (2.10), starting from a point (S_0,I_0) with $I_0\in\mathcal{O}(\epsilon)$ and $S_0>S_E$, follows $\mathcal{O}(\epsilon)$-closely from below, since the $\mathcal{O}(\epsilon)$ contribution is negative, a level curve of $\Gamma(S,I)$, until it reaches the nullcline of S given by $I=\frac{\epsilon\xi(1-S)}{\beta S}$, as shown on the right half of Figure 2.3, at a point with S coordinate $\mathcal{O}(\epsilon)$-close to S_∞.

It is also well known [33, 66] that the endemic equilibrium (S_E,I_E) is globally asymptotically stable, as stated below.

Theorem 2.3.1. *Consider* (2.10). *All trajectories with initial conditions* $0\le S(0)\le 1$, $0<I(0)\le 1$ *with* $S(0)+I(0)\le 1$ *converge asymptotically towards the (endemic) equilibrium point* (S_E,I_E).

The theorem can be proved using the Lyapunov function

$$L_1(S,I)=S+I-S_E\ln(S)-I_E\ln(I)-C_E, \tag{2.15}$$

with $C_E=S_E+I_E-S_E\ln(S_E)-I_E\ln(I_E)$, together with Lasalle's invariance principle [54]; or with [66, 74]

$$L_2(S,I)=I-I_E-I_E\ln(I/I_E)+\frac{\beta}{2(2\mu+\gamma)}(S+I-S_E+I_E)^2. \tag{2.16}$$

Here we are going to describe how solutions approach the equilibrium, for $\epsilon>0$ small. Once it is shown that solutions are in a neighbourhood of the equilibrium, local methods can be used

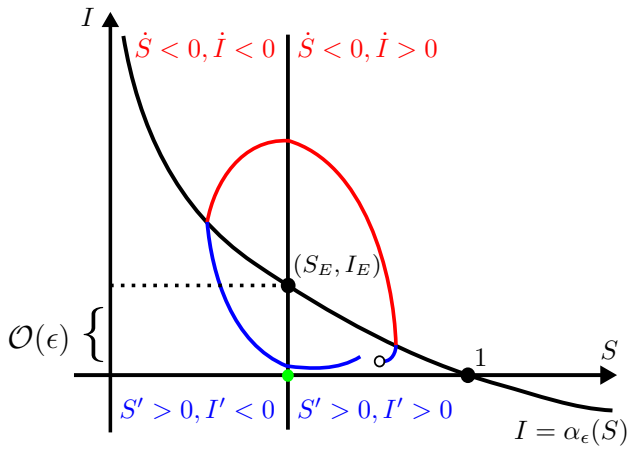

Figure 2.4: Schematic representation of the orbits of (2.10) on the two time scales. Red: fast orbit; blue: slow orbit; green: non-hyperbolic point.

to prove convergence to the equilibrium. Such an approach will be used for the other models as well. Our motivation is to present a method of analysis that does not depend on finding a Lyapunov function, which is, in general, a difficult task.

A convenient step, which is justified by the following Lemma, is to bring (2.10) to a standard form, in order to then apply the entry-exit formula.

Lemma 2. *Consider* (2.10) *and an initial condition* (S_*, I_*) *with* $0 < S_* \leq \frac{\gamma}{\beta} - \Delta < S_E$ *and* $I_* > 0$, *where* $\Delta \in \mathcal{O}(1)$ *and* $I_* \in \mathcal{O}(\epsilon) < \alpha_\epsilon(S_*)$. *Let* $0 < \Delta_1 < \Delta$, $\Delta_1 \in \mathcal{O}(1)$, *and* (S^*, I^*) *denote the point where the corresponding trajectory intersects the line* $\ell = \left\{(S, I) \in \mathbb{R}^2 \,|\, S = \frac{\gamma}{\beta} - \Delta_1\right\}$. *Then, for sufficiently small* $\epsilon > 0$ *we have that* I^* *is exponentially small. Furthermore, the first point at which the trajectory intersects the line* $\pi_\epsilon = \left\{(S, I) \in \mathbb{R}^2 \,|\, I = I_* \epsilon^k\right\}$, *for any* $k \in \mathbb{N}_{\geq 1}$, *satisfies* $S = S_* + O(\epsilon \log(\epsilon))$ *for* $\epsilon \to 0$.

Proof. We first note that the assumption on S_* simply means that S_* is bounded away from S_E uniformly in ϵ. For the proof it is convenient to define new coordinates (S, v) by $(S, I/\epsilon) = (S, v)$. Then (2.10) becomes

$$\begin{aligned} S' &= \epsilon(\xi(1 - S) - \beta S v), \\ v' &= v(\beta S - \gamma - \epsilon\xi). \end{aligned} \tag{2.17}$$

By classical Fenichel theory, a trajectory of (2.17) with initial condition (S_*, v_*) with $S_* < \frac{\gamma}{\beta}$ and $v_* = I_*/\epsilon \in \mathcal{O}(1)$ converges exponentially fast towards and stays $\mathcal{O}(\epsilon)$-close to the S-axis for some time. We know from the reduced system that $S' > 0$ on the critical manifold $I = 0$. Thus, since ℓ is sufficiently away from the non-hyperbolic point S_E, Fenichel's theory also guarantees that the trajectory crosses the line ℓ in a $\mathcal{O}(\epsilon)$ neighbourhood of the critical manifold. Let T denote the (slow) time it takes the trajectory to reach ℓ. During such time, $\beta S - \gamma \leq -\beta\Delta_1 < 0$ and therefore

$$v' \leq -Kv \implies v\left(\frac{T}{\epsilon}\right) \leq v_* e^{-K\frac{T}{\epsilon}} \implies I\left(\frac{T}{\epsilon}\right) \leq \epsilon v_* e^{-K\frac{T}{\epsilon}},$$

with $K = \beta\Delta_1 > 0$.
The last claim follows immediately from $v(t) \leq v_* \epsilon^{-Kt}$. □

Note in particular from Lemma 2 that, before the trajectory intersects ℓ, its corresponding I-coordinate is eventually $\mathcal{O}(\epsilon^2)$, which is what we need for the forthcoming arguments.

2.3.2 Applying the entry-exit function

We are now going to apply the entry-exit formula to describe the way trajectories pass near the non-hyperbolic point $(S, I) = (1/R_0, 0)$.

From Lemma 1 and 2, we can consider an initial point for system (2.10) with $S_0 < 1/R_0$ and $I_0 = \mathcal{O}(\epsilon^2)$. Next, we apply a change of variables defined by

$$S = \frac{u+1}{R_0}, \quad I = \epsilon v, \tag{2.18}$$

which brings the system to the standard form (2.2), with u slow and v fast, that is

$$\begin{aligned} v' &= \gamma(u - \epsilon\xi)v, \\ u' &= \epsilon(\xi(R_0 - u - 1) - \beta v(u+1)). \end{aligned} \tag{2.19}$$

So, using the notation of Section 2.2.2,

$$\begin{aligned} f(v, u, \epsilon) &= \gamma(u - \epsilon\xi), \\ g(v, u, \epsilon) &= \xi(R_0 - u - 1) - \beta v(u+1), \end{aligned} \tag{2.20}$$

which satisfy the hypotheses of the entry-exit function. Indeed, $S < 1$ implies $u < R_0 - 1$, which means $g(0, u, 0) > 0$ in the relevant region. Moreover, $f(0, u, 0) = \gamma u$, which clearly has the same sign as u.

Since $v_0 = I_0/\epsilon = \mathcal{O}(\epsilon)$, we can now apply the entry-exit formula, which gives $p_0(u_0)$ as the only positive solution of

$$\int_{u_0}^{p_0(u_0)} \frac{u}{R_0 - 1 - u} \mathrm{d}u = 0. \tag{2.21}$$

The integral (2.21) can be solved explicitly, giving $p_0(u_0)$ as the positive solution of

$$-p_0(u_0) + u_0 - (R_0 - 1)\ln\left(\frac{R_0 - 1 - p_0(u_0)}{R_0 - 1 - u_0}\right) = 0. \tag{2.22}$$

We now change back to the original (S, I) variables, and introduce, beyond Π_1 defined in (2.13), the map

$$\Pi_2 : \{S \in (0, 1/R_0)\} \to \{S \in (1/R_0, 1)\} \tag{2.23}$$

defined by $\dfrac{p_0(u_0) + 1}{R_0}$, where $u_0 = R_0 S_0 - 1$. Combining together the previous results, we can state the following:

Proposition 1. *Consider the solution of* (2.9) *with an initial condition* $S_0 > 1/R_0$ *and* $I_0 = \mathcal{O}(\epsilon^2)$. *Then the orbit* $\{S_\epsilon(t), I_\epsilon(t),\ t \in [0, T]\}$ *converges for* $\epsilon \to 0$ *to the union of the orbit under the fast flow*

$$\{(S, I) : \Gamma(S, I) = \Gamma(S_0, 0),\ \Pi_1(S_0) \le S \le S_0\}$$

and under the slow flow

$$\{(S, 0) :\ \Pi_1(S_0) \le S \le \Pi_2(\Pi_1(S_0))\}$$

where T *is such that the solution of* $S' = \xi(1 - S),\ S(0) = \Pi_1(S_0)$ *satisfies* $S(T) = \Pi_2(\Pi_1(S_0))$.

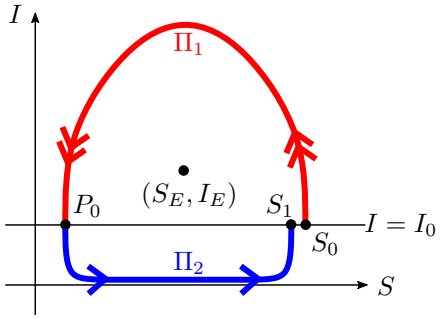

Figure 2.5: Sketch of the fast and slow dynamics defining the maps Π_1 and Π_2. The fact that $S_1 < S_0$ is shown below.

The limit orbit is sketched in Figure 2.5. Considering the composition of Π_1 and Π_2 gives the Poincaré map

$$\Pi : \{S \in [S_E, 1), I = I_0\} \to \{\Pi_2(\Pi_1(S)) \in [S_E, 1), I = I_0\}.$$

In this notation, we define $P_0 = \Pi_1(S_0)$, $S_1 = \Pi_2(P_0) = \Pi(S_0)$. These correspond, in the u-coordinate, to

$$u_0 = R_0 P_0 - 1 \approx R_0 S_\infty - 1, \quad p_0(u_0) = R_0 S_1 - 1.$$

We rewrite (2.22) as

$$P_0 - S_1 - \left(1 - \frac{1}{R_0}\right) \ln\left(\frac{1 - S_1}{1 - P_0}\right) = 0.$$

Which means that S_1, the exit point, is the only root greater than P_0 of

$$F(x) = x - P_0 + \left(1 - \frac{1}{R_0}\right) \ln\left(\frac{1 - x}{1 - P_0}\right). \tag{2.24}$$

It is clear that when the trajectory is in a neighbourhood of (S_1, I_0), as implied by the entry-exit map, one can reapply Proposition 1, obtaining $P_1 = \Pi_1(S_1)$ (reached through the fast flow), $S_2 = \Pi_2(P_1)$ (slow flow), and so on, obtaining two sequences

$$S_0,\ S_1 = \Pi_2(P_0), \ldots, S_n = \Pi_2(P_{n-1}), \ldots \qquad P_0 = \Pi_1(S_0)), \ldots, P_n = \Pi_1(S_n), \ldots \tag{2.25}$$

Lemma 3. *The sequence $\{S_n\}$ is decreasing and bounded below by $1/R_0$; the sequence $\{P_n\}$ is increasing and bounded above by $1/R_0$.*

Proof. We recall $S_1 = \Pi_2(P_0) = \Pi(S_0)$, so if, for any $S_0 \in (1/R_0, 1)$, such value is smaller/greater than S_0, $\{S_n\}$ is decreasing/increasing.
We notice that $\Pi(S_0) < S_0$ if and only if $\Pi_2(P_0) < \Pi_1^{-1}(P_0)$, where $\Pi_1^{-1}(P_0) > P_0$ is the only such root of

$$G(x) = x - P_0 + \frac{1}{R_0} \ln\left(\frac{P_0}{x}\right), \tag{2.26}$$

which comes from $\Gamma(x, 0) = \Gamma(P_0, 0)$; we recall that Γ describes the trajectories of the layer equation. The functions F and G are sketched in Figure 2.6.

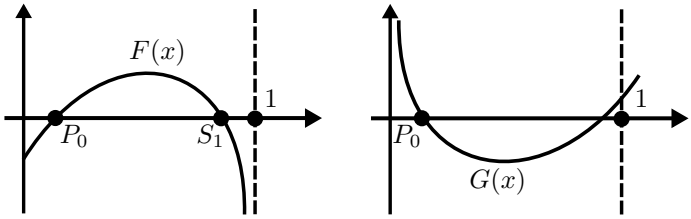

Figure 2.6: Sketch of the functions F and G, which implicitly define Π_2 and Π_1^{-1}, respectively.

Then, since G is increasing for $x > 1/R_0$,

$$\Pi_2(P_0) < \Pi_1^{-1}(P_0) \iff G(\Pi_2(P_0)) < 0.$$

The fact that $S_1 < S_0$ can be shown as a particular case of the following, more general proposition, by taking $a = P_0$, $b = 1/R_0$, $x^* = S_1$.

Lemma 4. *Let* $0 < a < b < 1$, $F(x) = x - a + (1-b)\ln(\frac{1-x}{1-a})$, $G(x) = x - a + b\ln(\frac{a}{x})$. *Let* $x^* \in (a, 1)$ *be the only zero greater than* a *of* F. *Then* $G(x^*) < 0$.

Proof. We use the auxiliary function $H(x) = F(x) + \frac{b}{1-b}G(x)$, which, under the hypotheses, is decreasing for $x \in (0, 1)$. Next we have that $H(a) = F(a) + \frac{b}{1-b}G(a) = 0$ which implies

$$0 > H(x^*) = F(x^*) + \frac{b}{1-b}G(x^*) = \frac{b}{1-b}G(x^*) \implies G(x^*) < 0.$$

□

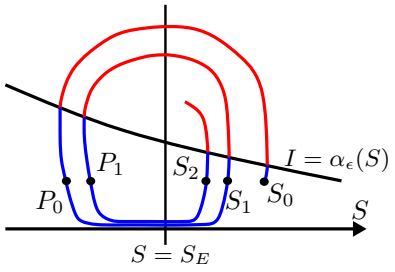

Figure 2.7: $\alpha_\epsilon(S) = \mathcal{O}(\epsilon)$; the red parts of the orbit are fast for both variables, the blue parts are fast for I, slow for S.

Since Π_1 is a decreasing function, from the fact that $\{S_n\}$ is decreasing, it follows that $\{P_n\}$ is increasing. □

Proposition 2. *The sequences* $\{S_n\}$ *and* $\{P_n\}$ *defined in* (2.25) *both converge to* $1/R_0$.

Proof. The convergence can be shown reasoning by contradiction, for example by looking at the sequence S_i. We know it is decreasing, and bounded below by $1/R_0$, so if it is not converging to this value, it must be converging to some other value $S_{\text{lim}} > 1/R_0$. But if this is the case, $\Pi(S_{\text{lim}}) < S_{\text{lim}}$, which contradicts the nature of S_{lim}.
Completely analogously we can see that $P_i \to 1/R_0$. □

Extending Proposition 1, one can easily show that, if $S_0 > 1/R_0$ and $I_0 = \mathcal{O}(\epsilon^2)$, the orbits $\{S_\epsilon(t), I_\epsilon(t), t \in [0,T]\}$ for any T converge for $\epsilon \to 0$ to a finite union of orbits (under the fast flow) from $(S_n, 0)$ to $(P_n, 0)$, and slow flows on the S-axis from $(P_n, 0)$ to $(S_{n+1}, 0)$.

The same can be shown for any initial condition, since starting from any (S_0, I_0) with $I_0 > 0$, the solutions will approach a point $(S_\infty, 0)$ with $S_\infty < 1/R_0$, so that setting $P_0 = S_\infty$, one can repeat the above argument.

What can we say of the orbits $\{S_\epsilon(t), I_\epsilon(t)\}$ for ϵ small but fixed as $t \to \infty$? When $1/R_0 - P_n = \mathcal{O}(\epsilon)$, the argument of Lemma 2 does not work. Hence, we cannot say, and indeed it is no longer true, that $I(t)$ becomes $\mathcal{O}(\epsilon^2)$ afterwards, and we cannot apply the entry-exit Lemma as above.

However, the previous argument shows that $\{S_\epsilon(t), I_\epsilon(t)\}$ reaches an ϵ-neighbourhood of the equilibrium (S_E, I_E). Linearization at the equilibrium then shows that all trajectories of (2.10) starting in the set $\{(S,I) \in \mathbb{R}^2 \,|\, S \geq 0, I > 0, S + I \leq 1\}$ converge towards (S_E, I_E), as already known (Theorem 2.3.1). This analysis provides an alternative proof, valid for $\epsilon > 0$ sufficiently small.

Biologically, the above analysis tells us that between two consecutive peaks of infection there is a long ($\mathcal{O}(1/\epsilon)$) time during which the fraction of infected population is exponentially small. On the other hand, the duration of high infected portion of the population is rather small (it occurs on the fast time scale). Ultimately, however, under the setting of this section the only possible asymptotic outcome is convergence towards the endemic equilibrium (S_E, I_E) via damped oscillations.

2.3.3 SIRS model

We now consider a SIRS compartment model. The SIRS model is a slight modification of the SIR model and thus we keep the same notation. The SIRS model is given by the following system:

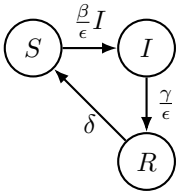

$$\begin{aligned} \dot{S} &= -\frac{\beta}{\epsilon} SI + \delta R, \\ \dot{I} &= \frac{\beta}{\epsilon} SI - \frac{\gamma}{\epsilon} I, \\ \dot{R} &= \frac{\gamma}{\epsilon} I - \delta R. \end{aligned} \tag{2.27}$$

Figure 2.8: Flow diagram for (2.27).

In this model there is no birth nor death, so the population remains constant. The small positive parameter $0 < \epsilon \ll 1$ gives rise to the difference in magnitude between the large infection rate β/ϵ, the large recovery rate γ/ϵ and the rate of loss of immunity δ. This difference models a highly contagious disease with a short infection period with possibility of reinfection. The main distinctions with the SIR system presented in Section 2.3.1 are the absence of demographic dynamics (no birth/death) and the possible loss of immunity (meaning that individuals can move from R to S). As we will see shortly, however, this important biological difference does not modify the qualitative behaviour of the system.

As we noticed in Section 2.3.1, $\dot{N} = \dot{S} + \dot{I} + \dot{R} = 0$, that is, the total population remains constant, so we assume without loss of generality $N(0) = 1$, which implies $N(\tau) \equiv 1$ for all $\tau \geq 0$;

this allows us, using $R = 1 - S - I$, to reduce the system to

$$\begin{aligned} \dot{S} &= -\frac{\beta}{\epsilon} SI + \delta(1 - S - I), \\ \dot{I} &= \frac{\beta}{\epsilon} SI - \frac{\gamma}{\epsilon} I. \end{aligned} \tag{2.28}$$

Proceeding as in the first model, we introduce the fast time variable $t = \tau/\epsilon$, which gives

$$\begin{aligned} S' &= -\beta SI + \epsilon\delta(1 - S - I), \\ I' &= I(\beta S - \gamma), \end{aligned} \tag{2.29}$$

where now the prime ($'$) indicates the derivative with respect to t. Note that system (2.29) is not in the standard form (2.2).

The critical manifold is, as before, the set $\mathcal{C}_0 = \{(S, I) \in \mathbb{R}^2 \,|\, I = 0\}$, and the slow flow along it is given by $\dot{S} = \delta(1 - S)$, which implies flow towards the point $(S, I) = (1, 0)$.

The $\epsilon \to 0$ limit system corresponding to (2.29) is

$$\begin{aligned} S' &= -\beta SI, \\ I' &= I(\beta S - \gamma), \end{aligned} \tag{2.30}$$

which is exactly the limit system we obtained in Section 2.3.1. Hence, we can apply the same qualitative reasoning as before, with some small changes: in the perturbed system the nullcline for S is slightly different, giving $I = \alpha(S) = (\epsilon\delta(1-S))/(\beta S + \epsilon\delta)$, and the value of S_E is exactly $1/R_0$.

The previous ansatz for the Lyapunov function does not work here; we could find another one, following what was done in [66], but we instead follow the analysis with the entry-exit function which, as we show below, does not change.

The trajectory starting from (S_0, I_0), with $I_0 \in \mathcal{O}(\epsilon^2)$, follows the same qualitative behaviour: after it intersects $I = \alpha(S)$ at a point $(S_\infty + \mathcal{O}(\epsilon), \mathcal{O}(\epsilon))$, it eventually intersects the horizontal line $I = I_0$. At that moment, we change the variables as before:

$$S = \frac{u + 1}{R_0}, \quad I = \epsilon v,$$

and we obtain a system in standard form:

$$\begin{aligned} v' &= \gamma u v, \\ u' &= \epsilon(-\beta v(u + 1) + \xi(R_0 - u - 1 - \epsilon v)). \end{aligned} \tag{2.31}$$

In the notation of the entry-exit function, then,

$$\begin{aligned} f(v, u, \epsilon) &= \gamma u, \\ g(v, u, \epsilon) &= -\beta v(u + 1) + \xi(R_0 - u - 1 - \epsilon v), \end{aligned} \tag{2.32}$$

which satisfy the hypotheses in the relevant region; hence, we can compute $p_0(u_0)$ with exactly the same integral equation

$$\int_{u_0}^{p_0(u_0)} \frac{u}{R_0 - 1 - u} \mathrm{d}u = 0, \tag{2.33}$$

and the procedure we followed for the SIR model can be applied to this SIRS one identically to show the global convergence to the unique equilibrium.

By following a similar analysis as the one performed so far one can also show that considering a SIRS model with demography would not change the qualitative behaviour of the system.

The results obtained so far for the SIR and SIRS models are summarized in the following Proposition.

Proposition 3. *The SIR, SIRS without and with demographic dynamics, with infection and recovery rates $\mathcal{O}(1/\epsilon)$ big compared to the other parameters, are all qualitatively equivalent. Their main common features are:*

- *boundedness of solutions in the set $\{(S,I,R) \in \mathbb{R}^3_{\geq 0} \mid 0 \leq S+I+R \leq 1\}$,*
- *population either constant, or converging uniformly and exponentially fast to a constant, which allows to reduce the number of compartments from 3 (S,I,R) to 2 (S,I),*
- *existence of an endemic equilibrium point of the form $(S_E, I_E) = (\frac{1}{R_0} + \mathcal{O}(\epsilon), \mathcal{O}(\epsilon))$,*
- *fast-slow decomposition in the I and S coordinate, respectively, $\mathcal{O}(\epsilon)$-close to the critical manifold $\mathcal{C}_0 = \{(S,I) \in [0,1]^2 \mid I = 0\}$,*
- *counterclockwise spiralling of the orbits towards (S_E, I_E), and consequent absence of periodic orbits.*

These common features mean that, in the long run, the population in each of these models converges to an equilibrium $\mathcal{O}(\epsilon)$ close to $(S,I,R) = (1/R_0, 0, 1-1/R_0)$, in the first octant of $\mathbb{R}^3$; each of the three variables have damped oscillations around the equilibrium value.

In the next section we study a more complete (but also more complicated) epidemic model, where the techniques developed so far shall be extended.

2.3.4 SIRWS model

We consider the SIRWS compartment model suggested by Dafilis et al. in [11]. As in the previous models, we assume that some parameters are $\mathcal{O}(\epsilon)$ small compared to others, making the corresponding processes slow, and the remaining ones fast (the changes correspond to every occurrence of ϵ in system (2.34)). This allows us to build on the analysis done in sections 2.3.1 and 2.3.3, and to apply the entry-exit function to a more challenging model.

The model we are concerned with in this section is given by:

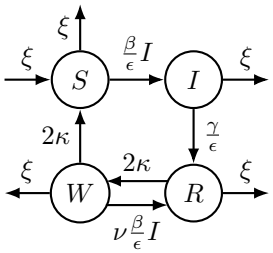

Figure 2.9: Flow diagram for (2.34)

$$
\begin{aligned}
\dot{S} &= -\frac{\beta}{\epsilon} SI + 2\kappa W + \xi(1-S), \\
\dot{I} &= \frac{\beta}{\epsilon} SI - \frac{\gamma}{\epsilon} I - \xi I, \\
\dot{R} &= \frac{\gamma}{\epsilon} I - 2\kappa R + \nu \frac{\beta}{\epsilon} IW - \xi R, \\
\dot{W} &= 2\kappa R - 2\kappa W - \nu \frac{\beta}{\epsilon} IW - \xi W.
\end{aligned}
\tag{2.34}
$$

As in the previous models, susceptible individuals $(S(\tau))$ become infectives $(I(\tau))$ upon contact with infectious individuals, who, at rate γ/ϵ become immune at their first stage $(R(\tau))$, and then, at a rate 2κ, become second-stage ('weakly') immune $(W(\tau))$. Weakly immune individuals

may then lose totally their immunity at rate 2κ, or, upon contact with infectious individuals, revert back to fully immune individuals ($R(\tau)$), thanks to the so-called immunity boosting. The constant ν is the ratio between the rate at which immunity boosting occurs in weakly immune individuals, and the rate at which susceptibles become infected. Finally, we assume a constant birth rate ξ, equal to the death rate, and that all individuals are born susceptible. Through the introduction of the small parameter ϵ we consider a highly contagious disease with a very short infection period, compared to other typical times of the system; indeed, the average length of the infectious period is ϵ/γ, while the average length of life is $1/\xi$ and the total average length of the immune period is $1/\kappa$ for individuals whose immunity is not boosted. Such relation between the parameters has been assumed, for example, for diseases such as pertussis, as described in [55], where the authors estimated $\beta = 260$, $\gamma = 17$, $\xi = 0.01$, $\kappa = 0.1$, $\nu = 20$; hence, the analysis which follows may be useful in the modelling of such diseases.

Analogous to the previous models, the set $\left\{(S, I, R, W) \in \mathbb{R}^4_{\geq 0} \,|\, 0 \leq S + I + R + W \leq 1\right\}$ is invariant. We can thus scale the total population to 1, so that we can use $R = 1 - S - I - W$. We notice that system (2.8) can be recovered from system (2.34) by setting $\kappa = \nu = 0$, and ignoring the consequently decoupled W coordinate.

As we shall describe in our analysis below, incorporating the waning state W modifies considerably the dynamics of the model; in fact, it induces the possibility of periodic limit cycles, a feature that the previous simpler models did not have. This is particularly important when comparing the dynamics of the SIRWS model with that of the SIRS model where, even if recovered portions of the population may become again susceptible, there is still no "long run periodic behaviour".

As we have done before, introducing the fast time variable $t = \tau/\epsilon$ brings the system into a fast-slow system, not in the standard form (2.2),

$$\begin{aligned} S' &= -\beta SI + \epsilon(2\kappa W + \xi(1 - S)), \\ I' &= \beta SI - \gamma I - \epsilon\xi I, \\ R' &= \gamma I + \nu\beta IW - \epsilon(2\kappa R + \xi R), \\ W' &= -\nu\beta IW + \epsilon(2\kappa R - 2\kappa W - \xi W). \end{aligned} \tag{2.35}$$

Remark 2. *Note that the critical manifold is (similarly to the previous models) given by*

$$\mathcal{C}_0 = \left\{(S, I, R, W) \in [0, 1]^4 \,|\, I = 0\right\}. \tag{2.36}$$

Furthermore, in the $\epsilon \to 0$ limit, S and I become independent of R and W, and orbits follow the same behaviour we have seen in the fast phases of the first two models. In other words, the (S, I)-orbits of the layer equation follow a power level of $\Gamma(S, I) = \gamma \ln(S) - \beta(S + I)$, and converge towards $(S_\infty, 0)$[1]. These observations motivate the following lemma.

Lemma 5. *Consider the layer equation corresponding to* (2.35)*. Then, as* $(S, I) \to (S_\infty, 0)$ *one has* $W \to W_\infty := W_0 \exp^{-\nu R_0(S_0 + I_0 - S_\infty)}$*, where* $W_0 = W(0)$*.*

Proof. We note that

$$\int_0^\infty \Big(S'(u) + I'(u)\Big)\mathrm{d}u = -\gamma \int_0^\infty I(u)\mathrm{d}u \implies S_0 + I_0 - S_\infty = \gamma \int_0^\infty I(u)\mathrm{d}u,$$

due to the fact that $\lim_{t\to+\infty} I(t) = 0$. Next, note from (2.35) that in the limit $\epsilon = 0$ one has $\frac{W'}{W} = -\nu\beta I$, which implies $W(t) = W_0 \exp^{-\nu\beta \int_0^t I(u)\mathrm{d}u}$. Letting $t \to \infty$ leads to the result, recalling that $R_0 = \frac{\beta}{\gamma}$. □

[1] We recall that S_∞ is defined as the nontrivial solution of $\Gamma(S, 0) = \Gamma(S_0, 0)$.

Since we have already shown that the layer equation is in the (S, I)-coordinates the same as before, we proceed just in the same way, that is, we apply first the change of coordinates

$$S = \frac{u+1}{R_0}, \quad I = \epsilon v,$$

which gives a system in standard singular perturbation form, with u, W slow and v fast, namely

$$\begin{aligned} v' &= (\gamma u - \epsilon\xi)v =: f(v,u,\epsilon)v, \\ u' &= \epsilon(-\beta v(u+1) + 2\kappa R_0 W + \xi(R_0 - u - 1)) =: \epsilon g(v,u,W,\epsilon), \\ W' &= \epsilon(-\nu\beta v W + 2\kappa - 2\kappa\frac{u+1}{R_0} - 4\kappa W - \xi W) + \mathcal{O}(\epsilon^2). \end{aligned} \tag{2.37}$$

And, accordingly, in the slow time scale τ:

$$\begin{aligned} \epsilon\dot{v} &= (\gamma u - \epsilon\xi)v, \\ \dot{u} &= -\beta v(u+1) + 2\kappa R_0 W + \xi(R_0 - u - 1), \\ \dot{W} &= -\nu\beta v W + 2\kappa - 2\kappa\frac{u+1}{R_0} - 4\kappa W - \xi W + \mathcal{O}(\epsilon). \end{aligned} \tag{2.38}$$

Naturally, the critical manifold in these new coordinates is $\mathcal{C}_0 = \big\{(u,v,W) \in \mathbb{R}^3 \,|\, v = 0\big\}$.

We want to compute the time during which a trajectory of (2.35) stays $\mathcal{O}(\epsilon^2)$-close to the critical manifold, as described in [35, equation (12)] and in [60, equation (11)]. A direct application of their result gives

$$\int_0^{T_E} u(\tau)\mathrm{d}\tau = 0.$$

In other words, T_E is defined as the time it takes to go from $u = u_0$ to $u = p_0(u_0)$. Then, remembering $u(\tau) = R_0 S(\tau) - 1$, T_E is given by

$$\int_0^{T_E} (R_0 S(\tau) - 1)\mathrm{d}\tau = 0. \tag{2.39}$$

To proceed with the calculations, let us look at the (S, W)-dynamics in the slow time variable t on the critical manifold $I = 0$:

$$\begin{aligned} \dot{S} &= 2\kappa W + \xi(1 - S), \\ \dot{W} &= 2\kappa(1 - S) - (4\kappa + \xi)W. \end{aligned} \tag{2.40}$$

This system of ODEs can be solved explicitly, assuming initial conditions $(S(0), W(0)) = (S_\infty, W_\infty)$, the limit values of the fast loop, we have:

$$\begin{aligned} S(\tau) &= 1 + [S_\infty - 1 + 2\kappa(S_\infty + W_\infty - 1)\tau]\exp(-(2\kappa + \xi)\tau), \\ W(\tau) &= [W_\infty - 2\kappa(S_\infty + W_\infty - 1)\tau]\exp(-(2\kappa + \xi)\tau) \\ &= 1 - S(\tau) - (1 - S_\infty - W_\infty)\exp(-(2\kappa + \xi)\tau). \end{aligned} \tag{2.41}$$

The phase-portrait of (2.40) is illustrated in Figure 2.10, where the only feasible region is the triangle $0 \le S + W \le 1$, $S, W \ge 0$, and all trajectories converge to $(S, W) = (1, 0)$.

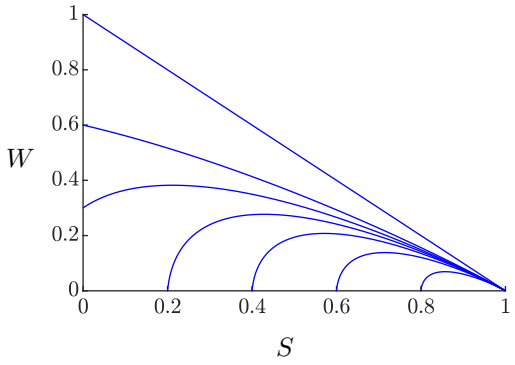

Figure 2.10: Phase plane for the S, W couple; values for $\kappa = 0.1$ and $\xi = 0.0125$ taken from [11]

Using the explicit equation for $S(\tau)$ given in (2.41), and introducing, for ease of notation, $A := 2\kappa + \xi$, $B := 2\kappa(S_\infty + W_\infty - 1)$, $C := S_\infty - 1$ so that

$$S(\tau) = 1 + C\exp(-A\tau) + Bt\exp(-A\tau),$$

the equation for the exit time T_E (2.39) becomes

$$-\frac{R_0\exp(-AT_E)(ABT_E + AC + B)}{A^2} + (R_0 - 1)T_E + \frac{R_0(AC + B)}{A^2} = 0. \tag{2.42}$$

Clearly $T_E = 0$ is a solution. Moreover, there is only one strictly positive solution, since $S(\tau)$ is strictly increasing and tends to 1 as $\tau \to +\infty$. Such solution provides the exit time.

Substituting the positive solution T_E of (2.42) it in (2.41) we obtain the exit point $(S(T_E), W(T_E))$. However, due to the implicit formulae we have obtained above, such a computation is only suitable numerically (see Section 2.3.4.1). Despite the previous obstacle, we can still check how the exit points depend on certain parameters. For example, from the first equation of (2.41) we observe that

$$\frac{\partial S}{\partial \xi}(\tau, \xi) = -\tau[S_\infty - 1 + 2\kappa(S_\infty + W_\infty - 1)\tau]\exp^{-(2\kappa+\xi)\tau} > 0, \tag{2.43}$$

which immediately suggests that the exit time is decreasing in ξ. Namely, let $T_{E,i}$ denote the exit time with $\xi = \xi_i$ and $i = 1, 2$. If $\xi_1 < \xi_2$ then, using (2.43), one sees that $T_{E,1} > T_{E,2}$.

To provide more insight on the dynamics of the SIRWS model, we are now going to complement our previous study with a numerical analysis, where the computed exit time T_E shall play an essential role.

2.3.4.1 Periodic orbits

Recall that in the SIR and SIRS models no periodic trajectories are possible. In this section we show that the SIRWS does have periodic solutions, and of particular biological relevance, stable limit cycles. Our motivation is that if a stable limit cycle exists, then a disease would have periodic outbursts. Furthermore, due to the time scales present in the model, there is the danger of missing such periodicity if only short time scale analysis is considered. Moreover, information regarding the parameter regions in which damped/sustained oscillations occur can give directions as to which parameter(s) to modify in order to have a desired control of the epidemic.

As it is usual in GSPT, the general idea to show existence of limit cycles of the perturbed (fast-slow) system is to first find a singular cycle, see for example [48, 80]. A singular cycle is a concatenation of limiting slow and fast orbits that form a cycle. Afterwards, given that some conditions are met, we argue that such singular cycle gives rise to a limit cycle of the fast-slow system. We further remark that a mixture of analytical and numerical methods is relevant since we have to combine local analytical results with global numerical results, which is a key theme in multiple time scale systems [26, 27, 50].

The steps to form a singular cycle of the SIRWS model are as follows:

1. Choose a section $J_1 = \left\{(S, I, W) = (S_0, 0, W) \,|\, S_0 > \frac{1}{R_0},\, W \in (0, 1 - S_0)\right\}$. This section is transversal to the reduced slow flow and is located on the unstable region of the critical manifold.

2. Consider the map Π_1 defined by the layer equation. Under such a map one obtains a new section on the critical manifold $J_2 := \Pi_1(J_1)$. The coordinates of J_2 are given by $(S_\infty, 0, W_\infty)$, as in Lemma 5.

3. Consider the map Π_2 defined by the slow flow *for a time* T_E implicitly given by (2.42), i.e. $\Pi_2(J_2) = (S(T_E), W(T_E))$ with $(S(\tau), W(\tau))$ given by (2.41), and let $J_3 := \Pi_2(J_2)$. Recall from the last part of section 2.3.4 that we can tune the exit time, for example, by changing the parameter ξ, without changing the map Π_1.

4. If J_3 intersects transversally J_1, then we have a robust singular cycle given precisely by the orbit corresponding to a fixed point of $\Pi_2 \circ \Pi_1$, see Figure 2.11 for a schematic representation of these four arguments.

   In the present context, robust means that the singular cycle persists under small smooth perturbations as a periodic orbit of the fast-slow system precisely due to the transverse intersection of J_1 and J_3 [81] (if it occurs).

   It is clear that for the particular SIRWS model, there is a priori no guarantee that such a transverse intersection occurs for a particular set of parameters and initial conditions. To clarify that indeed such a fixed point exists upon variation of parameter values, we refer to the situation shown in Figure 2.12 varying the parameter ξ, we argue as follows: let $F^\xi = (F_1^\xi, F_2^\xi) = \Pi_2 \circ \Pi_1 : \mathcal{C}_0 \to \mathcal{C}_0$ using the parameter ξ, and $X = \{\xi \,:\, J_3 \cap J_1 \neq \emptyset\}$. We can then define, for $\xi \in X$, $\bar{w}(\xi)$ as the value of w such that $F_1^\xi(S_0, w) = S_0$. Note moreover that for all w, the inequalities $0 < F_2^\xi(S_0, w) < 1 - S_0$ hold, as can be seen by (2.41).
   Consider finally

$$g : X \to \mathbb{R}, \quad g(\xi) = \bar{w}(\xi) - F_2^\xi(S_0, w)$$

   If $X = [\xi_1, \xi_2]$, we have $\bar{w}(\xi_1) = 0$ and $\bar{w}(\xi_2) = 1 - S_0$, or vice versa. Hence $g(\xi_1) < 0 < g(\xi_2)$, or vice versa. In either case, there exists $\bar{\xi} \in (\xi_1, \xi_2)$ such that $g(\bar{\xi}) = 0$, i.e. $F_1^{\bar{\xi}}(S_0, \bar{w}(\bar{\xi})) = S_0$ and $F_2^{\bar{\xi}}(S_0, \bar{w}(\bar{\xi})) = \bar{w}(\bar{\xi})$ as claimed.

   Moreover, since we know that both Π_1 and Π_2 are contractions in the W-direction (refer to (2.35), Lemma 5 and to Figure 2.10), such a singular cycle is locally attracting. Hence it persists as a locally attracting periodic orbit for $\epsilon > 0$ sufficiently small. We remark, however, that this does not mean that there are no other limit cycles for $\epsilon > 0$ sufficiently small. As we show in our numerical analysis of the forthcoming section, there is in fact a range of parameter for which a stable and an unstable limit cycle co-exist. The existence of the unstable limit cycle, however, does not follow from our previous perturbation arguments.

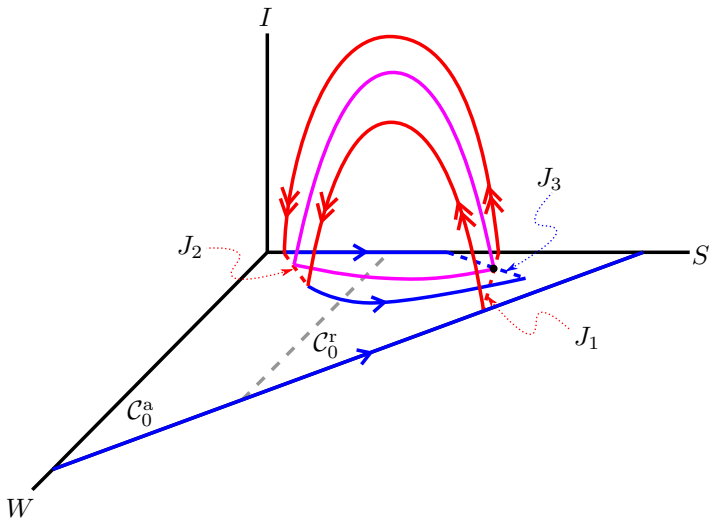

Figure 2.11: Schematic representation of the singular cycle, shown in magenta. The red arrows depict the map $\Pi_1 : (S_0, W_0) \mapsto (S_\infty, W_\infty)$ so that $\Pi_1(J_1) = J_2$. The blue arrows depict the map Π_2 given by the reduced flow on $\mathcal{C}_0$ and induced by (2.40) (for a finite time $T_E(S_\infty, W_\infty)$) so that $\Pi_2(J_2) = \Pi_2(\Pi_1(J_1)) = J_3$. If the sections J_1 and J_3 intersect, then such an intersection defines closed singular orbits. If J_1 and J_3 intersect transversally, then such intersection persists for $\epsilon > 0$ sufficiently small giving rise to a periodic orbit of the SIRWS model.

Naturally, the above procedure is only sufficient to show existence of limit cycles that pass close to the critical manifold and provides no information on other possible limit cycles of the fast-slow system, compare with [79]. Yet our attention is precisely focused on describing those limit cycles arising from the time scale separation.

An example of the above procedure is shown in Figure 2.12 where we set $\{\beta = 260, \gamma = 17, \kappa = 0.1, \xi = 0.0125, \nu = 5\}$, values taken from [11]. Figures in the left column show the evolution of J_1 (dashed red) in the fast system (red) and of J_2, too small to be visible, in the slow system (blue). Figures in the right column zoom to the interval J_3 (blue) for each parameter value, and its position relative to J_1 (dashed red). Note that

- For $\xi = 0.01$ (Figures 2.12 (a) and (b)) the interval J_3 lies to the right of J_1, so there might be a larger limit cycle further away from J_1.
- For $\xi = 0.0125$ (so Figures 2.12 (c) and (d)) the interval J_3 intersects transversally J_1, and the intersection certifies the existence the singular periodic orbit.
- For $\xi = 0.015$ (so Figures 2.12 (e) and (f)) the interval J_3 lies to the left of J_1, so there might be a smaller limit cycle further away from J_1, or the system might converge to the unique equilibrium point in the first octant.

It is worth noting that we chose to investigate the role of ξ, the birth/death rate, due to its biological relevance. However, by the same method one is able to numerically approach the existence of limit cycles upon variation of any other parameter. It is important to note that, in the limit systems, there is a clear separation between "fast parameters" (β, γ, ν) and "slow parameters" (ξ, κ); changing a single parameter will only influence either the layer or the reduced dynamics, and not both.

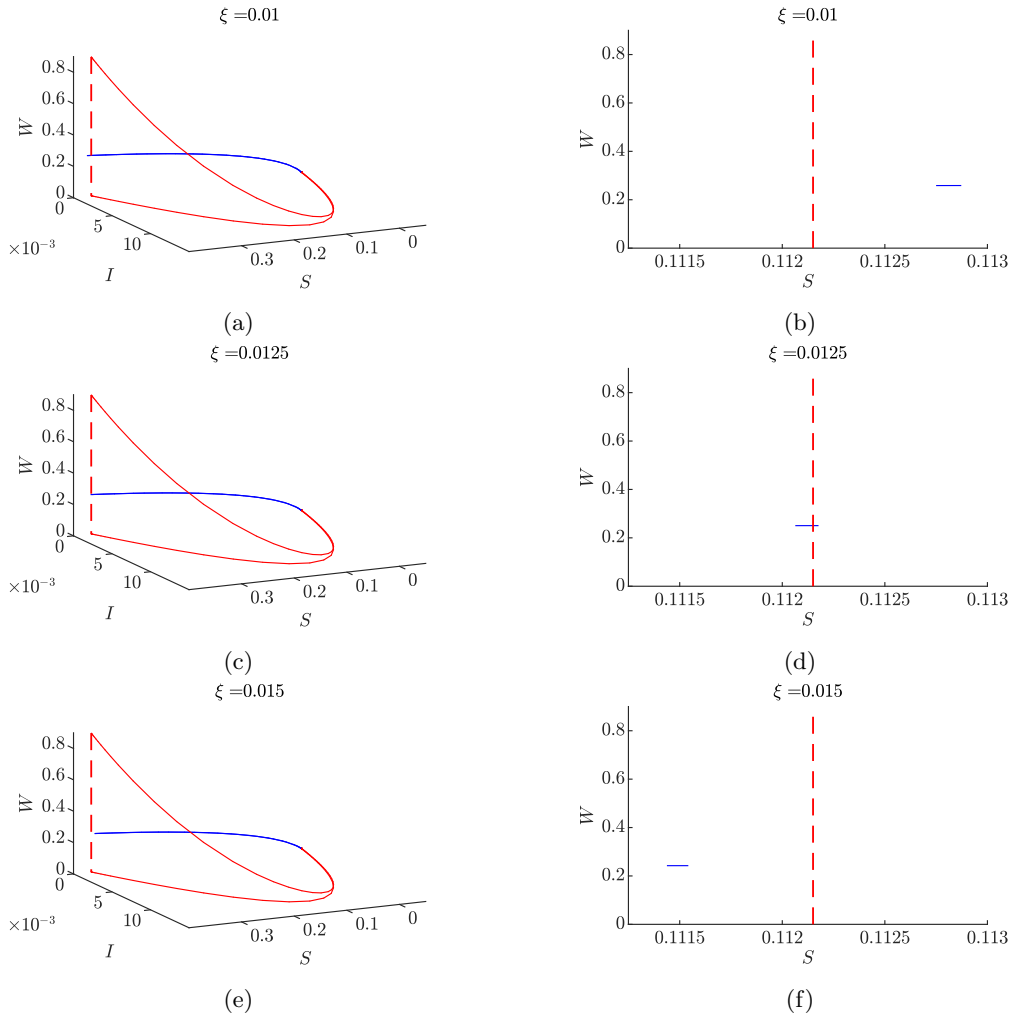

Figure 2.12: Numerical illustration of the effect of changing ξ on the slow dynamics. This numerical analysis shows that there is an interval around $\xi \sim 0.0125$ for which periodic orbits of (2.35) exists, for $\epsilon > 0$ sufficiently small. The dashed red line is J_1, while red curves indicate the evolution of such interval under the layer equation. Blue curve(s): evolution of the image of J_1 under the reduced flow on the critical manifold. The blue segments in (b), (d) and (f) correspond to J_3.

Remark 3. *One may also consider a finer decomposition of the return map and analyse each piece separately [50]; this would explain what happens for values of the parameters corresponding to a breakdown of transversality. Although this does add structural understanding, we leave this finer scale analysis as a problem for future work, since it would be lengthy and it would not add much to the analysis we present.*

Since we have already demonstrated the existence of limit cycles, the next question to investigate is the possible bifurcations that may arise upon variation of the parameters. Such analysis is presented in the forthcoming section.

2.3.4.2 Bifurcation analysis

In this section we carry out a bifurcation analysis, motivated by the one developed in [11], which we perform with MatCont [15]. Our goal is to investigate the way the bifurcation diagrams change as ϵ is decreased, i.e., we want to understand via numerical continuation how the fast-slow singular limit is approached; see also [14, 25, 36] where such a strategy has considerably improved our understanding of several fast-slow models. In our context, decreasing ϵ means, from a biological point of view, modelling an epidemiological system in which the difference in duration between life expectancy and infectious episodes becomes large. In the limit as $\epsilon \to 0$, infectious episodes become instantaneous, and the analysis of this limit case helps to understand the behaviour of the system for $\epsilon > 0$ small enough.

In fact, we note that the system studied in [11] is system (2.35), for the particular choice of $\epsilon = 1$. In what follows, we set $\beta = 260,\ \gamma = 17,\ \kappa = 0.1$, as in [11], and vary ϵ, ξ, ν, and later β as well. Notice that the values of the parameters $\beta,\ \gamma,\ \kappa$ and ξ already appear of different order of magnitude. It would be possible to use a different parametrization, letting $\tilde{\beta} = 0.26$, $\tilde{\gamma} = 0.017$ and $\epsilon = 0.001$. All the following analysis would be identical, except that the values obtained for ϵ, β and γ would be multiplied by 10^{-3}.

For consistency, we start by replicating Figure 5 from [11], by setting $\epsilon = 1$ and $\xi = 0.01$, in Figure 2.13a. For all parameter values there is a unique equilibrium in $\mathbb{R}^4_{\geq 0}$, as can be easily proved, but its stability changes varying ν through a subcritical and a supercritical Hopf bifurcation.

Next, in order to get the dependence of the bifurcation points with respect to ϵ, we continue the two Hopf points H_1 and H_2 and the Limit Point of Cycles (LPC) L in a (ν, ϵ) bifurcation diagram, obtaining the diagram shown in Figure 2.13b.

We notice from Figure 2.13b that H_1 converges to a positive value for $\nu \sim 1.32$ as $\epsilon \to 0$, while H_2 and L diverge; the latter much faster than the former. Moreover, we know from the analysis performed in Section 2.3.4 that as $\epsilon \to 0$ the equilibrium curve (black curve in Figure 2.13a) approaches the $\{I = 0\}$ axis. These two observations suggest that as $\epsilon \to 0$ the bifurcation diagram on Figure 2.13a gets stretched. One must also point out that the computation of the bifurcation diagrams for small ϵ becomes considerably expensive due to the high stiffness of the problem.

We next produce the analogous to Figure 2.13a, but for a smaller value of ϵ, namely $\epsilon = 0.05$, in Figure 2.14. In order to do so, due to stiffness of the problem, it is necessary to rescale the system by introducing a new variable $v = \ln(I)$. We emphasize that this rescaling is motivated by the fact that trajectories get exponentially close to the critical manifold, recall Lemma 2. Moreover, this rescaling might be useful for bifurcation analysis of systems with similar dynamics in which an exchange of stability of the critical manifold occur at a non-hyperbolic point, and trajectories of interest pass exponentially close to such a singularity. With the aforementioned

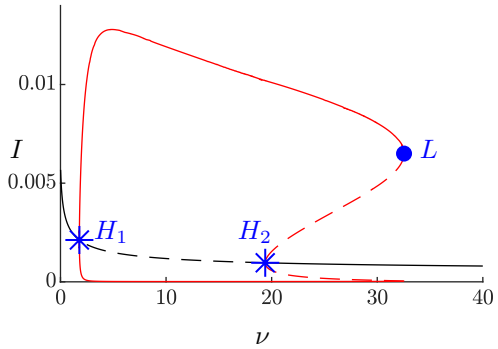

(a) One-parameter (ν) bifurcation diagram for (2.35) with $\epsilon = 1$: blue stars labelled H_1 and H_2 correspond to Hopf points; blue dot labelled L corresponds to the Limit Point of Cycles (LPC); red lines correspond to stable (solid) and unstable (dashed) limit cycles; the stable (solid) and unstable (dashed) equilibrium point is depicted by the black line.

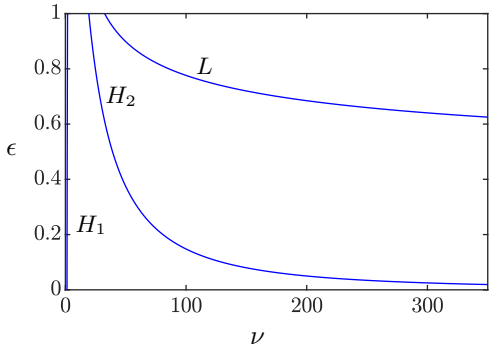

(b) The blue lines represent the Hopf points H_1 and H_2, and the LPC point L, plotted in Figure (2.13a), which are then continued while decreasing ϵ; compare with Figure 2.13a. We observe that H_1 does not tend to $\nu = 0$ as $\epsilon \to 0$ while H_2 and L diverge.

Figure 2.13: One and two parameter bifurcation diagrams for (2.35).

rescaling one obtains the following system of ODEs:

$$\begin{aligned} S' &= -\beta S\epsilon^v + \epsilon(2\kappa W + \xi(1-S)), \\ v' &= v(\beta S - \gamma - \epsilon\xi), \\ W' &= -\nu\beta W\epsilon^v + \epsilon(2\kappa(1-S-\epsilon^v-W) - 2\kappa W - \xi W). \end{aligned} \tag{2.44}$$

Thus, the bifurcation diagram in Figure 2.14 is obtained from (2.44) and confirms the behaviour anticipated in Figure 2.13b: as ϵ decreases, the distance between H_1 and H_2 increases, thus stretching the parameter region in which stable periodic solutions are to be observed. Most importantly, as is already evident in Figure 2.13b, we have that for ϵ sufficiently small the LPC is undetectable, implying that an eventual transition to stable (endemic) equilibrium due to increase of the immunity boosting rate ν is not possible any more.

Another important parameter is β, which regulates the infection rate. Thus, in order to further investigate the role of ϵ in the model, we next present in Figure 2.15 a (ν, β) bifurcation diagram.

For ease of notation, let us denote by $\nu(P)$ the value of ν corresponding to a point P. From Figure 2.15 we have that $\nu(GH_1) \approx 9.96$ and $\nu(GH_2) \approx 106.9$ for $\epsilon = 1$. Furthermore, for $\nu \leq \nu(GH_1)$, the system only exhibits stability of the equilibrium or of the limit cycle (zones 1 and 3). For $\nu(GH_1) < \nu \leq \nu(GH_2)$ there are two intervals of values for β which correspond to a stable equilibrium, one to a stable limit cycle and one to bistability (zones 1, 2, and 3). For $\nu(GH_2) < \nu \leq \nu_{\max}$, with $\nu_{\max} \approx 195.46$, there are two intervals of values for β which correspond to a stable equilibrium, one to a stable limit cycle and two to bistability, one of them being very thin. At $\nu = \nu_{\max}$ the two Hopf points H_1 and H_2 collide, and a codimension-2 Hopf-Hopf bifurcation occurs.

For $\epsilon = 0.05$, the diagram is qualitatively the same, but as already pointed-out before the diagram gets stretched both in β and in ν. The points GH_1 and GH_2 correspond now to $\nu \approx 7.04$

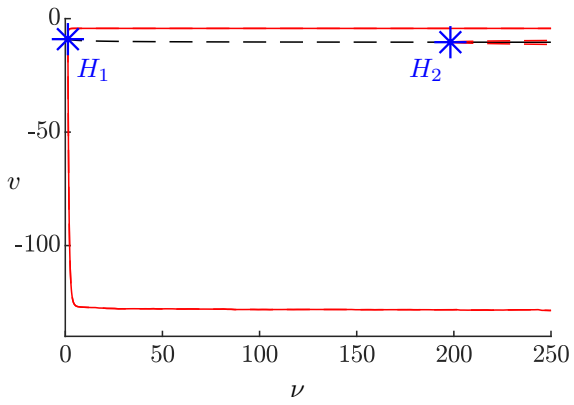

Figure 2.14: One-parameter (ν) bifurcation diagram for (2.44) with $\epsilon = 0.05$: blue stars labelled H_1 and H_2 correspond to Hopf points; red lines correspond to stable (solid) and unstable (dashed) limit cycles; the stable (solid) and unstable (dashed) equilibrium point is depicted by the black line.

and $\nu \approx 2282.6$, respectively. In particular, the bistability region 2 is enlarged.

To complement the previous description, and similar to Figure 9 (a) to (d) in [11] in Figures 2.16a-2.16c, we present the β-bifurcation diagram for different values of ν and continue all the Hopf points for decreasing ϵ, as shown in Figures 2.16d-2.16f.

As before, and for ease of notation, we denote by $\beta(P)$ the value of β corresponding to a point P. For each value of ν considered, we find two values $17 < \beta(H_1) < \beta(H_2)$ (17 was the fixed value of γ in each simulation; recall $R_0 = \beta/\gamma$) corresponding to Hopf points, and we continue them in ϵ, as shown in Figures 2.16d-2.16f. For $17 \leq \beta \leq \beta(H_1)$ the equilibrium point is stable, and there is no limit cycle. For $\beta(H_1) < \beta \leq \beta(H_2)$ the equilibrium point is unstable, and the limit cycle stable. For $\nu > \nu(GH_1)$ (resp. $\nu > \nu(GH_2)$), there is an interval (resp. there are two intervals) of values of $\beta(H_2) < \beta \leq \beta(L)$ (with L a LPC, whose existence and position depend on the choice of ν) for which the system exhibits bistability; eventually these two limit cycles collapse, and for $\beta > \beta(L)$ the system is characterized by a unique asymptotically stable equilibrium. Note, interestingly, that as the Hopf-Hopf bifurcation is approached, a new LPC (L_2 in Figure 2.16c) becomes visible.

We note that in the limit $\epsilon \to 0$, one has $\beta(H_1) \to 17$. This is due to the influence on the dynamics of the basic reproduction number $R_0 = \beta/\gamma$, which should remain greater than 1 for the endemic equilibrium to exist. Related to this, one has that $\beta(L_2) \to 17$ as $\epsilon \to 0$, whenever $\nu > \nu(GH_2)$. The values $\beta(H_2)$ and $\beta(L_1)$, instead, diverge to $+\infty$ as $\epsilon \to 0$; the region corresponding to the stable limit cycle stretches, as in the ν case. Lastly, we compute a (ξ, ν)-diagram and compare them for $\epsilon = 1$ and $\epsilon = 0.05$ in Figure 2.17, as we did for (β, ν) in Figure 2.15.

We observe in Figure 2.17 that not only the bifurcation diagram is stretched as ϵ decreases but also that the bistable region (region 2) is enlarged. GH_1 corresponds to $\xi \approx 0.0147$ for $\epsilon = 1$ and to $\xi \approx 0.03871$ for $\epsilon = 0.05$. Furthermore, in Figure 2.17 we show the existence of another Generalized Hopf point GH_3 (not considered in [11]), corresponding to $\xi \approx -0.1276$ for $\epsilon = 1$ and to $\xi \approx -0.1263$ for $\epsilon = 0.05$. We do not show the 2-parameter continuation of GH_3 since such a computation is not numerically feasible due to the high stiffness of the system in such parameter range. However, the previous observation suggests that all the bifurcation branches

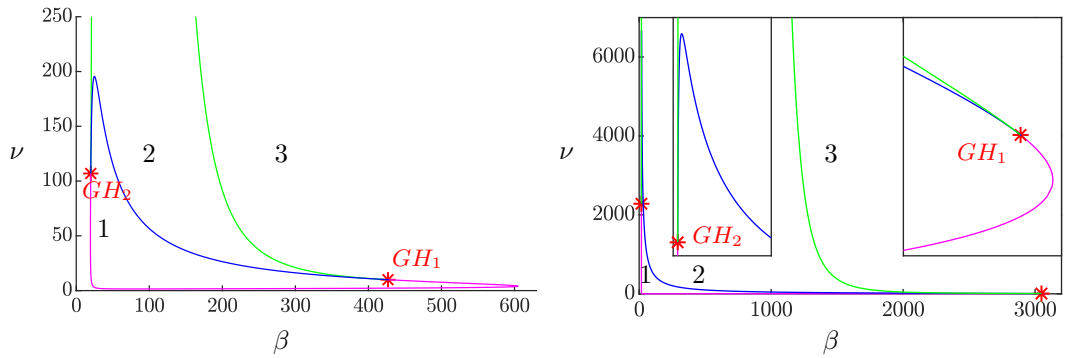

Figure 2.15: Two parameter bifurcation diagram for (2.35). Left and right represent $\epsilon = 1$ and $\epsilon = 0.05$, respectively. The red points labelled GH_i are generalised Hopf points. The blue (resp. magenta) branch is a curve of subcritical (resp. supercritical) Hopf bifurcation while the green branches correspond to limit point of cycles. We label the regions in the diagram according to the attractor as 1: Limit cycles, 2: Bistability, and 3: Point attractor. The insets in the right picture are "zoom-ins" near the two GH points.

corresponding to GH_3 are close to each other.

The numerical analysis shown in this section supports the existence of stable limit cycles for an increasing parameter range as $\epsilon \to 0$. Nonetheless, the dependence of the behaviour of the orbits on the parameters stays the same for sufficiently small parameters. This means that as in the $\epsilon = 1$ case, one still observes parameter ranges corresponding to the stability of the endemic equilibrium, and other parameter ranges corresponding to stable periodic orbits.

Based on the analysis performed so far, we can now give an interpretation of our results: first of all, the interplay between birth/death rate ξ and immune boosting ν remains qualitatively similar to the one described in [11], for small ϵ. However, the Hopf point H_2 moves according to the increasing difference in the time scales involved in the respective dynamics. H_1 does not converge to 0, supporting the result obtained in [11], where the authors showed that, for ν small enough, the dynamics are close to a SIRS system. The main difference, however, is that as ϵ decreases the role of the parameters can drastically change due to the changes in the bifurcation diagram. For example, for $\epsilon = 1$, a life expectancy of 50 years ($\xi = 0.02$) corresponds to convergence to the endemic equilibrium for all the possible values of ν. In contrast, for smaller values of ϵ the same ξ could correspond to stability of the limit cycle, bistability, or stability of the endemic equilibrium, depending on the value of ν (see Figure 2.17). Moreover, the effect of increasing life expectancy, i.e. decreasing ξ, results in the transition from point stability to stability of a limit cycle, possibly passing through a region of bistability. This means that, the higher the life expectancy of a certain population, the larger the interval for ν for which a stable limit cycle exists. Biologically, this means that ν must be sufficiently small to obtain a stable endemic equilibrium, otherwise periodic epidemic outbursts turn out to be robust.

2.4 Summary and Outlook

We have analysed the behaviour of three models given as a nonstandard singularly perturbed ODE. The first two models presented in Sections 2.3.1 and 2.3.3 proved to behave, under mild hypotheses on the parameters, qualitatively in the same way. In particular, their trajectories

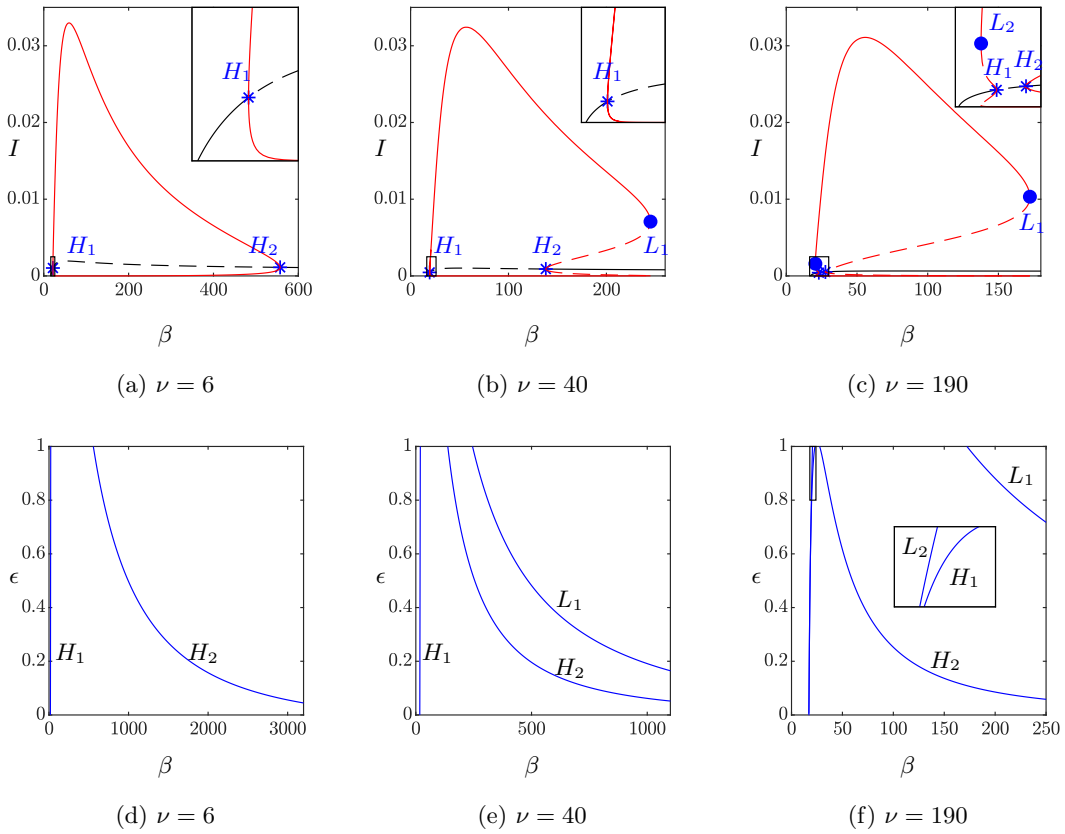

(a) $\nu = 6$ (b) $\nu = 40$ (c) $\nu = 190$

(d) $\nu = 6$ (e) $\nu = 40$ (f) $\nu = 190$

Figure 2.16: **First row:** one-parameter (β) bifurcation diagram for (2.35): blue stars labelled H_1 and H_2 correspond to Hopf points; blue circles labelled L_1 and L_2 correspond to Limit Point of Cycles; red lines correspond to stable (solid) and unstable (dashed) limit cycles; the stable (solid) and unstable (dashed) equilibrium point is depicted by the black line. The insets correspond to zoom-in near $\beta = 17$. **Second row:** continuation of the Hopf and LPC points while decreasing ϵ. We observe that H_1 (and L_2, when it exists) tends to $\beta = 17$ as $\epsilon \to 0$, while H_2 (and L_1, when it exists) diverges. The inset in (f) shows a zoom-in at the continuation of H_1 and L_2 from $\epsilon = 1$ to $\epsilon = 0.8$.

converge to the only (endemic) equilibrium in the open first quadrant, as long as the initial population of infected individuals is strictly positive. The SIRWS model, instead, proved to be much richer, with parameter regimes allowing for damped oscillations or sustained oscillations, or both.

The applications of such simplified models to actual data have to be viewed with some caution. Indeed, the fact that the solutions are exponentially close to the S-axis implies that, if ϵ is small, the values predicted for $I(t)$ are, over long stretches of time, very close to 0. Thus, in reality the infection will be prone to extinction, and may depend on reinfections from outside for persistence (see the discussion in [16] about the minimum community size). Our analysis aims at the qualitative properties of the system, rather than at precise predictions.

For our analysis we have combined techniques from GSPT, and in particular the entry-exit function, introduced in section 2.2.2. One must point-out that GSPT is usually employed for

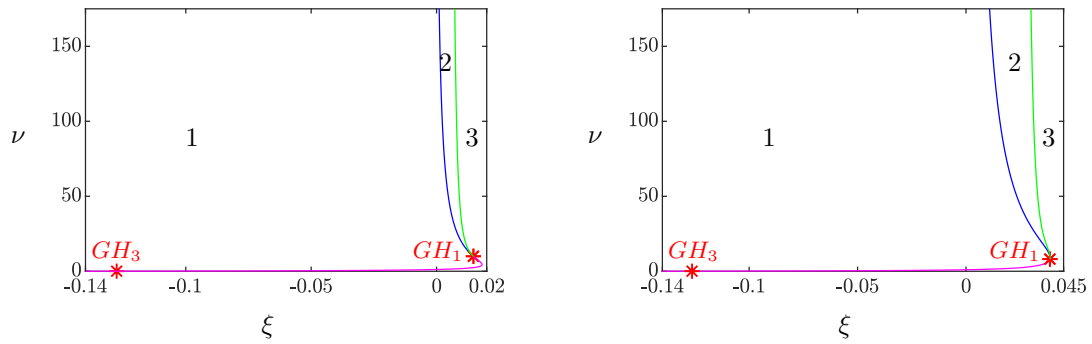

Figure 2.17: Two parameter bifurcation diagram for (2.35). Left and right represent $\epsilon = 1$ and $\epsilon = 0.05$, respectively. The red points labelled GH_i are generalised Hopf points. The blue (resp. magenta) branch is a curve of subcritical (resp. supercritical) Hopf bifurcation while the green branch corresponds to a limit point of cycles. Thus, we label the regions in the diagram according to the attractor as 1: Limit cycles, 2: Bistability, and 3: Point attractor.

singular perturbation problems in standard form, and just recently it has been shown that non-standard problems can also be dealt with. More precisely, GSPT allowed us to show the existence of stable limit cycles for certain parameter ranges. Based on such analysis, we further performed numerical studies and computed several insightful bifurcation diagrams, which allowed us to provide a complete qualitative description of the perturbed SIRWS model.

We concluded comparing previous results appearing in [11], and extending them by taking into account the role of the (small) parameter ϵ, which does not change the overall qualitatively behaviour of the system, but it does drastically change the parameter ranges corresponding to each dynamic regime. The parameter region characterized by stable limit cycles becomes unbounded as ϵ tends to 0. It would be interesting to properly analyse this extra singular behaviour. Likewise, our analysis does not suggest the presence of MMOs, however it would be interesting to consider such problem more thoroughly in epidemic models under further conditions, see for example [19]. We leave these, and other interesting problems motivated by our work, as future research topics to be explored.

Finally, our studies show that GSPT together with numerical tools seem to be suitable to analyse and comprehend epidemiological models with vastly different rates.

Once the bifurcation structure of epidemic models is known, one can then be more ambitious and aim to not only control epidemic outbreaks better after they have occurred but even try to anticipate them using early-warning signs [69, 87]. Therefore, our results on bifurcation structure presented here are strongly expected to contribute to the design of these warning signs.

3. A geometric analysis of the SIRS epidemiological model on a homogeneous network

3.1 Introduction

Mathematical epidemics modelling is, now more than ever, an important and urgent field to explore. A deep understanding of how diseases evolve and spread can give, and has given, us strategies to contain, treat and even prevent them.
Over the years, mathematical modellers have made a variety of different assumptions, in order to obtain a tractable trade-off between simplicity, which allows for more in-depth analysis, and realism, which allows to make more precise predictions.
In particular, compartment models build on the core idea that the population can, at any time, be portioned into compartments characterized by a specific state with respect to the ongoing epidemic. The first of such models divides the population into Susceptible, Infected and Recovered individuals, from which the SIR acronym is used. A Susceptible can become Infected ($S \to I$) by making contact with an already infected individuals, and can then either Recover ($I \to R$) or die, if we assume the disease to be characterized by permanent immunity after a first infection. If we do not make such an assumption, and allow recovered individuals to become susceptible again ($R \to S$), we obtain a so called SIRS model. Many more models, with different compartments, have been proposed and analysed in the past, see e.g. [32, 59, 11, 23].
Classical compartmental models are based on the homogeneous mixing assumption, i.e. the assumption that any individual in a population may have contacts with any other. Such an assumption, however, is quite unrealistic for many situations in which the observed population is large, and possibly divided in classes, families or generally sub-populations. One possible extension is to subdivide the population into groups, assuming homogeneous mixing within each group, but representing inter-group interactions through a contact matrix [65]. Another possible approach is to take into account the network structure of contacts. Often, epidemic dynamics on a network is analysed only through simulations [61, 75, 89, 9, 84, 22]. The method of pair approximations, introduced in epidemiology by Satō et al. [71] and Keeling et al. [41], allows to build a system of differential equations that retains some aspects of the network structure. The ideas and some applications of the methods are presented in detail in the monograph by Kiss et al. [46]. However, not much analytical progress has been made in the study of the resulting systems, possibly because they are generally rather complex.
This chapter aims at introducing methods from Geometric Singular Perturbation Theory (GSPT) to analyse these systems, building on the ideas introduced in Chapter 2. The difference in time-scales between epidemic spread and demographic turnover, which can be observed in many

diseases, is the motivation for the use of techniques from GSPT. We refer to Chapter 2 for a brief introduction of the techniques we use, or to the references therein, and in particular to [39] and [51], for a more detailed explanation. In particular, we will exploit the *entry-exit function* [12, 13] to analyse the behaviour of the system on its critical manifold, which is characterized by a change in stability over a hyperplane.
In this work, we assume homogeneity of the network, in order to obtain analytical results, before validating them numerically. Even with such an assumption, the additional complexity brought by the network structure must be treated properly. In fact, in order to completely describe the evolution of a network in time, one needs to have an equation for each possible state of its nodes, one for each possible state of its edges (along which the epidemic spreads), one for each possible state of triples, i.e. three nodes connected by two edges, and so on. This procedure, however, would generate an infinite system of ODEs, which would once again be hardly treatable with analytical tools. In order to overcome this difficulty, one can apply the so-called *moment closure* [52, 46], i.e. approximation formulas which allow us to truncate the dimension of the objects we want to analyse. If we truncate at the node level, we lose the network structure, and we recover a homogeneously mixing system. Instead, we truncate at the edge level, using the pair approximation discussed above, and analyse the system which derives from this choice.
To our knowledge, there are relatively few articles in which GSPT has been applied rigorously to epidemics models [70, 29, 90, 7, 85]; however, for most infectious diseases, the presence of different time scales is natural. Moreover, though a SIR model on networks has been studied with moment closure already [5, 46], the SIRS extension has not. Likewise, a thorough bifurcation analysis on compartment models such as the one we analyse in this chapter is not present in the literature.
The additional feature of the network structure, even in its most simplified version, i.e. homogeneous network, unravels new dynamics for the SIRS system we study. Indeed, there exists a set in the parameter space which allows the system to exhibit a stable limit cycle. To complement the bifurcation analysis, we extend the geometrical argument from Chapter 2 to the higher dimensional system we study, providing additional justification for the existence of stable limit cycles.
It is worth noticing that the model we study is not globally in fast-slow standard form; as in [53, 48] and Chapter 2, the fast-slow dynamics are only evident in specific regions of the phase space, in which a local change of coordinates brings the system to a standard two time scales form. In particular, we refer to the very recent monograph [86], in which the properties of perturbed systems in non-standard form are thoroughly analysed.
The chapter is structured as follows: in Section 3.2, we recall the derivation of the model, and introduce the moment closure technique. In Section 3.3, we obtain analytical results on the model, in particular on the fast and slow limit systems and on the application of the entry-exit function. In Section 3.4, we perform a bifurcation analysis and numerical exploration of the model. Finally, in Section 3.5, we conclude with a summary of the results, and with possible research outlooks.

3.2 Formulation of the SIRS model on a network

In this section we describe and propose an SIRS model for epidemics on graphs, building on the model proposed in [46, Sec. 4.2.2]. We are interested in the graph generalization of the model studied in Chapter 2, in order to drop the homogeneous-mixing hypothesis, under which we assumed that each individual in the population could have contacts with any other. We then assume loss of immunity to be slower, compared to the other rates (this is the case e.g.

for pertussis [11, 55], and it could potentially be true for the recent SARS-CoV-2 [47, 68]); this assumption brings the model to a non-standard perturbed system of ODEs, which we study with techniques from GSPT.

3.2.1 The model

The construction of the model is essentially what is presented in detail in [46, Ch. 4], extended to the SIRS case. For ease of reading, we briefly repeat the whole method.
We consider a network of N nodes, with N large, representing the individuals of a population, and we assume this network to be homogeneous, meaning that each node has fixed degree $n \in \mathbb{N}_{\geq 2}$, representing the number of direct neighbours each individual has. We assume the network to be undirected and connected, meaning that, given any two nodes in the network, there is a finite sequence of edges (or an *undirected path*) which starts in the first and ends in the second.
Each node can be in three states, namely S (susceptible), I (infected) or R (recovered). We will indicate the number of each state at time t with $[\cdot](t)$; we stress the distinction between the notation X, indicating a state, and $[X]$, indicating the number of individuals in the state X. We indicate the number of edges connecting a node in state X to one in state Y at time t with $[XY](t)$ for all $t \geq 0$. We distinguish between an edge XY, counted starting from a node in state X, and the same edge counted starting from the other node in state Y, for a reason of conserved quantities, namely (3.7a), (3.7b) and (3.7c) to be defined below. For example, we count the number of edges SI by "visiting" each node in state S, and counting all its neighbours in state I, then summing over all the nodes in state S; this implies that, at all times, by definition, $[SI] = [IS]$. The edges connecting a node with another in the same state, such as SS, hence, will always be counted twice.
Infection can only spread if a node in state S is connected to a node in state I through an edge SI; we denote the infection rate with $\beta \geq 0$. Nodes in state I recover, independently from their neighbours, at a rate $\gamma > 0$; and nodes in state R lose their immunity, again independently from their neighbours, at a slow rate ϵ, with $0 < \epsilon \ll \beta, \gamma$. Based upon these modelling assumptions, it is then straightforward to prove using the master equation of the epidemic model, that one obtains the following system of ODEs:

$$\begin{aligned} [S]' &= -\beta[SI] + \epsilon[R], \\ [I]' &= \beta[SI] - \gamma[I], \\ [R]' &= \gamma[I] - \epsilon[R]. \end{aligned} \tag{3.1}$$

From our assumptions, the sum of $[S] + [I] + [R] \equiv N$ is conserved at all times; we normalize by dividing both nodes and edges by N, and we do not rename the new variables, which now indicate the density of nodes, and a rescaled fraction of edges, in each state. Now $[S] + [I] + [R] \equiv 1$, so we can reduce the dimension of system (3.1) by removing $[R]$, obtaining the system

$$\begin{aligned} [S]' &= -\beta[SI] + \epsilon(1 - [S] - [I]), \\ [I]' &= \beta[SI] - \gamma[I]. \end{aligned} \tag{3.2}$$

In order to fully describe the dynamics of the system, we need an ODE for $[SI]$ as well. To understand how the number of edges $[SI]$ evolve in time, we need to consider the role of triples, as exemplified in Figure 3.1. A triple is a path of length 2 through a central node in state Y, connected to two nodes in state X and Z, respectively; we indicate such a triple with XYZ. The positions of X and Z are interchangeable, and the most important node is the central one, as we will explain shortly.

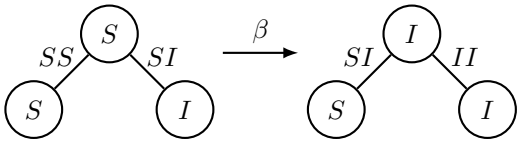

Figure 3.1: Example of the role of triples. The rightmost edge (of the triple on the left) turns from SI to II because the infection spreads to the central node; the leftmost edge turns from SS to SI because it belongs to a triple SSI.

The only change of the system which depends on the presence of a specific edge is the contagion which brings $SI \to II$. Direct neighbours of a node in the state S which get infected, i.e. the node X in a triple XSI, see their edge XS change to XI due to their belonging to the triple. The two other possible changes in the system, namely the recovery (a node in state I becoming R, which happens at a rate γ) and the loss of immunity (a node in state R becoming S, which happens at a rate ϵ) only happen at a node level, so the only nodes which see this change are the direct neighbours of the node changing state, and we do not need to consider their belonging to a triple.

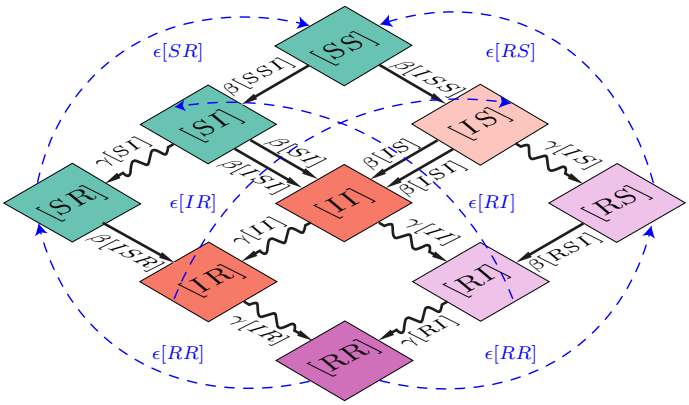

Figure 3.2: Complete description of the edges dynamics considering edges and triples. Straight lines: infections; wobbly lines: recovery; dashed lines: loss of immunity. The base diagram is the same which appears in [46], to visually describe their SIR model; the new, slow dynamics in our model are the dashed blue arrows, symbolizing loss of immunity.

For clarity, we fix a lexicographic order $S \prec I \prec R$ for nodes and edges, and write the explicit equations for the edges which follow this order only. If we take into account all the triples with a central node in state S and at least one node I, which could infect the central one (as described in Figure 3.2), we obtain the following system of ODEs, which describes the evolution in time of

nodes and edges:

$$\begin{aligned}
[S]' &= -\beta[SI] + \epsilon(1 - [S] - [I]),\\
[I]' &= \beta[SI] - \gamma[I],\\
[SS]' &= 2\epsilon[SR] - 2\beta[SSI],\\
[SI]' &= -(\gamma+\beta)[SI] + \epsilon[IR] + \beta[SSI] - \beta[ISI],\\
[SR]' &= \gamma[SI] - \epsilon[SR] + \epsilon[RR] - \beta[ISR],\\
[II]' &= 2\beta[SI] - 2\gamma[II] + 2\beta[ISI],\\
[IR]' &= \gamma[II] - (\gamma+\epsilon)[IR] + \beta[ISR],\\
[RR]' &= 2\gamma[IR] - 2\epsilon[RR].
\end{aligned} \tag{3.3}$$

Notice the 2 which multiplies the right hand sides of edges connecting nodes in the same state: as we mentioned above, they are always counted twice, whether they are created or lost. To fully describe the system, we would then need to have ODEs for triples, quadruples, etc. Instead, we proceed as in [46], and apply *moment closures*.

3.2.2 Moment closures

Moment closure methods are approximation methods used in many contexts, in order to reduce large (or infinite) dimensional systems of equations to a smaller finite dimension [52]. Proceeding as in [46, Sec. 4.2], one can approximate the edges as functions of the nodes, or triples as functions of nodes and edges. If we choose the first option, assuming independence between the state of nodes, we can approximate all edges as follows:

$$[XY] \approx n[X][Y]. \tag{3.4}$$

This implies that we lose the network structure and, up to rescaling the infection parameter by $\tilde{\beta} = n\beta$, we recover the SIRS system already studied in Chapter 2.

Lemma 6. *Consider* (3.2). *Applying approximation* (3.4) *and rescaling* $\tilde{\beta} = n\beta$, *one recovers the* SIRS *system studied in Chapter 2, which is characterized by an asymptotic stability of the endemic equilibrium for orbits starting in the set* $\left\{(S,I,R) \in \mathbb{R}^3_{\geq 0} \mid S+I+R \leq 1, I > 0\right\}$.

Instead, in this chapter we choose to apply the second order approximation, and hence we approximate each triple with the formula given in equation (4.6) of [46], namely

$$[XYZ] \approx \frac{n-1}{n}\frac{[XY][YZ]}{[Y]}. \tag{3.5}$$

This approximation is based on the conditional independence between the states of neighbors of a node, using a counting argument, which for clarity we recall from [46]. The total number of edges starting from a node in state Y is $n[Y]$, while the total number of edges in state XY is $[XY]$; this means that a fraction $[XY]/(n[Y])$ of edges starting from a node in state Y reach a node in state X. With the same procedure, we obtain a fraction $[YZ]/(n[Y])$ of edges which connect a node in state Y, from which we start, with one in state Z. Hence, selecting a node in state Y and two of his direct neighbours u and v, and using the conditional independence of u and v, the probability of them forming a triple XYZ is $[XY][YZ]/(n^2[Y]^2)$. Combinatorics tell us there are $n(n-1)$ ways of picking u and v, and $[Y]$ nodes in state Y; multiplying $n(n-1)\cdot[Y]\cdot[XY][YZ]/(n^2[Y]^2)$, we obtain formula (3.5).

3.3 Analysis of the model

In this section we present the pair approximation SIRS model, and give our main analytical results. First, we are going to reduce the dimension of the system, exploiting three conserved quantities. Second, we are going to introduce a formulation for the basic reproduction number for the system, and we describe the behaviour of the fast limit system. Third, we are going to derive the equilibria of the system in the biologically relevant region, and we show that the slow manifold of our perturbed system is exponentially close to the critical manifold. Last, we are going to rescale the system in an $\mathcal{O}(\epsilon)$-neighbourhood of the critical manifold, with a scaling similar to the one proposed in Chapter 2, and we apply the entry-exit procedure.
Throughout the analysis, we notice that the parabola $[SS] = n[S]^2$, i.e. approximation (3.4) applied to the edges in state $[SS]$, on the critical manifold is of particular importance for the dynamics.

3.3.1 Fast-slow model

In this section, we derive the system we will study for the remainder of the chapter, applying moment closure to (3.3) and reducing its dimension.

Recall Definition 1. Applying approximation (3.5) to every triple in system (3.3), we obtain the following singularly perturbed autonomous system, which is not in the standard form (2.2):

$$\begin{aligned}
[S]' &= -\beta[SI] + \epsilon(1 - [S] - [I]),\\
[I]' &= \beta[SI] - \gamma[I],\\
[SS]' &= 2\epsilon[SR] - 2\beta\frac{n-1}{n}\frac{[SS][SI]}{[S]},\\
[SI]' &= -(\gamma+\beta)[SI] + \epsilon[IR] + \beta\frac{n-1}{n}[SI]\left(\frac{[SS]}{[S]} - \frac{[SI]}{[S]}\right),\\
[SR]' &= \gamma[SI] - \epsilon[SR] + \epsilon[RR] - \beta\frac{n-1}{n}\frac{[SI][SR]}{[S]},\\
[II]' &= 2\beta[SI] - 2\gamma[II] + 2\beta\frac{n-1}{n}\frac{[SI]^2}{[S]},\\
[IR]' &= \gamma[II] - (\gamma+\epsilon)[IR] + \beta\frac{n-1}{n}\frac{[SI][SR]}{[S]},\\
[RR]' &= 2\gamma[IR] - 2\epsilon[RR],
\end{aligned} \tag{3.6}$$

in which, as from our assumptions, the processes of infection and recovery are fast, and the process of loss of immunity is slow. By construction, the sum of all the edges starting from a node in the state $[S]$ (or $[I]$ or $[R]$, respectively) is equal to

$$[SS] + [SI] + [SR] = n[S], \tag{3.7a}$$
$$[SI] + [II] + [IR] = n[I], \tag{3.7b}$$
$$[SR] + [IR] + [RR] = n[R], \tag{3.7c}$$

which allows us to remove the equation governing $[SR]$ (and $[IR]$ and $[RR]$, respectively). This can be checked by carefully computing the difference of the derivatives of the right hand side(s)

and the left hand side(s) of (3.7). By doing so, we reduce the dimension of the system, obtaining

$$[S]' = -\beta[SI] + \epsilon(1 - [S] - [I]), \tag{3.8a}$$
$$[I]' = \beta[SI] - \gamma[I], \tag{3.8b}$$
$$[SS]' = 2\epsilon(n[S] - [SS] - [SI]) - 2\beta\frac{n-1}{n}\frac{[SS][SI]}{[S]}, \tag{3.8c}$$
$$[SI]' = -(\gamma+\beta)[SI] + \epsilon(n[I] - [SI] - [II]) + \beta\frac{n-1}{n}[SI]\left(\frac{[SS]}{[S]} - \frac{[SI]}{[S]}\right), \tag{3.8d}$$
$$[II]' = 2\beta[SI] - 2\gamma[II] + 2\beta\frac{n-1}{n}\frac{[SI]^2}{[S]}. \tag{3.8e}$$

The *basic reproduction number* R_0 can be obtained [46, p. 140] for the limit as $\epsilon \to 0$ of system (3.8) as

$$R_0 = \frac{\beta(n-2)}{\gamma}. \tag{3.9}$$

We notice that, for (3.9) to be well-defined and dependent on the parameters of the system, we need $n > 2$. The equality $n = 2$ describes the very special case of a ring network, i.e., a connected network in which all nodes have exactly two neighbours. In the remainder of the chapter we assume $R_0 > 1$ and $n > 2$.

Remark 4. *We notice that the threshold $R_0 \lessgtr 1$ in (3.9) is equivalent to*

$$R_1 := \frac{\beta(n-1)}{\beta+\gamma} \lessgtr 1 \iff R_2 := \frac{\beta n}{2\beta+\gamma} \lessgtr 1, \tag{3.10}$$

since they all correspond to $\beta(n-2) \lessgtr \gamma$. A formula corresponding to R_1 is given in [46], shortly after the definition of R_0.

We notice that R_1 has a much more intuitive biological interpretation than R_0. Consider a network with all the nodes in susceptible state S, except one in state I. Consider one of the n edges in state IS: this could either transition to RS, at a rate γ, and the epidemics would die out immediately, or spread the infection to the node in state S, at a rate β, and become an edge II. If the latter happens, with probability $\beta/(\beta+\gamma)$, $(n-1)$ new edges move to state SI; hence, R_1 can be interpreted in the classical meaning of "the number of edges infections caused by one infected edge in an otherwise susceptible population". Recall that the disease spreads only through edges SI (or IS, equivalently), so their number should be the quantity we measure in order to quantify the contagiousness of the disease; an edge II can not be used to spread the disease.
Now we compute the basic reproduction number R_1 for system (3.8) and $\epsilon > 0$ sufficiently small.

Proposition 4. *The basic reproduction number R_1 for system (3.8) is given by*

$$R_1 = \frac{\beta(n-1)(\gamma+\epsilon)}{\gamma(\gamma+\beta+\epsilon)}. \tag{3.11}$$

Proof. We use the method first introduced in [17], and then generalized in [82] (see also [18]). We linearize system (3.6) at the disease free equilibrium

$$([S],[I],[SS],[SI],[SR],[II],[IR],[RR]) = (1,0,n,0,0,0,0,0)$$

focusing on the infected compartments. In this case we choose as variables describing the infected compartments $[SI]$, $[II]/2$ and $[IR]$ obtaining

$$\begin{pmatrix} [SI] \\ [II]/2 \\ [IR] \end{pmatrix}' = A \begin{pmatrix} [SI] \\ [II]/2 \\ [IR] \end{pmatrix},$$

with the matrix A given by

$$A = \begin{pmatrix} \beta(n-2)-\gamma & 0 & \epsilon \\ \beta & -2\gamma & 0 \\ 0 & 2\gamma & -(\gamma+\epsilon) \end{pmatrix}.$$

We split $A = M - V$, with V invertible, M and V^{-1} having non-negative entries. There are clearly many ways of doing that, but the preferred splitting is such that M and V can be interpreted as the *transmission* (i.e. relative to new infections) and *transition* matrix (i.e. relative to any other change of state), respectively. Then, we compute

$$R_1 = \rho(MV^{-1}),$$

where ρ indicates the spectral radius of a matrix. The choice for the two matrices is

$$M = \begin{pmatrix} \beta(n-1) & 0 & 0 \\ 0 & 0 & 0 \\ 0 & 0 & 0 \end{pmatrix}, \quad V = \begin{pmatrix} \gamma+\beta & 0 & -\epsilon \\ -\beta & 2\gamma & 0 \\ 0 & -2\gamma & \gamma+\epsilon \end{pmatrix}.$$

It can easily be checked, then, that V^{-1} has non-negative entries, and that, since MV^{-1} has two rows of zeros,

$$\rho(MV^{-1}) = (MV^{-1})_{1,1} = R_1 := \frac{\beta(n-1)(\gamma+\epsilon)}{\gamma(\gamma+\beta+\epsilon)}. \tag{3.12}$$

This finishes the proof. □

Remark 5. *The perturbed R_1 given in (3.11) has a similar biological interpretation for the perturbed system to the one given for the corresponding R_1 (3.10) of the limit system as $\epsilon \to 0$. We need to compute R_1, the average number of SI edges produced by an SI edge in a totally susceptible population; as in the previous case, an edge SI will become an edge II with probability $\beta/(\beta+\gamma)$, producing in this case $n-1$ edges SI; however, the original edge II, after having become IR can become again an IS edge with probability $\epsilon/(\epsilon+\gamma)$. After having returned SI, the edge will produce other R_1 SI edges, since the pairwise model does not consider higher order correlation and does not "remember" that the neighbours of S had already been infected once. Hence*

$$R_1 = \frac{\beta}{\beta+\gamma}\left(n-1+\frac{\epsilon}{\epsilon+\gamma}R_1\right),$$

from which one obtains (3.12).
Through this argument, we see that threshold for the SIRS model is different from the one for the SIR model, while in the homogeneous mixing case the two coincide.

Lemma 7. *System (3.8) is well posed in the convex set*

$$\begin{aligned} \Delta = \{([S],[I],[SS],[SI],[II]) \in \mathbb{R}^5_{\geq 0} | \\ 0 \leq [S]+[I] \leq 1\} \cap \{0 \leq [SS]+[SI] \leq n[S], 0 \leq [SI]+[II] \leq n[I]\}. \end{aligned} \tag{3.13}$$

The set is forward invariant under the flow of (3.8), for $\epsilon \geq 0$, so that solutions of (3.8) are global in time.

Proof. Apparently the right-hand side of (3.8) has a singularity at $[S] = 0$; however, in the set Δ, the terms $[SI]/[S]$ and $[SS]/[S]$ are both bounded by n, so that the right-hand side is indeed Lipschitz. Hence, system (3.8) has a local solution. Furthermore, it can be easily checked that the system is forward invariant by showing that the flow is pointing inwards on the boundary of Δ. Hence, solutions of system (3.8) are global in time. □

3.3.2 Fast limit

In this section, we study the fast subsystem (or layer equations) corresponding to the limit of system (3.8) as $\epsilon \to 0$ on the fast time scale. Hence, we have to take the limit $\epsilon \to 0$ in system (3.8), to obtain the layer equations

$$[S]' = -\beta[SI], \tag{3.14a}$$
$$[I]' = \beta[SI] - \gamma[I], \tag{3.14b}$$
$$[SS]' = -2\beta\frac{n-1}{n}\frac{[SS][SI]}{[S]}, \tag{3.14c}$$
$$[SI]' = -(\gamma+\beta)[SI] + \beta\frac{n-1}{n}[SI]\left(\frac{[SS]}{[S]} - \frac{[SI]}{[S]}\right), \tag{3.14d}$$
$$[II]' = 2\beta[SI] - 2\gamma[II] + 2\beta\frac{n-1}{n}\frac{[SI]^2}{[S]}. \tag{3.14e}$$

For ease of notation, we introduce

$$[\cdot]_0 = [\cdot](0),$$
$$[\cdot]_\infty = \lim_{t\to+\infty}[\cdot](t).$$

In the fast dynamics, the susceptible population can only decrease, and eventually the infected population will not have any more susceptibles to "recruit" and will decrease as well. In particular, we prove the following:

Proposition 5. *Consider system (3.14); $[S]$ and $[SS]$ are decreasing for all $t \geq 0$, and they tend to positive constants $[S]_\infty$ and $[SS]_\infty$. The variables $[I]$, $[SI]$, $[II]$ and $[IR]$ all have the limit $[I]_\infty = [SI]_\infty = [II]_\infty = [IR]_\infty = 0$.*

Proof. We proceed to show the claims of the proposition: for $[SS]$ (and implicitly for $[SR]$, referring to (3.7a)), we give the limit value as a function of $[S]_\infty$, $[S]_0$ and $[SS]_0$. We introduce the auxiliary variables $u := \frac{[SI]}{[S]}$ and $v := \frac{[SS]}{[S]}$. From (3.14a) and (3.14d) we see that

$$u' = -(\gamma+\beta)u + \beta u\left(\frac{n-1}{n}v + \frac{1}{n}u\right),$$

while from (3.14a) and (3.14c) we see that

$$v' = -\beta\frac{n-2}{n}uv. \tag{3.15}$$

From our analysis, for any initial point we have $0 \leq [SS] + [SI] \leq n[S]$ and $[SS], [SI] \geq 0$. This implies that, for all times

$$u \geq 0, \quad v \geq 0, \quad u + v \leq n.$$

Note that from (3.15) v is clearly decreasing for $n > 2$, and we see that

$$u' + v' = -\gamma u - \beta u\left(1 - \frac{u+v}{n}\right) < 0. \tag{3.16}$$

Recall Lemma 7, which implies $v \geq 0$; if $v = 0$, then $[SS] = 0$, and from equation (3.14c) we observe that $[SS]$ will not change, so 0 is its corresponding limit value. Assume then $v > 0$: since $v' < 0$, $v \to v_\infty$ monotonically as $t \to \infty$, and since $0 \leq u + v \leq n$, this implies that $u \to u_\infty$ as $t \to \infty$ as well. Then we notice that

$$0 < -\int_0^\infty (u'(z) + v'(z))\, \mathrm{d}z = u_0 + v_0 - u_\infty - v_\infty < \infty. \tag{3.17}$$

We notice that we can rewrite (3.17) using (3.16) and obtain

$$\infty > -\int_0^{+\infty} (u'(z) + v'(z))\mathrm{d}z = \int_0^{+\infty} \left(\gamma u(z) + \beta u(z)\left(1 - \frac{1}{n}(u(z) + v(z))\right)\right)\mathrm{d}z \tag{3.18}$$

$$> \gamma \int_0^{+\infty} u(z)\mathrm{d}z. \tag{3.19}$$

This means that

$$\int_0^{+\infty} u(z)\mathrm{d}z < +\infty \implies u_\infty = 0, \tag{3.20}$$

which implies, recalling that $[SI] = u[S]$ and $[S]_\infty < \infty$, that $[SI]_\infty = 0$. We can now rewrite (3.14a) as

$$[S]' = -\beta u[S],$$

which implies

$$[S]_\infty = [S]_0 \exp\left(-\beta \int_0^{+\infty} u(z)\mathrm{d}z\right) > 0, \tag{3.21}$$

Similarly, using (3.15), we can show that

$$v_\infty = v_0 \exp\left(-\beta \frac{n-2}{n} \int_0^{+\infty} u(z)\mathrm{d}z\right) > 0, \tag{3.22}$$

which implies, using (3.20) and (3.21), and recalling that $[SS] = v[S]$, that $[SS]_\infty > 0$. In particular, combining (3.21) and (3.22), we can write

$$[SS]_\infty = [SS]_0 \left(\frac{[S]_\infty}{[S]_0}\right)^{\frac{2n-2}{n}}. \tag{3.23}$$

We notice, from (3.7a), that this implies that $[SR]$ converges to a non-negative limit as well. Combining (3.14a) and (3.14b) as above, we show that $[I]$ vanishes as $t \to \infty$ as well:

$$[S]' + [I]' = -\gamma[I] < 0.$$

Since $[S] \to [S]_\infty$ as $t \to +\infty$, also $[I] \to [I]_\infty$. Proceeding as in (3.19), it can be shown that $[I]_\infty = 0$. This yields, by (3.7b), that $[II]_\infty = 0$ and $[IR]_\infty = 0$. □

Remark 6. *A relation between $[SS](t)$ and $[S](t)$ for system (3.14) analogous to (3.23) holds for all t. Indeed, noticing that*

$$V(t) = \ln([SS](t)) - 2\frac{n-1}{n}\ln([S](t)),$$

is a constant of motion for system (3.14), we observe that for any $t \geq 0$ the relation

$$[SS](t) = [SS]_0\left(\frac{[S](t)}{[S]_0}\right)^{\frac{2n-2}{n}}, \tag{3.24}$$

holds.

The equilibria of the limit system are all of the form $[S] = S^* \in [0,1]$, $[I] = 0$, $[R] = 1 - S^*$; $[SS] = SS^* \geq 0$, $[SI] = 0$, $[SR] = SR^* \geq 0$, $[II] = 0$, $[IR] = 0$, $[RR] = RR^* \geq 0$ with $SS^* + SR^* = nS^*$ and $SR^* + RR^* = n(1 - S^*)$; i.e., they lie on the critical manifold (3.25).
The eigenvalues of the linearization of system (3.8) on the critical manifold

$$\mathcal{C}_0 := \{([S],[I],[SS],[SI],[II]) \in \mathbb{R}^5_{\geq 0} | [I] = [SI] = [II] = 0\}, \tag{3.25}$$

are

$$\lambda_1 = \lambda_2 = 0,$$

corresponding to the slow variables $[S]$ and $[SS]$,

$$\lambda_3 = \frac{\lambda_4}{2} = -\gamma < 0,$$

and

$$\lambda_5 = \beta\frac{(n-1)[SS]}{n[S]} - (\gamma + \beta). \tag{3.26}$$

In particular, λ_5 changes sign on the hyperplane $\beta(n-1)[SS] - n(\gamma+\beta)[S] = 0$. We notice that $\beta(n-1) > 0$, since we suppose $n > 2$.
Considering (3.26), we define the *loss of hyperbolicity line* on the critical manifold $\mathcal{C}_0$

$$[SS] = \frac{n(\beta+\gamma)}{\beta(n-1)}[S] =: L[S]. \tag{3.27}$$

We now give a closed formula for the value of $[S]_\infty$.

Proposition 6. *Consider a generic initial condition $([S]_0, [SS]_0)$ in the repelling region of $\mathcal{C}_0$, i.e. satisfying $R_1[S]_0 > 1$ and $[SS]_0 > L[S]_0$. The entry point $[S]_\infty$ is given as the unique zero smaller than $[S]_0$ of the function*

$$H(x) = n\frac{\beta+\gamma}{\beta}(x^{\frac{1}{n}} - [S]_0^{\frac{1}{n}}) - [SS]_0([S]_0^{\frac{2}{n}-2}x^{1-\frac{1}{n}} - [S]_0^{\frac{1}{n}-1}). \tag{3.28}$$

Proof. We proceed as in [5, Sec. 3]. From our assumptions, $[SI](0) = \mathcal{O}(\epsilon)$.
Combining (3.14a), (3.14d) and (3.24), we obtain

$$[SI]' - \frac{n-1}{n}\frac{[SI]}{[S]}[S]' = \frac{\beta+\gamma}{\beta}[S]' - \frac{n-1}{n}[SS]_0[S]_0^{\frac{2}{n}-2}[S]^{\frac{n-2}{n}}[S]'.$$

Multiplying both sides by the integrating factor $[S]^{\frac{1-n}{n}}$ we obtain

$$\frac{\mathrm{d}}{\mathrm{d}t}\left([SI][S]^{\frac{1-n}{n}}\right) = \frac{\beta+\gamma}{\beta}[S]^{\frac{1-n}{n}}[S]' - \frac{n-1}{n}[SS]_0[S]_0^{\frac{2}{n}-2}[S]^{-\frac{1}{n}}[S]'. \tag{3.29}$$

Integrating (3.29) from $t=0$ to $t=+\infty$, and recalling that, by Proposition 5, $[SI]_\infty = 0$, we obtain

$$-[SI](0)S_0^{\frac{1-n}{n}} = n\frac{\beta+\gamma}{\beta}[S]^{\frac{1}{n}}\Big|_{t=0}^{+\infty} - [SS]_0[S]_0^{\frac{2}{n}-2}[S]^{\frac{n-1}{n}}\Big|_{t=0}^{+\infty}. \tag{3.30}$$

Since, by assumption, the left-hand side of (3.30) is $\mathcal{O}(\epsilon)$, we ignore it, and we consider the right-hand side only. Hence, we find $[S]_\infty$ by solving

$$n\frac{\beta+\gamma}{\beta}[S]^{\frac{1}{n}}\Big|_{t=0}^{+\infty} = [SS]_0[S]_0^{\frac{2}{n}-2}[S]^{\frac{n-1}{n}}\Big|_{t=0}^{+\infty},$$

from which we immediately obtain that $[S]_\infty$ is given as a zero of the function $H(x)$ defined in (3.28). We now prove that such a zero is unique.
Recall $\frac{[SS]_0}{[S]_0} \le n$; we have

$$H(0) = [S]_0^{\frac{1}{n}}\left(-n\frac{\beta+\gamma}{\beta} + \frac{[SS]_0}{[S]_0}\right) < 0, \quad H([S]_0) = 0.$$

Moreover,

$$H'(x) = \frac{\gamma+\beta}{\beta}x^{\frac{1}{n}-1} - \frac{n-1}{n}[SS]_0[S]_0^{\frac{2}{n}-2}x^{-\frac{1}{n}} = x^{\frac{1}{n}-1}\left(\frac{\gamma+\beta}{\beta} - \frac{n-1}{n}[SS]_0[S]_0^{\frac{2}{n}-2}x^{1-\frac{2}{n}}\right).$$

Recall (3.27). We see that $H'(x) > 0$ for

$$x < \left(\frac{L[S]_0}{[SS]_0}\right)^{\frac{n}{n-2}}[S]_0 =: [S]_*([S]_0, [SS]_0).$$

Clearly, $[S]_* = [S]_*([S]_0, [SS]_0) < [S]_0$, since we assumed $[SS]_0 > L[S]_0$. Lastly,

$$H'([S]_0) = [S]_0^{\frac{1}{n}-1}\left(\frac{\gamma+\beta}{\beta} - \frac{n-1}{n}\frac{[SS]_0}{[S]_0}\right) < 0 \quad \text{if} \quad [SS]_0 > L[S]_0.$$

Hence, $H(x)$ increases on the interval $[0, [S]_*)$, has a positive maximum in $x = [S]_*$, and then decreases towards 0; in particular, it has a unique zero on the interval $[0, [S]_*)$, and hence in the interval $[0, [S]_0)$. □

Remark 7. *Recall (3.27) and Proposition 5. Given a couple $([S]_0, [SS]_0)$ in the repelling region $\mathcal{C}_0^R$ above the line $[SS] = L[S]$ (i.e., where $\lambda_5 > 0$), its image under the fast flow (3.14), approximated up to $\mathcal{O}(\epsilon)$ by formulas (3.28) and (3.23), is in the attracting region $\mathcal{C}_0^A$ below the line $[SS] = L[S]$ (i.e., where $\lambda_5 < 0$); refer to Figure 3.3 for a visualization.*

Remark 8. *Recall (3.9), and that we assume $R_1 > 1$. Then $L = \frac{n(\beta+\gamma)}{\beta(n-1)} = \frac{n}{R_1} < n$. Hence, the purple line $[SS] = L[S]$ in Figure 3.3 is always below the line $[SS] = n[S]$.*

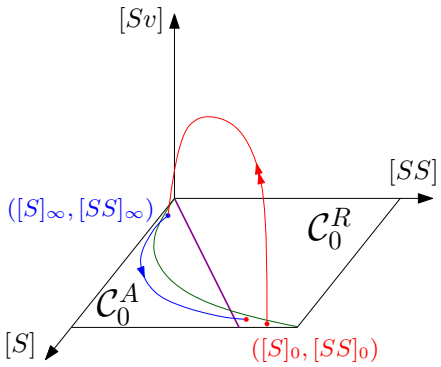

Figure 3.3: Red curve: evolution of the point $([S]_0, [SS]_0)$ under the fast flow. Blue curve: evolution of the point $([S]_\infty, [SS]_\infty)$ under the slow flow. Green curve: curve $[SS] = \alpha([S])$ defined in (3.39). Purple line: line of loss of hyperbolicity $[SS] = L[S]$ of the critical manifold of system (3.8), which divides the attracting region $\mathcal{C}_0^A$ and the repelling one $\mathcal{C}_0^R$.

3.3.3 Equilibria of the perturbed system

The following Lemma discusses the equilibria of system (3.8).

Proposition 7. *For $\epsilon > 0$ sufficiently small and $R_0 > 1$, system (3.8) has 2 equilibria in the relevant region of $\mathbb{R}^5$.*
Disease free equilibrium:

$$[S] = 1, \quad [I] = 0, \quad [SS] = n, \quad [SI] = 0, \quad [II] = 0.$$

Endemic equilibrium: *to their lowest order of ϵ the components are given by:*

$$\begin{aligned}
[S] &= \frac{(n-1)(\gamma+\beta)}{(n^2-n-1)\,\beta-\gamma} + \mathcal{O}(\epsilon),\\
[I] &= \epsilon\frac{n((n-2)\beta-\gamma)}{\gamma\,((n^2-n-1)\,\beta-\gamma)} + \mathcal{O}(\epsilon^2),\\
[SS] &= \frac{n(\gamma+\beta)^2}{\beta((n^2-n-1)\,\beta-\gamma)} + \mathcal{O}(\epsilon),\\
[SI] &= \epsilon\frac{n((n-2)\beta-\gamma)}{\beta\,((n^2-n-1)\,\beta-\gamma)} + \mathcal{O}(\epsilon^2),\\
[II] &= \epsilon\frac{n((n-2)\beta-\gamma)}{\gamma\,((n^2-n-1)\,\beta-\gamma)} + \mathcal{O}(\epsilon^2).
\end{aligned} \tag{3.31}$$

Proof. The disease free equilibrium is trivial. The endemic equilibrium is computed by expanding the variables in power series of ϵ, e.g. $[S] = S_0 + \epsilon S_1 + \mathcal{O}(\epsilon^2)$, substituting them in system (3.8), equating the right-hand sides to 0 and matching powers of ϵ. □

Remark 9. *Since we assume $R_0 = \frac{\beta(n-2)}{\gamma} > 1$, recall Remark 4 and (3.11), the numerators of $[I]$, $[SI]$ and $[II]$ of (3.31), as well as all the denominators, are strictly positive for $\epsilon > 0$ small enough.*

We notice that the disease free equilibrium belongs to $\mathcal{C}_0$ defined in (3.25), and by computing the corresponding $\lambda_5 = \beta(n-2) - \gamma = \gamma(R_0 - 1) - \mathcal{O}(\epsilon) > 0$, we show that it is unstable.

Moreover, we notice that the endemic equilibrium is $\mathcal{O}(\epsilon)$ close to the line $[SS] = L[S]$ defined in (3.27); hence, it approaches it as $\epsilon \to 0$.

3.3.4 Slow manifold

Next, we provide a multiple time scale description of the disease-free, or near disease-free states:

Proposition 8. *The slow manifold of system (3.8) is exponentially close in ϵ to the critical manifold $\mathcal{C}_0$ given by (3.25).*

Proof. The invariant manifold $\mathcal{C}_0$ is an invariant manifold also for system (3.8) with $\epsilon > 0$: by direct substitution, we have that $[I]'$, $[SI]'$ and $[II]'$ are zero on $\mathcal{C}_0$. Hence, $\mathcal{C}_0$ is invariant and satisfies all the conclusions of Fenichel's theorem, and so it is one possible slow manifold. By Fenichel's theorem, all slow manifolds are exponentially close to each other in the normally hyperbolic region; invariance allows us to extend at least one slow manifold across the line where we do not have normal hyperbolicity, namely $\mathcal{C}_0$. □

The slow dynamics on the slow manifold $[I] = [SI] = [II] = 0$ are given by:

$$\begin{aligned}[S]' &= \epsilon(1 - [S]),\\ [SS]' &= 2\epsilon(n[S] - [SS]),\end{aligned}$$

which, rescaling the system to the slow time variable $\tau = \epsilon t$, becomes

$$\begin{aligned}\dot{[S]} &= (1 - [S]),\\ \dot{[SS]} &= 2(n[S] - [SS]).\end{aligned} \tag{3.32}$$

Recall that $[S]_\infty$ and $[SS]_\infty$ are the initial conditions for the slow flow. Solving (3.32) explicitly yields

$$\begin{aligned}[S](\tau) &= ([S]_\infty - 1)e^{-\tau} + 1,\\ [SS](\tau) &= 2([S]_\infty - 1)ne^{-2\tau}(e^{\tau} - 1) + ([SS]_\infty - n)e^{-2\tau} + n,\end{aligned} \tag{3.33}$$

meaning that $[S] \to 1$, $[SS] \to n$ exponentially fast, as we would expect, since in the slow dynamics, on the node level, the variable $[R]$ can only decrease, and $[S]$ can only increase.
For its importance in the dynamics, we introduce the following notation

$$\Gamma := \{([S], [SS]) \in [0, 1] \times [0, n] | [SS] = n[S]^2\}. \tag{3.34}$$

Lemma 8. *The parabola Γ (3.34) is uniformly attracting for system (3.32).*

Proof. Recall (3.33). Then, introducing the function $d(\cdot)$ to indicate the distance between a point and the parabola, we have

$$\begin{aligned}d(\tau) = |[SS](\tau) - n[S]^2(\tau)| =& |2n([S]_\infty - 1)e^{-\tau} - 2n([S]_\infty - 1)e^{-2\tau} + ([SS]_\infty - n)e^{-2\tau} + n -\\ &-n([S]_\infty - 1)^2e^{-2\tau} - n - 2n([S]_\infty - 1)e^{-\tau}| = |e^{-2\tau}([SS]_\infty - n[S]_\infty^2)| = e^{-2\tau}d(0),\end{aligned}$$

which means that an orbit starting in any point $([S]_\infty, [SS]_\infty) \in (0, 1) \times (0, n)$ approaches exponentially fast the parabola Γ (3.34). □

Lemma 9. *Consider an orbit starting (i.e. exiting the slow manifold) $\mathcal{O}(\delta_2)$, where $0 < \delta_2 \ll 1$, away from the parabola $[SS] = n[S]^2$, in a point with $[S](0) = [S]_0$ in the repelling region of $\mathcal{C}_0$, i.e. satisfying $R_1[S]_0 > 1$, $[SS]_0 > L[S]_0$. Its entry point in the slow flow $[S]_\infty$ after a fast piece is given as the unique zero smaller than $[S]_0$ of*

$$G(x) = \frac{\beta+\gamma}{\beta}(x^{\frac{1}{n}} - [S]_0^{\frac{1}{n}}) - [S]_0^{\frac{2}{n}} x^{1-\frac{1}{n}} + [S]_0^{1+\frac{1}{n}}. \tag{3.35}$$

Proof. Notice that, considering Lemma 8, the assumption of starting close to the parabola is not restrictive. The derivation of $G(x)$ is analogous to the derivation of $H(x)$ of Proposition 6, using

$$[SS](t) = n[S]_0^{\frac{2}{n}} ([S](t))^{\frac{2n-2}{n}}$$

instead of (3.24), since we assume $[SS]_0 = n[S]_0^2$. The uniqueness of the zero is obtained applying Proposition 3 to this specific initial condition. □

Remark 10. *Recall (3.23). Since we showed that the parabola Γ (3.34) is attracting in the slow flow, we can assume that, after the first slow piece of any orbit, $[SS]_0 = n[S]_0^2 + \mathcal{O}(\delta_1)$, where $0 < \delta_1 \ll 1$. We can then rewrite (3.23) as*

$$[SS]_\infty = [SS]_0 \left(\frac{[S]_\infty}{[S]_0}\right)^{\frac{2n-2}{n}} \approx n[S]_0^2 \left(\frac{[S]_\infty}{[S]_0}\right)^{\frac{2n-2}{n}} = n[S]_\infty^2 \left(\frac{[S]_\infty}{[S]_0}\right)^{-\frac{2}{n}},$$

where the $\approx$ symbol indicates an $\mathcal{O}(\delta_1)$ error. For n large enough, the last factor is close to 1, and the entry point for the slow flow is approximately on the parabola.

3.3.5 Rescaling

As we showed in Section 3.3.2, under the fast flow eventually $[I]$, $[SI]$ and $[II]$ will be $\mathcal{O}(\epsilon)$; recall (3.7b), from which we see that $[I] = \mathcal{O}(\epsilon)$ implies $[SI], [II], [IR] = \mathcal{O}(\epsilon)$. Proceeding as in Chapter 2, we rescale $[I] = \epsilon[v]$. This implies, using (3.7b),

$$[SI] = \epsilon[Sv], \quad [II] = \epsilon[vv].$$

This brings the model, after rearranging the variables, to a singularly perturbed system of ODEs, namely

$$\begin{aligned}
[S]' &= -\epsilon\beta[Sv] + \epsilon(1 - [S] - \epsilon[v]),\\
[SS]' &= 2\epsilon(n[S] - [SS] - \epsilon[Sv]) - 2\epsilon\beta\frac{n-1}{n}\frac{[SS][Sv]}{[S]},\\
\epsilon[v]' &= \epsilon\beta[Sv] - \epsilon\gamma[v],\\
\epsilon[Sv]' &= -\epsilon(\gamma+\beta)[Sv] + \epsilon^2(n[v] - [Sv] - [vv]) + \epsilon\beta\frac{n-1}{n}[Sv]\left(\frac{[SS]}{[S]} - \epsilon\frac{[Sv]}{[S]}\right),\\
\epsilon[vv]' &= 2\epsilon\beta[Sv] - 2\epsilon\gamma[vv] + \epsilon^2\beta\frac{n-1}{n}\frac{[Sv]^2}{[S]},
\end{aligned} \tag{3.36}$$

which can be rewritten in a standard form, and rescaled to the slow time scale, denoting now the time derivative with an overdot, giving

$$\begin{aligned}
[\dot{S}] =& -\beta[Sv] + (1 - [S] - \epsilon[v]),\\
[\dot{SS}] =& 2(n[S] - [SS] - \epsilon[Sv]) - 2\beta\frac{n-1}{n}\frac{[SS][Sv]}{[S]},\\
\epsilon[\dot{v}] =& \beta[Sv] - \gamma[v],\\
\epsilon[\dot{Sv}] =& -(\gamma+\beta)[Sv] + \epsilon(n[v] - [Sv] - [vv]) + \beta\frac{n-1}{n}[Sv]\left(\frac{[SS]}{[S]} - \epsilon\frac{[Sv]}{[S]}\right),\\
\epsilon[\dot{vv}] =& 2\beta[Sv] - 2\gamma[vv] + \epsilon\beta\frac{n-1}{n}\frac{[Sv]^2}{[S]}.
\end{aligned} \tag{3.37}$$

Taking now the $\lim_{\epsilon\to 0}$, we obtain the system of algebraic-differential equations

$$\begin{aligned}
[\dot{S}] =& -\beta[Sv] + (1 - [S]),\\
[\dot{SS}] =& 2(n[S] - [SS]) - 2\beta\frac{n-1}{n}\frac{[SS][Sv]}{[S]},\\
0 =& \beta[Sv] - \gamma[v],\\
0 =& -(\gamma+\beta)[Sv] + \beta\frac{n-1}{n}\frac{[Sv][SS]}{[S]},\\
0 =& 2\beta[Sv] - 2\gamma[vv].
\end{aligned} \tag{3.38}$$

The last three equations of (3.38) are satisfied for $[v] = [Sv] = [vv] = 0$. This is exactly the critical manifold of (3.8), on which the dynamics is described by (3.32).
Using (3.32), we can show how λ_5 changes in time, in the slow flow, by deriving its formulation (3.26) with respect to time, obtaining

$$\dot{\lambda}_5 = \beta\frac{n-1}{n}\frac{2n[S]^2 - [SS]([S]+1)}{[S]^2}.$$

This implies that λ_5 is increasing if $[SS] < \alpha([S])$, where the function α is defined by

$$\alpha(x) = \frac{2nx^2}{x+1}. \tag{3.39}$$

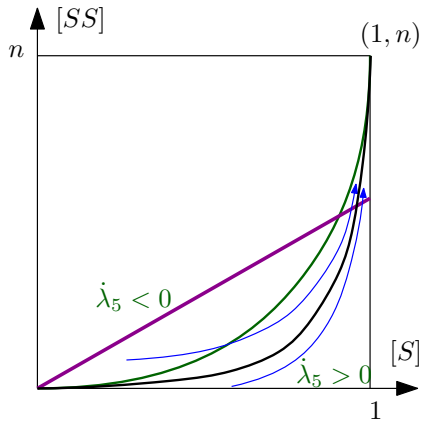

Figure 3.4: Sign of the derivative in time of λ_5 under the slow flow. Blue: sketch of orbit starting above/below the green curve $[SS] = \alpha([S])$. Purple: loss of hyperbolicity line $[SS] = L[S]$ (3.27). Black: the parabola Γ (3.34). Notice that orbits always land below the purple line, which is the region of the rectangle in which the critical manifold is attracting.

In Figure 3.4 we visualize the behaviour of two orbits in the slow dynamics. We note that, even if an orbit enters the slow flow in a point below the purple line but above the green curve, i.e. in the region where $\dot{\lambda}_5 < 0$, it eventually has to cross the green line before crossing the purple curve, since they represent respectively $\dot{\lambda}_5 = 0$ and $\lambda_5 = 0$. Hence, any orbit will eventually evolve in the region $\dot{\lambda}_5 > 0$. We prove the following:

Proposition 9. *The subset* $\{([S], [SS]) \in (0,1) \times (0,n) | \dot{\lambda}_5 > 0\}$ *is forward invariant for system (3.32).*

Proof. The normal vector to the curve $\alpha([S])$ is given by $\nu = (-\dot{\alpha}([S]), 1)$, with

$$\dot{\alpha}([S]) = \frac{2n[S]([S]+2)}{([S]+1)^2}.$$

If we take the scalar product of ν with the vector field F given by (3.32), we obtain

$$\nu \cdot F = 2\left(\frac{n(2[S]^3 + 3[S]^2 - [S])}{([S]+1)^2} - [SS]\right) < 2(\alpha([S]) - [SS]),$$

meaning that on the curve $[SS] = \alpha([S])$, this scalar product is negative, hence orbits approaching the curve from below will not cross it. □

Remark 11. *By comparing (3.34) and (3.39), we notice that the curve* α *is always above the parabola* Γ*; hence, by invariance of* Γ *and Proposition 9, an orbit starting above the parabola will eventually be "squeezed" between* α *and* Γ*.*

3.3.6 Entry-exit function

Dividing the last three equations of system (3.36) by ϵ on both sides, we obtain

$$\begin{aligned}
[S]' &= \epsilon(-\beta[Sv] + (1 - [S] - \epsilon[v])),\\
[SS]' &= \epsilon\bigg(2(n[S] - [SS] - \epsilon[Sv]) - 2\beta\frac{n-1}{n}\frac{[SS][Sv]}{[S]}\bigg),\\
[v]' &= \beta[Sv] - \gamma[v],\\
[Sv]' &= -(\gamma+\beta)[Sv] + \epsilon(n[v] - [Sv] - [vv]) + \beta\frac{n-1}{n}[Sv]\bigg(\frac{[SS]}{[S]} - \epsilon\frac{[Sv]}{[S]}\bigg),\\
[vv]' &= 2\beta[Sv] - 2\gamma[vv] + \epsilon\beta\frac{n-1}{n}\frac{[Sv]^2}{[S]}.
\end{aligned} \tag{3.40}$$

System (3.40) can be rewritten as

$$\begin{aligned}
x' &= \epsilon f(x,z) + \epsilon^2 m(z,w),\\
z' &= zg(x,z) + \epsilon h(x,z,w),\\
w' &= -Dw + Az + \epsilon l(x,z),
\end{aligned} \tag{3.41}$$

where we denote $x := \binom{[S]}{[SS]}$, $z := [Sv]$, and $w := \binom{[v]}{[vv]}$. The critical manifold $\mathcal{C}_0 = \{z = 0, w = \binom{0}{0}\}$ is invariant for system (3.41) both when $\epsilon > 0$ and $\epsilon = 0$. Recall (3.26); it is clear that $g(x,0) = \lambda_5 \lesseqgtr 0$ when $x \in \mathcal{C}_0^A$ or $x \in \mathcal{C}_0^R$, respectively.

To control the relation between the starting point of the slow dynamics and the transition point back to the fast dynamics, we are going to employ the entry-exit function [13]. This tool relies on calculating a fast variational equation along a slow orbit to calculate the exit point from the slow dynamics after a change from fast attraction to fast repulsion has taken place. We now describe this idea in more detail in our current setting, and we apply it to system (3.41).

Similarly to what was done in Chapter 2, we want to find a formulation for an entry-exit function to apply to system (3.41), in order to obtain more information on the slow part of the dynamics. We can not apply [60, equation (11)], since (3.41) has three fast variables; we refer to a generalization of such result, which is given in [72, p. 417]. However, one of the hypotheses necessary for the application of such formula is not satisfied on the whole critical manifold $\mathcal{C}_0$; namely, the separation of negative eigenvalues from the eigenvalue which causes the loss of stability. The eigenvalues on $\mathcal{C}_0$ are -2γ, $-\gamma$ and λ_5; the result can be applied to trajectories contained in the portion of $\mathcal{C}_0$ in which $\lambda_5 > -\gamma$. Recall (3.26): indeed, we have that $\lambda_5 \leq -\gamma$ if

$$[SS] \leq \frac{n-1}{n}[S].$$

For trajectories which lie completely in the region of $\mathcal{C}_0$ in which $[SS] > \frac{n-1}{n}[S]$, we can apply the entry-exit formula given as the function π in [72, p. 417] to system (3.41), obtaining formula (3.42). We conjecture that the same formula can be applied to the whole $\mathcal{C}_0$, and leave the proof of such conjecture as future research work.

We denote with $x_0 := ([S]_\infty, [SS]_\infty)$. Then, if $x(\tau; x_0)$ is the solution of

$$\begin{cases} \dot{x} &= f(x,0,0),\\ x(0) &= x_0, \end{cases}$$

we can implicitly compute the exit time T_E of an orbit on the slow manifold through the integral

$$\int_0^{T_E} g(x(\tau; x_0), 0)\mathrm{d}\tau = 0. \tag{3.42}$$

Recall (3.33); for ease of notation, we introduce $A := [S]_\infty - 1 < 0$ and $B := [SS]_\infty - n < 0$. Then, (3.42) becomes

$$\begin{aligned}\int_0^{T_E} \lambda_5(\tau)\mathrm{d}\tau = \int_0^{T_E} \Big(-(\gamma+\beta) + \beta\frac{n-1}{n}\frac{[SS](\tau)}{[S](\tau)}\Big)\mathrm{d}\tau = \\ \int_0^{T_E} \Big(-(\gamma+\beta) + \beta\frac{n-1}{n}\frac{2Ane^{-2\tau}(e^{\tau}-1)+Be^{-2\tau}+n}{Ae^{-\tau}+1}\Big)\mathrm{d}\tau = 0,\end{aligned} \tag{3.43}$$

which gives the following equation for T_E

$$\begin{aligned}-(\gamma+\beta)T_E + \beta\frac{n-1}{n}\Big(\frac{A^2nT_E + Ae^{-T_E}(2An-B) + (B-A(A+2)n)\ln(Ae^{-T_E}+1)}{A^2} \\ - \frac{2An-B}{A}\Big) = 0.\end{aligned} \tag{3.44}$$

Clearly, $T_E = 0$ is a solution of (3.44); the integrand of (3.43), i.e. λ_5, along the slow flow, is eventually always increasing, recall Proposition 9; as we remarked, even though it is negative in the first part of the flow, it becomes eventually (and definitely) positive.

Lemma 10. *The exit time T_E is finite for any initial point $([S]_\infty, [SS]_\infty) \in \mathcal{C}_0^A$.*

Proof. Recall (3.43). For small positive values of τ, $\lambda_5(\tau) < 0$, since the slow dynamics begins in the attracting region $\mathcal{C}_0^A$. Hence, for small values of $\tau \geq 0$ the integral

$$\int_0^{\tau} \lambda_5(\sigma)\mathrm{d}\sigma < 0.$$

From (3.44), we observe that

$$\lim_{T_E\to+\infty} \int_0^{T_E} \lambda_5(\sigma)\mathrm{d}\sigma = +\infty,$$

hence there exists at least one finite T_E which satisfies (3.42). From our previous analysis, we know that $\lambda_5(\tau) = 0$ only once during the slow flow, and it remains positive afterwards; hence, such T_E is unique. □

3.3.7 Application of the entry-exit formula to the parabola

As we have remarked so far, the parabola (3.34) is of particular interest for the dynamics, even more so for large values of n. Hence, we are interested in understanding the entry-exit relation on this specific invariant set. We now consider the evolution, under the slow flow, of the point $([S]_\infty, [SS]_\infty) = (0,0)$; with these initial conditions, (3.33) becomes

$$\begin{aligned}[S](\tau) &= 1 - e^{-\tau}, \\ [SS](\tau) &= n + ne^{-2\tau} - 2ne^{-\tau} = n[S]^2(\tau).\end{aligned} \tag{3.45}$$

Being able to write $[SS]$ as a function of $[S]$ allows us to compute the exit point for the origin, which in general is not possible, since λ_5 depends on both slow variables. Combining (3.45) and (3.43) we obtain

$$\begin{aligned}&\int_0^{[S]_1} \Big(\frac{-(\gamma+\beta)+\beta(n-1)x}{1-x}\Big)\mathrm{d}x = 0 \\ &\implies \beta(n-1)(1-[S]_1) + (\gamma-(n-2)\beta)\ln(1-[S]_1) - \beta(n-1) = 0, \\ &\implies -\beta(n-1)[S]_1 + (\gamma-(n-2)\beta)\ln(1-[S]_1) = 0,\end{aligned} \tag{3.46}$$

where $[S]_1$ indicates the exit point of the orbit which starts at the origin.
It can easily be shown, by direct substitution, that orbits with initial conditions $([S]_\infty, [SS]_\infty) = ([S]_\infty, n[S]_\infty^2)$ evolve, under the slow flow (3.33), along the curve $[SS] = n[S]^2$; moreover, this follows from Lemma 8. The exit point of such an orbit can be computed implicitly, with the same procedure as (3.46).

Lemma 11. *Orbits entering the slow flow in a point of the form* $([S]_\infty, [SS]_\infty) = ([S]_\infty, n[S]_\infty^2)$ *exit at a point of the form* $([S]_1, n[S]_1^2)$*, with* $[S]_1$ *given by*

$$-\beta(n-1)[S]_1 + (\gamma - (n-2)\beta)\ln(1-[S]_1) = -\beta(n-1)[S]_\infty + (\gamma-(n-2)\beta)\ln(1-[S]_\infty), \quad (3.47)$$

which can be equivalently rewritten, introducing for ease of notation $C := ((n-2)\beta-\gamma)/(\beta(n-1))$*, as*

$$(1-[S]_1)^C e^{[S]_1} = (1-[S]_\infty)^C e^{[S]_\infty}. \quad (3.48)$$

Proof. Straightforward computation from the integral in (3.46), where we substitute the lower bound of integration 0 with a generic $[S]_\infty$. □

Lemma 12. *If two entry points on the parabola satisfy* $[S]_{\infty,1} < [S]_{\infty,2}$*, then the corresponding exit points satisfy* $[S]_{1,1} > [S]_{1,2}$*.*

Proof. Recall that the parabola is invariant under the slow flow. The entry-exit relation (3.48) implicitly defines a function

$$h(x) := (1-x)^C e^x,$$

meaning that the entry-exit relation can be written as $h([S]_\infty) = h([S]_1)$ (see Figure 3.5 for a sketch of the function h, and a visualization of the argument of this proof). We observe that $h(0) = 1$ and $h(1) = 0$. Deriving $h(x)$, we see that

$$h'(x) = (1-x)^{C-1}(1-C-x)e^x > 0 \iff x < 1-C = \frac{\gamma+\beta}{(n-1)\beta} = \frac{1}{R_1}.$$

Hence, $h(x)$ is increasing before $x = 1/R_1$, decreasing afterwards. This implies that if $[S]_{\infty,1} < [S]_{\infty,2}$ we have that $h([S]_{\infty,1}) < h([S]_{\infty,2})$, and the corresponding exit points satisfy $[S]_{1,1} > [S]_{1,2} > 1/R_1$. □

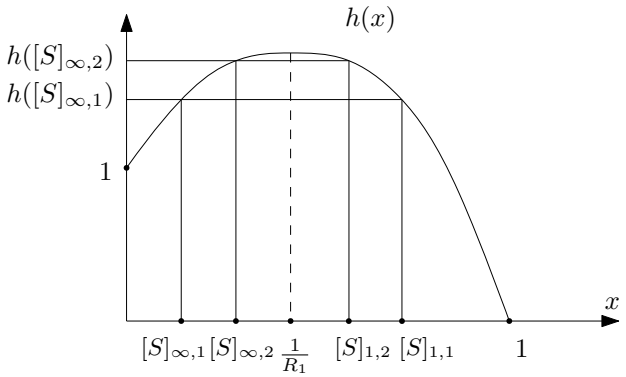

Figure 3.5: Sketch of the function $h(x)$ used in the proof of Lemma 12.

The study of the asymptotic behaviour of system (3.8) is then reduced to two 2-dimensional maps, from $\mathcal{C}_0$ to itself; specifically, we have that $\Pi_1([S]_0, [SS]_0) = ([S]_\infty, [SS]_\infty)$, while $\Pi_2([S]_\infty, [SS]_\infty) = ([S]_1, [SS]_1)$. We now explain the reasoning under the approximation that Π_1 and Π_2 map the parabola Γ to itself, and can hence be seen as near one-dimensional (see Figure 3.6); in fact, the occurrence of near one-dimensional return maps is an important theme in multiple time scale systems [6, 26, 50, 64].
Next, consider a point with $[S]$ coordinate $[S]_0$, $\mathcal{O}(\epsilon)$ away from the parabola Γ (3.34), in the repelling part of the critical manifold. Its image $[S]_\infty$ under the fast flow, which defines the map Π_1 sketched in Figure 3.6, is given by (3.35). We notice that this value depends on both β and γ, as well as on n. For n large enough, the entry point in the slow flow will be close to the parabola, as argued in Remark 10; hence, we will be able to compute its exit point $[S]_1$ using (3.47), which again depends explicitly on all the parameters of the system in a highly non-trivial way. This is different from the SIRWS model studied in Chapter 2, in which there was a clear separation between fast parameters, which dictated the fast dynamics, and had no influence on the slow one, and slow parameters, which characterised the viceversa. The map Π_2 in Figure 3.6 sketches the relation between the entry point $[S]_\infty$ and its corresponding exit point $[S]_1$, i.e. (3.35).

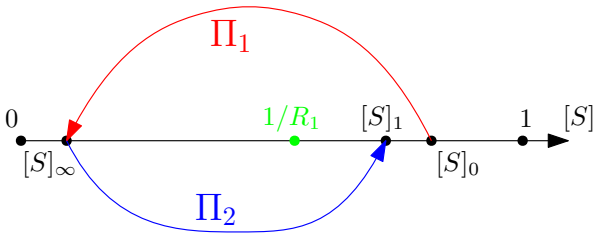

Figure 3.6: Sketch of the map which relates $[S]_0$ to $[S]_\infty$ (red) and $[S]_\infty$ to $[S]_1$ (blue). The green dot represents the value $1/R_1$: the epidemics can only start for values of $[S]_0 > 1/R_1$.

Depending on the relative position of $[S]_0$ and $[S]_1$, we might be able to deduce the asymptotic behaviour of the system. However, the high dimensionality of the layer equation and the complex implicit relation between $[S]_0$ and $[S]_\infty$ hinders the analysis of the system with non-numerical tools. See Figure 3.7 for comparisons between formula (3.35) and direct integration of the layer system (3.14).
We proceed now to a bifurcation analysis of system (3.8), and finally, with a technique similar to the one detailed Chapter 2, Section 2.3.4.1, to numerically investigate the existence of periodic orbits by concatenation of fast and slow pieces. We stress the versatility of the numerical argument we present, which is similar to the one we used in Chapter 2, applied now to a higher dimensional system.

3.4 Bifurcation analysis and numerical simulations

In this section, we carry out a bifurcation analysis for the behaviour of system (3.8), which will then be verified by numerical simulations and by a geometrical argument. Bifurcation analysis is done on system (3.8), which for small values of ϵ is stiff (as we showed in Proposition 8, the slow manifold is exponentially close to the critical manifold), while the numerical simulation concern a combination of systems (3.14) and (3.32), which are both non-stiff.
It is important to notice that, even though the layer system (3.14) converges to the critical

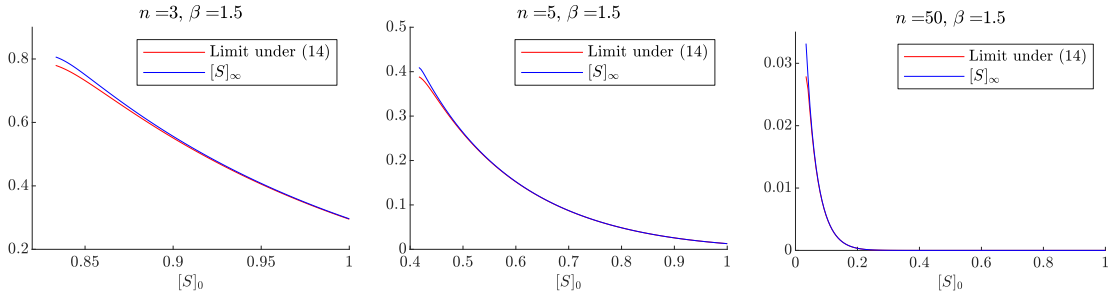

(a) (b) (c)

Figure 3.7: Comparison of the limit value of $[S]$ as $t \to \infty$ of system (3.14) (red) and formula (3.35) (blue). We set $[I]_0 = [SI]_0 = [II]_0 = 0.001$, $\gamma = 1$. With the values of the parameters of (a) (respectively, (b) and (c)), $1/R_1 \approx 0.833$ (resp., 0.417 and 0.034), and we only consider values of $[S]_0 \geq 1/R_1$, for which the epidemics can start.

manifold forwards in time, the slow flow (3.32) would converge to the point $([S], [SS]) = (1, n)$ if we let it evolve freely; the derivation of the exit time (3.44) is fundamental, in this setting, to carry out a meaningful numerical exploration of the model.

Without loss of generality, we set γ, which is the inverse of the average infection interval, to 1; this simply amounts to an $\mathcal{O}(1)$ rescaling of time, and we rescale the other parameters accordingly, keeping however the same symbols, for ease of notation. System (3.8) then has only three parameters, namely ϵ, n and β.

Using MatCont [15], we are able to completely characterize system (3.8) through numerical bifurcation analysis. We only consider the first octant of $\mathbb{R}^3$, for the biological interpretation of the parameters. Numerical analysis shows the existence of a Hopf surface Σ, whose "skeleton" is depicted in Figure 3.8. For values of the parameters between the plane $\epsilon = 0$ and Σ, the system exhibits a stable limit cycle, while for values above Σ, the system exhibits convergence to the endemic equilibrium (3.31). Our bifurcation analysis suggests the existence of a value $\epsilon^* \approx 0.18$ such that, for $\epsilon > \epsilon^*$, the system only exhibits convergence to the endemic equilibrium, regardless of the values of β and n.

To make Figure 3.8 more readable, we provide intersections of the surface Σ with some planes $n = k$ (Figure 3.9a), $\beta = k$ (Figure 3.9b), and finally $\epsilon = k$ (Figure 3.10). As in Chapter 2, we see an expansion of the parameter region which exhibits stable limit cycles as ϵ decreases, see Figure 3.10. This means that, as ϵ decreases, i.e. as the ratio between the average lengths of the infectious phase and the immunity interval decreases, we are more likely to observe occurrence of stable limit cycles in the disease dynamics. We do not observe, however, a divergence in the n direction, as the limit as $\epsilon \to 0$ of the surface contained in the green curves of Figure 3.10 is still bounded.

Counter-intuitively from a biological viewpoint, from which one would expect a greater diffusion of an epidemic in a population consisting of more social individuals, our numerical exploration of system (3.8) shows that limit cycles are only possible for small values of n (specifically 3, 4 and 5). This means that, for a disease with small enough ratio between the infection period and the immunity window (i.e., ϵ), each individual in the population having really few direct neighbours can lead, depending on the force of infection τ, to periodic outbreaks, while having more than 5 drives the population towards the unique endemic equilibrium. The homogeneous mixing hypothesis can be interpreted, in this network setting, as having n large. In this regard, the bifurcation analysis is in agreement with the results of Chapter 2, in which the SIRS model

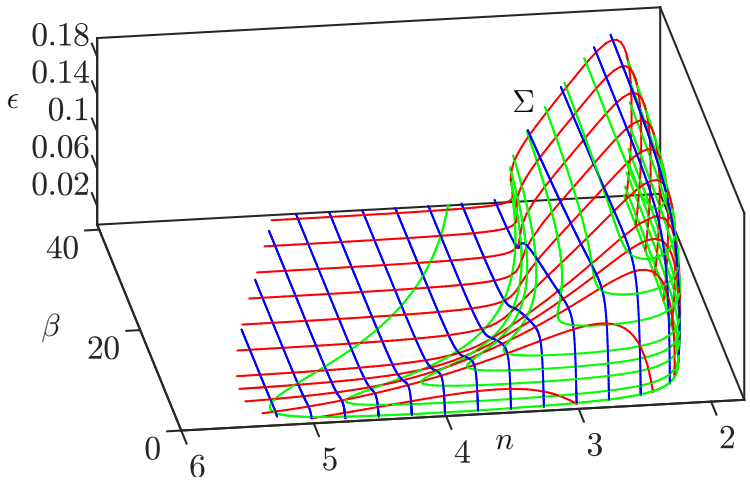

Figure 3.8: A skeleton of the bifurcation surface Σ. Green (respectively, red and blue) curves correspond to constant values of ϵ (respectively, β and n). We notice that, for values of $n \geq 6$, system (3.8) converges to the endemic equilibrium (3.31) regardless of the value of ϵ and β.

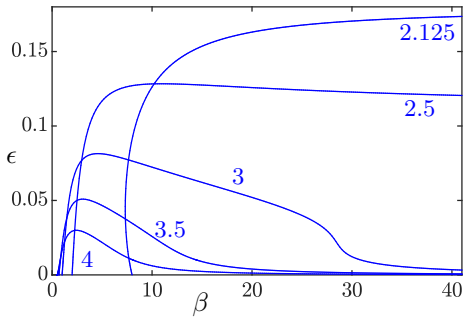

(a) Intersections of the surface Σ with planes $n = k$. The values of n are indicated near the corresponding curves.

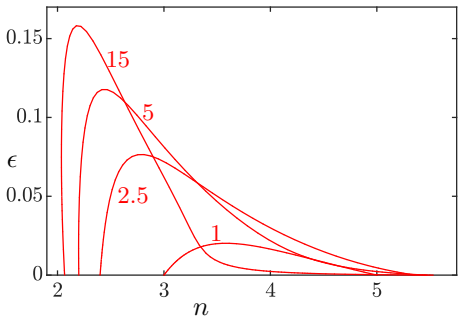

(b) Intersections of the surface Σ with planes $\beta = k$. The values of β are indicated near the corresponding curves.

Figure 3.9: A subset of the blue and red curves from Figure 3.8.

with homogeneous mixing is characterized by convergence towards the endemic equilibrium, as long as $R_0 > 1$; recall that the endemic equilibrium (3.31) is characterized by a quantity of infected which is $\mathcal{O}(\epsilon)$ small.

In order to verify the accuracy of the surface Σ, we investigate the system via a numerical implementation of the same geometrical argument used in Chapter 2, Section 2.3.4.1. There, we numerically showed the existence of a candidate orbit by concatenating heteroclinic orbits of the layer equation, from the critical manifold to itself, and orbits of the slow flow, truncating each at the corresponding exit time. The system studied in Chapter 2 was 3-dimensional, but the slow flow evolved on a 2-dimensional plane in $\mathbb{R}^3$; as we showed thus far, system (3.8) is

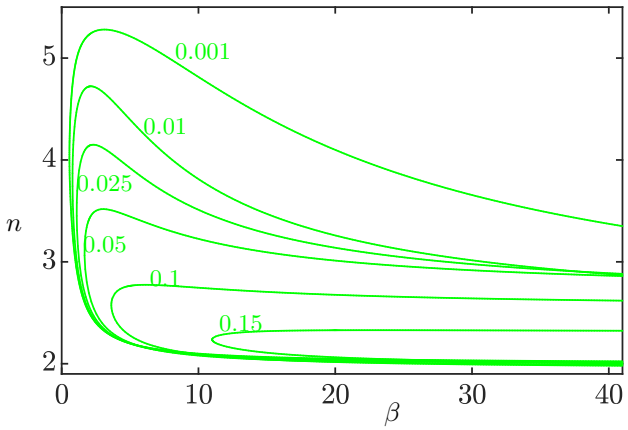

Figure 3.10: Intersections of the surface Σ with planes $\epsilon = k$. The values of ϵ are indicated near the corresponding curves.

characterized by a 2-dimensional slow manifold, as well. We now briefly recall the construction of the geometrical argument.
We fix $\epsilon = 0$, $n = 4$, and vary β to be below and above Σ, respectively; we compare the results in Figure 3.11. In both cases, a candidate starting point for a periodic orbit was found by iterating multiple times the layer system (3.14) and the slow flow (3.32), stopped when the slow piece of the orbit reached its exit time (3.44). Once we have obtained the candidate value for $[S]_0$, we take a small interval J_1 in the $[SS]$ coordinate around its corresponding value $[SS]_0$, and we map it forward in time to obtain an interval of starting points for the slow flow, J_2. Finally, we map J_2 forward in time, stopping each orbit at the corresponding exit time, obtaining a third interval J_3. In Chapter 2, we argued that if J_3 intersects J_1 transversally, then the perturbed system, for $\epsilon > 0$ small enough, exhibits stable limit cycles.
Figures 3.11 (a) and (c) depict the numerical realization of the two limit systems for a couple (n, β) for which we do not expect limit cycles: indeed, J_1 and J_3 (respectively, the vertical red line and the blue line in (b)) do not intersect, and bifurcation analysis confirms that, for this choice of the parameters, there are no limit cycles, but global convergence to the endemic equilibrium.
Figures 3.11 (b) and (d), instead, depict the numerical realization of the two limit systems for a couple (n, β) for which we do expect limit cycles: indeed, J_1 and J_3 intersect, and bifurcation analysis confirms that, for this choice of the parameters, there is a stable limit cycle. Since the underlying idea is the same as Chapter 2, Section 2.3.4.1, we refer to that for a more in-depth explanation of the method.
Figures 3.11 (e) and (f), finally, are projections on the $[S] - [I]$ plane of orbits of system (3.8), starting from a random initial point. As we expected, for ϵ sufficiently small, the perturbed system exhibits either convergence to equilibrium, as the combination of the two limit systems showed in Figures 3.11 (a) and (c), or towards a stable limit cycle, as argued from (b) and (d). This numerical analysis shows that there is an interval around $\beta \sim 2$ for which periodic orbits of (3.8) exists, for $\epsilon > 0$ sufficiently small.

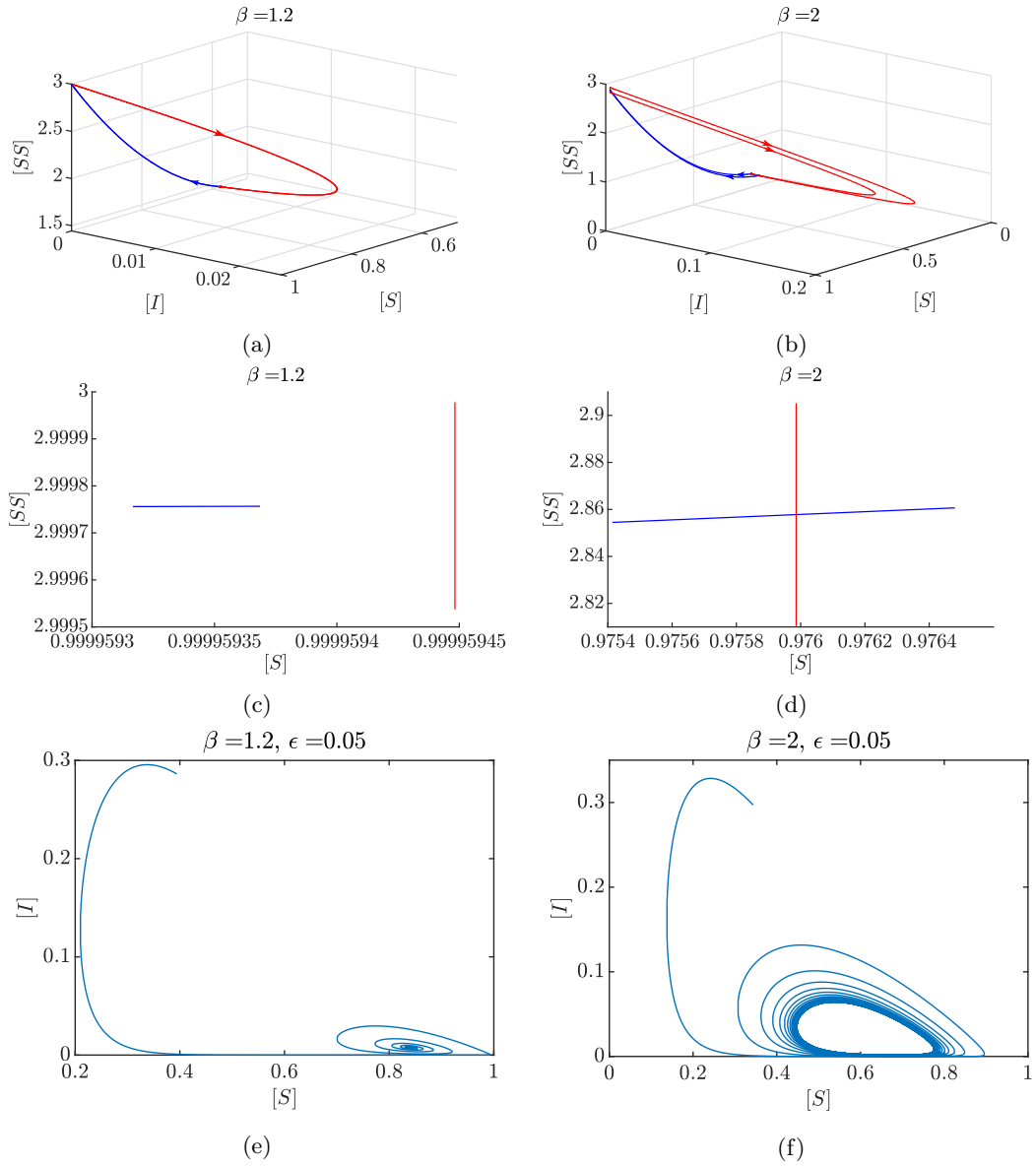

Figure 3.11: Numerical illustration of the effect of changing β on the system dynamics. Figures (a) and (b): evolution under the layer system (red) of a small interval J_1, in the $[SS]$ direction. Its image defines the entry interval J_2 on the critical manifold; evolution of each point of J_2 under the slow flow (blue), stopped at its exit time, giving the exit interval J_3. Notice that the blue curves lie on the $[S], [SS]$ plane, while the red curves represent a fast excursion in the region $[I], [SI], [II] > 0$. Figures (c) and (d): zoom on the relative position of J_1 and J_3 on the critical manifold. Figures (e) and (f): projections on the $[S] - [I]$ plane of numerical simulations of system (3.8) from a random point, exhibiting convergence to the endemic equilibrium and the stable limit cycle, respectively.

3.5 Summary and Outlook

We have analysed the behaviour of a model for epidemics on networks, given in a nonstandard singularly perturbed form, after reducing its dimension exploiting multiple conserved quantities.

Even though the model derived from the SIRS model studied in Chapter 2, which is characterized by global convergence to equilibrium, our bifurcation analysis and geometric numerical argument show that, for a significant open subset of the parameter space, the network generalization exhibits stable limit cycles. The main characteristic of this set is the value of n, the number of neighbours every individual has, which must be between 3 and 5 included. In practical terms, this is not a major restriction as most real-world networks have sub-networks, where individuals have around three to five very close friends. It is clear that there is further motivation to intensify the investigation of more complex compartment networks with techniques from GSPT, since dropping the homogeneous mixing hypothesis unveiled asymptotic behaviours which are impossible in the corresponding system studied without network structure. In particular, it would be interesting to check whether the periodic solutions identified in the pair-approximation model of a network can be detected also in simulations of the original network model.

Moreover, the analysis of this network generalization of the SIRS model studied in Chapter 2 qualitatively confirmed its results, since for large values of n (in the homogeneous mixing hypothesis, $n = N - 1$, which is by assumption large), the system only exhibits convergence towards the endemic equilibrium.

We stress the versatility of our geometric procedure, which gives us a numerical intuition of the asymptotic behaviour of a stiff system, i.e. system (3.8) with $0 < \epsilon \ll 1$, without having to *actually* integrate it, but through simple integration of the corresponding two non-stiff limit systems, which we derived through the use of GSPT. This is particularly important for the high(er) dimensionality of the system, which hinders analytical results on the perturbed system. In particular, the same strategy is likely to generalize to more complicated network-based ODE models derived from moment closure.

Furthermore, it would be interesting to rigorously investigate how the system changes as we let $n \to +\infty$. One intermediate step between having two independent perturbation parameters (*i.e.*, $\epsilon \to 0$ and $n \to +\infty$) could be to couple n and ϵ, for example taking $n = \mathcal{O}(1/\epsilon^\alpha)$, for some $\alpha > 0$. However, this goes beyond the scope of this project, and we leave this as a prompt for future research.

4. Bibliography

[1] R. M. Anderson and R. McM. May. *Infectious diseases of humans*, volume 1. Oxford university press Oxford, 1991.

[2] V. Andreasen. The effect of age-dependent host mortality on the dynamics of an endemic disease. *Math. Biosci.*, 114(1):29–58, 1993.

[3] E. Benoît, M. Brøns, M. Desroches, and M. Krupa. Extending the zero-derivative principle for slow–fast dynamical systems. *Zeitschrift für angewandte Mathematik und Physik*, 66(5):2255–2270, 2015.

[4] R. Bertram and J. E. Rubin. Multi-timescale systems and fast-slow analysis. *Mathematical biosciences*, 287:105–121, 2017.

[5] S. Bidari, X. Chen, D. Peters, D. Pittman, and P. L. Simon. Solvability of implicit final size equations for SIR epidemic models. *Mathematical biosciences*, 282:181–190, 2016.

[6] K. Bold, C. Edwards, J. Guckenheimer, S. Guharay, K. Hoffman, J. Hubbard, R. Oliva, and W. Weckesser. The forced van der Pol equation II: canards in the reduced system. *SIAM Journal of Applied Dynamical Systems*, 2(4):570–608, 2003.

[7] F. Brauer. A singular perturbation approach to epidemics of vector-transmitted diseases. *Infectious Disease Modelling*, 4:115–123, 2019.

[8] D. Breda, O. Diekmann, W. F. De Graaf, A. Pugliese, and R. Vermiglio. On the formulation of epidemic models (an appraisal of Kermack and McKendrick). *Journal of biological dynamics*, 6(sup2):103–117, 2012.

[9] C. Castellano and R. Pastor-Satorras. Thresholds for epidemic spreading in networks. *Physical review letters*, 105(21):218701, 2010.

[10] S. S. Chaves, P. Gargiullo, J. X. Zhang, R. Civen, D. Guris, L. Mascola, and J. F. Seward. Loss of vaccine-induced immunity to varicella over time. *New England Journal of Medicine*, 356(11):1121–1129, 2007.

[11] M. P. Dafilis, F. Frascoli, J. G. Wood, and J. M. McCaw. The influence of increasing life expectancy on the dynamics of SIRS systems with immune boosting. *The ANZIAM Journal*, 54(1-2):50–63, 2012.

[12] P. De Maesschalck. Smoothness of transition maps in singular perturbation problems with one fast variable. *J. Differ. Equ.*, 244(6):1448–1466, 2008.

[13] P. De Maesschalck and S. Schecter. The entry–exit function and geometric singular perturbation theory. *J. Differ. Equ.*, 260(8):6697–6715, 2016.

[14] M. Desroches, B. Krauskopf, and H.M. Osinga. The geometry of mixed-mode oscillations in the Olsen model for the perioxidase-oxidase reaction. *DCDS-S*, 2(4):807–827, 2009.

[15] A. Dhooge, W. Govaerts, Y. A. Kuznetsov, H. G. E. Meijer, and B. Sautois. New features of the software MatCont for bifurcation analysis of dynamical systems. *Math. Comput. Model. Dyn. Syst.*, 14(2):147–175, 2008.

[16] O. Diekmann, H. Heesterbeek, and T. Britton. *Mathematical Tools for Understanding Infectious Disease Dynamics*. Princeton Univ. Press, 2013.

[17] O. Diekmann, J. A. P. Heesterbeek, and J. A. J. Metz. On the definition and the computation of the basic reproduction ratio R 0 in models for infectious diseases in heterogeneous populations. *Journal of mathematical biology*, 28(4):365–382, 1990.

[18] O. Diekmann, J. A. P. Heesterbeek, and M. G. Roberts. The construction of next-generation matrices for compartmental epidemic models. *Journal of the Royal Society Interface*, 7(47):873–885, 2010.

[19] E. K. Ersöz, M. Desroches, A. Guillamon, J. Rinzel, and J. Tabak. Canard-induced complex oscillations in an excitatory network. *Journal of Mathematical Biology*, 2020.

[20] N. Fenichel. Geometric singular perturbation theory for ordinary differential equations. *J. Differ. Equ.*, 31(1):53–98, 1979.

[21] K. O. Friedrichs, W. R. Wasow, et al. Singular perturbations of non-linear oscillations. *Duke Mathematical Journal*, 13(3):367–381, 1946.

[22] A. Ganesh, L. Massoulié, and D. Towsley. The effect of network topology on the spread of epidemics. In *Proceedings IEEE 24th Annual Joint Conference of the IEEE Computer and Communications Societies.*, volume 2, pages 1455–1466. IEEE, 2005.

[23] G. Giordano, F. Blanchini, R. Bruno, P. Colaneri, A. Di Filippo, A. Di Matteo, and M. Colaneri. Modelling the COVID-19 epidemic and implementation of population-wide interventions in italy. *Nature Medicine*, pages 1–6, 2020.

[24] J. Guckenheimer, K. Hoffman, and W. Weckesser. The forced van der Pol equation I: The slow flow and its bifurcations. *SIAM Journal on Applied Dynamical Systems*, 2(1):1–35, 2003.

[25] J. Guckenheimer and C. Kuehn. Homoclinic orbits of the FitzHugh-Nagumo equation: The singular limit. *DCDS-S*, 2(4):851–872, 2009.

[26] J. Guckenheimer, M. Wechselberger, and L.-S. Young. Chaotic attractors of relaxation oscillations. *Nonlinearity*, 19:701–720, 2006.

[27] R. Haiduc. Horseshoes in the forced van der Pol system. *Nonlinearity*, 22:213–237, 2009.

[28] M. J. B. Hauser and L. F. Olsen. Mixed-mode oscillations and homoclinic chaos in an enzyme reaction. *Journal of the Chemical Society, Faraday Transactions*, 92(16):2857–2863, 1996.

[29] J. A. P. Heesterbeek and J. A. J. Metz. The saturating contact rate in marriage-and epidemic models. *Journal of Mathematical Biology*, 31(5):529–539, 1993.

[30] G. Hek. Geometric singular perturbation theory in biological practice. *Journal of mathematical biology*, 60(3):347–386, 2010.

[31] H. W. Hethcote. Qualitative analyses of communicable disease models. *Mathematical Biosciences*, 28(3-4):335–356, 1976.

[32] H. W. Hethcote. The mathematics of infectious diseases. *SIAM review*, 42(4):599–653, 2000.

[33] H. W. Hethcote. The Basic Epidemiology Models: Models, Expressions for R_0, Parameter Estimation, and Applications. In *Epidemiology*, volume 9, pages 1–135. World Scientific, 2005.

[34] F. C. Hoppensteadt. Singular perturbations on the infinite interval. *Transactions of the American Mathematical Society*, 123(2):521–535, 1966.

[35] T.-H. Hsu and S. Ruan. Relaxation Oscillations and the Entry-Exit Function in Multi-Dimensional Slow-Fast Systems. *arXiv preprint arXiv:1910.06318*, 2019.

[36] A. Iuorio, C. Kuehn, and P. Szmolyan. Geometry and numerical continuation of multiscale orbits in a nonconvex variational problem. *Discr. Cont. Dyn. Syst. S*, 13(2):1269–1290, 2020.

[37] H. Jardón-Kojakhmetov and C. Kuehn. A survey on the blow-up method for fast-slow systems. *arXiv preprint arXiv:1901.01402*, 2019.

[38] S. Jelbart and M. Wechselberger. Two-stroke relaxation oscillators. *Nonlinearity*, 33(5):2364, 2020.

[39] C. K. R. T. Jones. Geometric singular perturbation theory. In *Dynamical systems*, pages 44–118. Springer, 1995.

[40] T. J. Kaper. An introduction to geometric methods and dynamical systems theory for singular perturbation problems. In J. Cronin and R. E. Jr. O' Malley, editors, *Analyzing multiscale phenomena using singular perturbation methods*, volume 56, page 85–132. American Mathematical Society, Providence, 1999.

[41] M. J. Keeling, D. A. Rand, and A. J. Morris. Correlation models for childhood epidemics. *Proceedings of the Royal Society of London. Series B: Biological Sciences*, 264(1385):1149–1156, 1997.

[42] M. J. Keeling and P. Rohani. *Modeling Infectious Diseases in Humans and Animals*. Princeton University Press, 2008.

[43] M. J. Keeling, P. Rohani, and B. T. Grenfell. Seasonally forced disease dynamics explored as switching between attractors. *Phys. D*, 148:317–335, 2001.

[44] W. O. Kermack and A. G. McKendrick. A contribution to the mathematical theory of epidemics. *Proc. R. Soc. Lond. Series A, Containing papers of a mathematical and physical character*, 115(772):700–721, 1927.

[45] W. O. Kermack and A. G. McKendrick. Contributions to the mathematical theory of epidemics-ii . the problem of endemicity. *Proc. R. Soc. Lond. Series A*, 138A:55–83, 1932.

[46] I. Z. Kiss, J. C. Miller, P. L. Simon, et al. *Mathematics of epidemics on networks*. Springer, 2017.

[47] S. M. Kissler, C. Tedijanto, E. Goldstein, Y. H. Grad, and M. Lipsitch. Projecting the transmission dynamics of SARS-CoV-2 through the postpandemic period. *Science*, 368(6493):860–868, 2020.

[48] I. Kosiuk and P. Szmolyan. Geometric analysis of the Goldbeter minimal model for the embryonic cell cycle. *J. Math. Biol.*, 72(5):1337–1368, 2016.

[49] M. Krupa and M. Wechselberger. Local analysis near a folded saddle-node singularity. *Journal of Differential Equations*, 248(12):2841–2888, 2010.

[50] C. Kuehn. On decomposing mixed-mode oscillations and their return maps. *Chaos: An Interdisciplinary Journal of Nonlinear Science*, 21(3):033107, 2011.

[51] C. Kuehn. *Multiple time scale dynamics*, volume 191. Springer, 2015.

[52] C. Kuehn. Moment closure—a brief review. In *Control of self-organizing nonlinear systems*, pages 253–271. Springer, 2016.

[53] C. Kuehn and P. Szmolyan. Multiscale geometry of the Olsen model and non-classical relaxation oscillations. *J. Nonlinear Sci.*, 25(3):583–629, 2015.

[54] J. LaSalle. Some extensions of Liapunov's second method. *IRE Transactions on circuit theory*, 7(4):520–527, 1960.

[55] J. S. Lavine, A. A. King, and O. N. Bjørnstad. Natural immune boosting in pertussis dynamics and the potential for long-term vaccine failure. *Proc. Natl. Acad. Sci. U.S.A*, 108(17):7259–7264, 2011.

[56] B. Letson and J. E. Rubin. A new frame for an old (phase) portrait: Finding rivers and other flow features in the plane. *SIAM Journal on Applied Dynamical Systems*, 17(4):2414–2445, 2018.

[57] N. Levinson. Perturbations of discontinuous solutions of non-linear systems of differential equations. *Acta Mathematica*, 82(1):71–106, 1950.

[58] M. Y. Li, W. Liu, C. Shan, and Y. Yi. Turning points and relaxation oscillation cycles in simple epidemic models. *SIAM Journal on Applied Mathematics*, 76(2):663–687, 2016.

[59] M. Y. Li and J. S. Muldowney. Global stability for the SEIR model in epidemiology. *Mathematical biosciences*, 125(2):155–164, 1995.

[60] W. Liu. Exchange lemmas for singular perturbation problems with certain turning points. *Journal of Differential Equations*, 167(1):134–180, 2000.

[61] M. López-García. Stochastic descriptors in an SIR epidemic model for heterogeneous individuals in small networks. *Mathematical biosciences*, 271:42–61, 2016.

[62] A. M. Mandel, M. Akke, and A. G. Palmer. Dynamics of ribonuclease h: temperature dependence of motions on multiple time scales. *Biochemistry*, 35(50):16009–16023, 1996.

[63] M. Martcheva. *An Introduction to Mathematical Epidemiology*, volume 61. Springer, 2015.

[64] G. S. Medvedev. Reduction of a model of an excitable cell to a one-dimensional map. *Physica D*, 202(1):37–59, 2005.

[65] J. Mossong, N. Hens, M. Jit, P. Beutels, K. Auranen, R. Mikolajczyk, M. Massari, S. Salmaso, G. S. Tomba, J. Wallinga, et al. Social contacts and mixing patterns relevant to the spread of infectious diseases. *PLoS Med*, 5(3):e74, 2008.

[66] S. M. O' Regan, T. C. Kelly, A. Korobeinikov, M. J. A. O' Callaghan, and A. V. Pokrovskii. Lyapunov functions for SIR and SIRS epidemic models. *Appl. Math. Lett.*, 23(4):446–448, 2010.

[67] L. S. Pontryagin. Asymptotic behavior of solutions of systems of differential equations with a small parameter in the derivatives of highest order. *Izvestiya Rossiiskoi Akademii Nauk. Seriya Matematicheskaya*, 21(5):605–626, 1957.

[68] H. E. Randolph and L. B. Barreiro. Herd immunity: Understanding COVID-19. *Immunity*, 52(5):737–741, 2020.

[69] S. M. O' Regan and J. M. Drake. Theory of early warning signals of disease emergence and leading indicators of elimination. *Theor. Ecol.*, 6(3):333–357, 2013.

[70] F. Rocha, L. Mateus, U. Skwara, M. Aguiar, and N. Stollenwerk. Understanding dengue fever dynamics: a study of seasonality in vector-borne disease models. *Int J Comput Math*, 93(8):1405–1422, 2016.

[71] K. Satō, H. Matsuda, and A. Sasaki. Pathogen invasion and host extinction in lattice structured populations. *Journal of mathematical biology*, 32(3):251–268, 1994.

[72] S. Schecter. Exchange lemmas 2: General exchange lemma. *Journal of Differential Equations*, 245(2):411–441, 2008.

[73] S. Schecter. Geometric singular perturbation theory analysis of an epidemic model with spontaneous human behavioral change. *arXiv preprint arXiv:2006.09237*, 2020.

[74] Z. Shuai and P. van den Driessche. Global stability of infectious disease models using Lyapunov functions. *SIAM J. Appl. Math.*, 73(4):1513–1532, 2013.

[75] D. Smilkov, C. A. Hidalgo, and L. Kocarev. Beyond network structure: How heterogeneous susceptibility modulates the spread of epidemics. *Scientific reports*, 4(1):1–7, 2014.

[76] H. L. Smith. Subharmonic bifurcation in an SIR epidemic model. *J. Math. Biol.*, 17:163–177, 1983.

[77] H. E. Soper. The Interpretation of Periodicity in Disease Prevalence. *J. Royal Statistical Society*, 92:34–73, 1929.

[78] A. N. Swart, M. Tomasi, M. Kretzschmar, A. H. Havelaar, and O. Diekmann. The protective effects of temporary immunity under imposed infection pressure. *Epidemics*, 4(1):43–47, 2012.

[79] H. Taghvafard, H. Jardón-Kojakhmetov, and M. Cao. Parameter-robustness analysis for a biochemical oscillator model describing the social-behaviour transition phase of myxobacteria. *Proc. R. Soc. Lond. Series A*, 474(2209):20170499, January 2018.

[80] H. Taghvafard, H. Jardón-Kojakhmetov, P. Szmolyan, and M. Cao. Geometric analysis of Oscillations in the Frzilator model. *arXiv preprint arXiv:1912.00659*, 2019.

[81] R. Thom. Quelques propriétés globales des variétés différentiables. *Comment. Math. Helv.*, 28(1):17–86, 1954.

[82] P. Van den Driessche and J. Watmough. Reproduction numbers and sub-threshold endemic equilibria for compartmental models of disease transmission. *Mathematical biosciences*, 180(1-2):29–48, 2002.

[83] V. Venkatasubramanian. Singularity induced bifurcation and the van der Pol oscillator. *IEEE Transactions on Circuits and Systems I: Fundamental Theory and Applications*, 41(11):765–769, 1994.

[84] E. Volz. SIR dynamics in random networks with heterogeneous connectivity. *Journal of mathematical biology*, 56(3):293–310, 2008.

[85] X. Wang, L. Wei, and J. Zhang. Dynamical analysis and perturbation solution of an SEIR epidemic model. *Applied Mathematics and Computation*, 232:479–486, 2014.

[86] M. Wechselberger. *Geometric singular perturbation theory beyond the standard form*. Springer, 2020.

[87] A. Widder and C. Kuehn. Heterogeneous population dynamics and scaling laws near epidemic outbreaks. *Math. Biosci. Eng.*, 13(5):1093–1118, 2016.

[88] R. G. Woolthuis, J. Wallinga, and M. van Boven. Variation in loss of immunity shapes influenza epidemics and the impact of vaccination. *BMC infectious diseases*, 17(1):1–11, 2017.

[89] H. Zhang, Z.-H. Guan, T. Li, X.-H. Zhang, and D.-X. Zhang. A stochastic SIR epidemic on scale-free network with community structure. *Physica A: Statistical Mechanics and its Applications*, 392(4):974–981, 2013.

[90] Z. Zhang, Y. Suo, J. Peng, and W. Lin. Singular perturbation approach to stability of a SIRS epidemic system. *Nonlinear Analysis: Real World Applications*, 10(5):2688–2699, 2009.